Study of Spectral Characteristics of Low Frequency Conducted EMI in Power Electronic Based Systems

Esfetanaj, Naser Nourani

DOI (link to publication from Publisher):
10.54337/aau443238170

Publication date:
2021

Document Version
Publisher's PDF, also known as Version of record

STUDY OF SPECTRAL CHARACTERISTICS OF LOW FREQUENCY CONDUCTED EMI IN POWER ELECTRONIC BASED SYSTEMS

BY
NASER NOURANI ESFETANAJ

DISSERTATION SUBMITTED 2021

AALBORG UNIVERSITY
DENMARK

STUDY OF SPECTRAL CHARACTERISTICS OF LOW FREQUENCY CONDUCTED EMI IN POWER ELECTRONIC BASED SYSTEMS

Ph.D. Dissertation

Naser Nourani Esfetanaj

Dissertation submitted Apr. 29, 2021

Dissertation submitted:	Apr. 29, 2021
PhD supervisor:	Assoc. Prof. Pooya Davari, Aalborg University, Denmark
Assistant PhD supervisor:	Prof. Huai Wang, Aalborg University, Denmark
PhD committee:	Professor Francesco Iannuzzo (chairman) Aalborg University
	Professor Braham Ferreira University of Twente
	Professor Jorma Kyyrä Aalto University
PhD Series:	Faculty of Engineering and Science, Aalborg University
Department:	Department of Energy Technology

ISSN (online): 2446-1636
ISBN (online): 978-87-7210-943-5

Published by:
Aalborg University Press
Kroghstræde 3
DK – 9220 Aalborg Ø
Phone: +45 99407140
aauf@forlag.aau.dk
forlag.aau.dk

Printed in Denmark by Rosendahls, 2021

Curriculum Vitae

Naser Nourani Esfetanaj

Naser Nourani Esfetanaj (S'19) received the B.Sc. degrees in electrical engineering from the Department of Electrical & Computer Engineering from Tabriz University, Tabriz, Iran, in 2011. And an MSC from the Department of Electrical Engineering from Sahand University of Technology, Tabriz, Iran in 2013.

His main responsibility was as an HV expert in substation design at the MONA consultants company from 2013 to 2018. He is pursuing a Ph.D. degree in power electronics at the Department of Energy Technology, Aalborg University, Aalborg, Denmark. He joined the Electrical Engineering and Information Technology Department, Dresden University of Technology, Germany, as a Visiting Scholar, where he focused on several research activities under the supervision of Dr. Jan Meyer. He is responsible for the IEEE student branch newsletter at Aalborg University. His main study interests include EMI/EMC in power electronics-based systems. He is a student member of IEEE and PELS, and EMC society, where he contributes to several working groups.

ABSTRACT

Power electronics (PE) converters are increasingly applied in grid-connected systems. While they provide efficient and flexible control of electrical energy, they also bring new challenges concerning electromagnetic interference (EMI). In fact that, the EMC standards are in place to ensure the compatibility of power electronics. But, the current standards cover below 2 kHz and above 150 kHz. Therefore, there is a gap in standard as there is no general emission standard for 2 – 150 kHz as it only covers some specific products. The 2-150 kHz is of particular interest due to: 1) many power converters have switched in this frequency range, and 2) the mains communication systems (MCS) are communicated together to transfer the data in this frequency range. Consequently, generated noise from the PE converter may severely deteriorate MCS communication signals. Hence, to assure proper and reliable grid operation, EMI challenging issues at device and system levels should be investigated appropriately.

Firstly, seen from the technical perspective, one major concern is the lack of systematically understanding of noise propagation into the power grid within 2-150 kHz regarding the upcoming emission standard (i.e., 61000-6-3). Hence, accurate modeling of the different power converters is needed to characterize low-frequency EMI emissions up to 150 kHz. Further, this analytical model needs to extended to single-phase and three-phase applications. Further, as the penetration of power electronic systems to the grid increases, the noise level should be limited based on the standard requirement, thereby a proper EMI filter should be better designed as well in the single-phase and three-phase.

Secondly, one of the main challenges in the new frequency range is the lack of a suitable model which covers the interaction analysis between the units in multi-converter systems. Further, it is necessary to simplify the multi-converter systems analysis model. Additionally, the parallel operation of various PE converters within similar power switching frequencies has led to unprecedented emissions within high frequencies, including a beating frequency and EMI under 150 kHz. Moreover, the factory switching tolerance, which brings the unsynchronized scenario on the multi converter systems, should be included in the modeling.

To tackle those issues and thus understand noise propagation mechanism and limit the emission following the standard regulations, this Ph.D. project discusses modeling and analyzing of low-frequency noise emission. Consequently, it can provide a proper EMI filter design and identify dominant parameters leading to power converter noise model order reduction and simplification. The analytical low-frequency EMI emission model through closed-loop impedance modeling is developed up to 150 kHz throughout this project. Among different power converters, a voltage source inverter (VSI) and a boost power factor correction (PFC) converter will be intensively studied as they are common in grid-connected single-phase applications. Utilizing closed-loop models can speed up the design process, prevent time-consuming trial and error, empirical measurements, and reduce cost. Further, it is necessary to limit the noise level based on the standards requirement. Hence, designing a proper EMI filter for the frequency between 2-150 kHz based on the proposed modeling approach is analyzed. The performance of the proposed analytical approach with and without EMI filter has

been validated through experiments and simulations. The reduced-order model is achieved to use in the multi-converter system analysis.

Next, the analytical model is extended to the three-phase converter to characterize noise behavior in the low-frequency EMI range. Hence, the proposed technique estimates the generated emissions of the three-phase converter by utilizing double Fourier analysis and closed-loop input/output admittance. Three-phase voltage VSI and active rectifier will be studied as the most common topologies utilized in grid-connected three-phase applications. The impact of a sampling frequency and loading conditions on the closed-loop admittance have been analyzed. The performance of the proposed method is shown through the experimental and simulation results.

Furthermore, the impact of interleaving techniques on the analytical method has also been analyzed by applying phase shift effects. Moreover, the EMI filter design is done by considering various phase shifts to decrease the filter volume. Next, the interaction current between the multi-converter is also analyzed, where unsynchronized scenarios are regarded due to the switching frequency tolerance. Moreover, the effects of the different EMI filter designs on the interaction current between the units and grid are investigated. Finally, an aggregated analytical EMI emission estimation approach is achieved on the multi-converter systems. The proposed analytical method is validated by simulations and experiments with different phase shifts.

Accordingly, by employing the analytical proposed models for EMI noise propagation assessment and prevention, future power-electronics-based power systems may be designed and operated in a desirable fashion and compatible with the new standard.

DANSK RESUME

Power elektronik (PE) konvertere anvendes i stigende grad i net-tilsluttede systemer. Mens de giver effektiv og fleksibel kontrol af elektrisk energi, medfører de også nye udfordringer vedrørende elektromagnetisk interferens (EMI). EMC-standarderne er på plads for at sikre kompatibilitet imellem effektelektronik systemer. De nuværende standarder dækker kun for båndene under 2 kHz og over 150 kHz. Derfor er der et hul i standarderne, da der ikke er nogen generel emissionsstandard for 2 - 150 kHz, men kun visse specifikke til nogle produkter. 2-150 kHz er af særlig interesse af flere grunde: 1) mange effektomformere arbejder i dette frekvensområde, og 2) hovedkommunikationssystemerne (MCS) overfører data i dette frekvensområde. Derfor kan genereret støj fra PE-konverteren alvorligt forringe MCS-kommunikationssignalerne. For at sikre korrekt og pålidelig drift bør EMI udfordringerne på enheds- og systemniveau derfor undersøges korrekt.

Fra et teknisk perspektiv er den manglende systematiske forståelse af støjformering i elnettet bekymrende. Her menes specifikt inden for 2-150 kHz båndet, også i den kommende emissionsstandard (dvs. 61000-6-3). Derfor er der behov for nøjagtig modellering af de forskellige effektomformere for at karakterisere lavfrekvente EMI-emissioner op til 150 kHz.

Desuden skal analysemodellerne udvides til enfasede og trefasede applikationer. Efterhånden som mængden af effekt elektroniske systemer i nettet øges, bør interferensniveauet begrænses baseret på standardkrav, hvorved et korrekt EMI-filter også skal designes bedre i enfasede og trefasede systemer.

For det andet er en af de største udfordringer i det nye frekvensområde manglen på en passende model, der dækker interaktionsanalysen mellem enhederne i multi-converter-systemer. Yderligere er det nødvendigt at forenkle analyseanalysemodellen til multi-konverteringssystemer. Derudover har den parallelle drift af forskellige PE-konvertere inden for lignende strømskiftefrekvenser ført til hidtil usete emissioner inden for høje frekvenser, herunder en slagfrekvens og EMI under 150 kHz. Desuden bør fabriksomskiftningstolerancen, som bringer det usynkroniserede scenarie på multikonverteringssystemerne, medtages i modelleringen.

For at tackle disse problemer og dermed forstå støjformeringsmekanismen og begrænse emissionen i henhold til standardbestemmelserne, vil dette Ph.D. projekt diskutere modellering og analyse af lavfrekvent støjemission. Derfor kan det tilvejebringe et ordentligt EMI-filterdesign og identificere dominerende parametre, der fører til støjmodel forenkling. Den analytiske lavfrekvente EMI-emissionsmodel gennem lukket sløjfeimpedansmodellering er udviklet op til 150 kHz gennem hele dette projekt. Blandt forskellige effektomformere vil en spændingskildeinverter (VSI) og en boost effektfaktorkorrigering (PFC) konverter blive undersøgt intensivt, da de er almindelige i netforbundne enfasede applikationer. Designprocessen vil forhindre tidskrævende trial-and-error og reducere omkostningerne. Desuden er det nødvendigt at begrænse støjniveauet baseret på standardkravet. Derfor analyseres designet af EMI-filtre til frekvensen mellem 2-150 kHz baseret på den foreslåede modelleringsmetode. Udførelsen af den foreslåede analytiske tilgang med og uden EMI-filter er blevet valideret gennem eksperimenter og simuleringer.

Dernæst udvides den analytiske model til trefasekonverteren for at karakterisere støjadfærd i det lavfrekvente EMI-område.
Derfor estimerer den foreslåede teknik de genererede emissioner fra trefasekonverteren ved hjælp af dobbelt Fourier-analyse og lukket sløjfe-input/output adgang. Tre-faset spændings VSI og aktiv ensretter vil blive undersøgt som de mest almindelige topologier, der anvendes i nettilsluttede trefaseapplikationer. Virkningen af samplingsfrekvens og belastningsforhold på et lukket kredsløb er blevet analyseret. Udførelsen af den foreslåede metode vises gennem de eksperimentelle og simuleringsresultater.

Desuden er virkningen af sammenflettede teknikker i analysemetoden også blevet analyseret ved anvendelse af faseforskydningseffekter. Derudover udføres EMI-filterdesignet ved at overveje forskellige faseskift for at mindske filtervolumenet. Dernæst analyseres interaktionsstrømmen mellem multikonverteren også, hvor usynkroniserede scenarier betragtes på grund af skiftefrekvenstolerancen. Desuden undersøges virkningerne af de forskellige EMI-filterdesign på interaktionsstrømmen mellem enhederne og elnettet. Endelig opnås en aggregeret analytisk EMI-estimeringsmetode på multikonverteringssystemerne. Den foreslåede analysemetode valideres ved simuleringer og eksperimenter med forskellige faseforskydninger.

Ved anvendelse af de analytisk foreslåede modeller til vurdering og forebyggelse af støjudbredelse af EMI kan fremtidige effektelektroniske baserede energisystemer designes og drives på en ønskelig måde som er kompatible med den nye standard.

PREFACE

The work presented in this dissertation summarizes the outcome from the Ph.D. project " Study of the spectral characteristic of low frequency conducted EMI in power electronic-based systems.", which was definition at the Department of Energy Technology Aalborg University, Denmark. This Ph.D. project is supported by the Department of Energy Technology, Aalborg University, Otto Mønsteds Fond, Dresden University of Technology. The author would like to give an acknowledgment to the institutions mentioned above.

First, I would like to express my sincere gratitude to my supervisor and co-supervisor, Assoc. Prof. Pooya Davari and Prof. Huai wang for their continuous support of my Ph.D. study and research, for motivation, interest, and immense knowledge. Their support and encouragement are the main drivers for me to complete my Ph.D. study.

I am also appreciative to Doctor Jan Meyer for granting me an opportunity to visit The Dresden University of Technology during my study abroad. I would also like to thank my colleagues at the Dresden University of Technology for their great welcome during my stay.

Special thanks go to Professor Frede Blaabjerg and Assistant Professor Saeed Peyghami for their valuable suggestions and help. I would also like to thank all my colleagues and secretaries at the Department of Energy Technology, Aalborg University, for their support and fruitful discussion.

In the end, I would like to express my thankfulness to my family for their endless care and continued support, which is the most fantastic assistance in many ways. Most importantly, I wish to appreciate my lovely wife, Safa, who provides continued support. I am incredibly grateful for her patience, motivation, and the love that she gave to me during my Ph.D. and my life.

Naser Nourani Esfetanaj,
Aalborg University, April 29, 2021

CONTENTS

Chapter 1. Introduction

1.1. Background

1.1.1. Standardization Gap Between 2-150 kHz EMI Emission Frequency Range

Power converters are widely employed in grid-connected energy generation or utilization systems for power conversion. In recent years, power electronics (PE) converters have witnessed an ever-increasing advancement, especially PE converters operating within the switching frequency of 2-150 kHz. This progress is expected to be dramatically increased within the aforementioned frequency range in the near future [J1]. The vast increase of PE converters enables more flexible power grids, nevertheless, it brings new EMI concerns. This is majorly caused by inherent pulse energy conversion characteristics. Fig. 1.1 depicts an overall view of power electronic-based power system which some of them be modeled in the thesis.

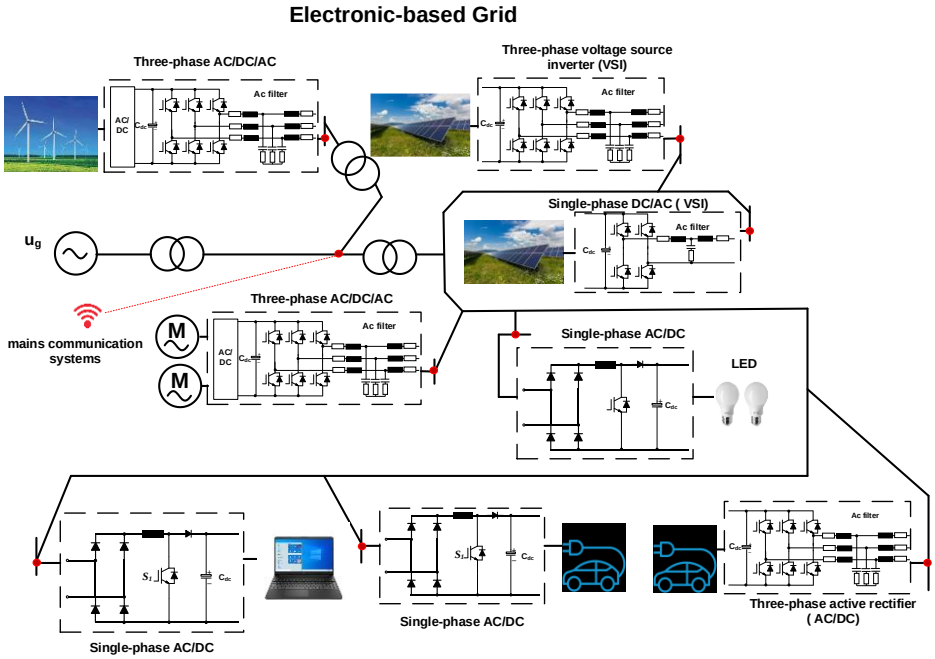

***Fig. 1.1**: General view of power electronic-based power system.*

Indeed, the pulsed energy conversion related to PE converters and the required communications throughout the electric power lines results in serious EMI emissions that may compromise the power grid reliability [1]. As an obvious reason, the smart grid is considered as a major area that may be affected by EMI emissions. Many PE converters utilized in smart grids are operated by relying on mains communication systems (MCS) [J1]. Moreover, the PE converters' injected noise into the power grid may extremely distort MCS operational signals. Thus, limit the maximum EMI peak under the standard level is a great important factor conditioning the appropriate design of systems based upon PE. MCS, in particular, is a smart meter measuring the supply/demand of electric power energy. This is mandatory in smart grids, and the related importance is only highlighted due to supply-side and/or demand-side management requirements. Additionally, regarding Fig. 1.2, most MCSs are operated purposefully for communication within a given frequency range (2-150 kHz); however, PE converters produce unintentional emissions. Extensive penetrations of PE converters and MCSs because of their state-of-the-art technology within this frequency range is regarded as the main logic behind the critical importance of this frequency range. For example, converters used for energy conversion and management of photovoltaics (PVs)[2], electric vehicles (EVs) on-board chargers [3], and laptop/PC chargers [4] have an operating frequency in between 2 – 150 kHz.

***Table 1-1**: IEC standard and report classification for 2-150 kHz frequency range.*

Standard's number	**Standard's name**	**Publication date**
IEC TR 61000-3-10 ED1 [5]	Emission limits in the frequency range 2- 9 kHz [5]	2023*
IEC 61000-6-3 [6]	Electromagnetic compatibility (EMC)- Generic standards - Emission standard for equipment in residential environments [6]	2020
IEC 61000-2-2 [7]	EMC-Environment - Compatibility levels for low-frequency conducted disturbances and signalling in public low-voltage power supply systems [7]	2002
IEC 61000-2-4 [8]	EMC -Environment - Compatibility levels in industrial plants for low-frequency conducted disturbances [8]	2002, 2023*

* The standard group is working on it, it will be published in the future.

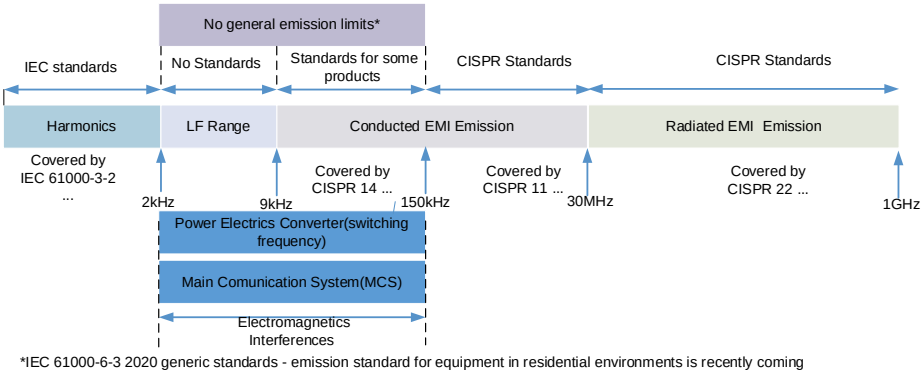

***Fig. 1.2**: The classification of IEC standard frequency ranges for the harmonics and different EMI types for the electric power system [C1, J1].*

Additionally, a number of noise emission interferences have been recently reported for various PE converters within this frequency range [5, 6]. The mutually operating groups in IEC SC77A/CISPR, NASI, and CIGRE standard committees are currently working on defining the limits of the emissions below 150 kHz [7-10]. Table 1-1 provides the view for the IEC standard and report classification for 2-150 kHz frequency range from emission and compatibility perspective view [6].

Generally, to reach an ensured electromagnetic compatibility (EMC) of PE systems, the produced noise emissions need to be limited for observing the available international standards. As depicted in Fig. 1.2, the frequencies below 2 kHz and above 150 kHz are in the standard ranges; but, there is no generally-accepted standards for the noise emissions within 2−150 kHz except for unique products [12]. The given EMI standardization gap in the frequency range between 2 – 150 kHz results in challenging interferences created by PE converters [1], [10], [12, 13]. Even though many research works have been recently reported on measuring/observing the interference issues, there are no obligatory perceptions of noise emissions and mitigation and their impacts within the 2−150 kHz frequency range. Thus, it is required for a systematic technique to model multi-parallel converters and evaluate their interactions, such as their frequency behavior and the influences on the electric power grid.

1.1.2. Conducted EMI Modeling in Power Electronic

Due to the presence of inherent pulsed energy conversion in PE converters, EMI appears within a broad frequency range, and the created unintentional emissions may partially/entirely interfere with the operation of the other grid-connected PE devices. As discussed earlier, there has been no reported EMI analytical model in the new frequency range regarding the lack of general standards. It is required to find the EMI

analytical model to hasten the understanding and analysis of the converter's frequency behavior. It would be more effective to find EMI mitigation techniques to limit EMI based on the standard requirements. It would also be essential in the multi-converter systems analysis in which many converters are connected via a common point. So far, EMI analysis and/or modeling have been investigated within frequencies above 150 kHz. For example, in [14– 16], PE converters' modeling within high frequencies was applied to assess EMI emissions based upon Thevenin/Norton equivalent circuit models. A number of EMI filters, including DM filter, CM, and CM+DM filters, have been already suggested for frequencies above 150 kHz [10], [17– 19] with regard to recommended standard limits[20– 22]. Most of the modeling approaches focusing on EMI analysis within frequencies above 150 kHz are based on simulations. All of the suggested techniques suffer from higher complexity due to existing parasites caused mainly by components and PCB layout. Thus, all techniques that are appropriate for high-frequency modeling of EMI (that is >150 kHz) may be employed for estimation of the EMI within frequencies under 150 kHz at the cost of higher complexity and computation time.

Accordingly, just a few simulation/experimental-based reports are available in the literature focusing on EMI issues within the frequencies below 150 kHz [1], [5, 6], [15], [23, 24]. Therefore, this thesis aims to propose an analytic modeling technique for noise in DM EMI propagating within this frequency. The proposed model is extended considering the analysis within the time-frequency domain; therefore, demonstrating the PE converter's behavior which leverages its switching function as the major source of noise and the related closed-loop impedance for EMI estimations as shown in Fig. 1.3. The majority of modeling approaches employed for high-frequency modeling of EMI are based on computer simulation model and semi-experimental model because of complex behavior of various parts/components and the reliance of EMI behavior on PE converter design. As a result, the parasitic effect model is not designed in the current thesis as long as their impacts are trivial [J1]. This thesis aims to propose an appropriate order-reduction technique within low-frequency ranges regarding PE converters having various topologies and modulations.

Additionally, only some analytical approaches are appropriate for differential-mode noise, as in [28] mentioned as a "conventional approach" in this thesis. According to the comparative investigations, it has been revealed that the traditional methodology is only appropriate for designing/sizing the EMI filter because it only forecasts the emission's first peak with acceptable accuracy. Furthermore, within the frequency range of interest, the DM noise is more important than CM noise because of small parasitic capacitor limiting the EMI level subjected to standards [J1], [8– 10], which is acceptable in most applications except in a few particular cases, including motor drives [29]. More importantly, besides modeling PE converters according to CISPR standards [24], EMI measurements must be carried out with an EMI receiver and line impedance stabilization network (LISN). Thus, the equivalent model of the circuit for LISN and EMI receiver must also be obtained for modeling the EMI emissions. The LISN presents a fixed impedance, decouples PE converters and power grids within high frequencies, and repeats measurements when conducted emission tests.

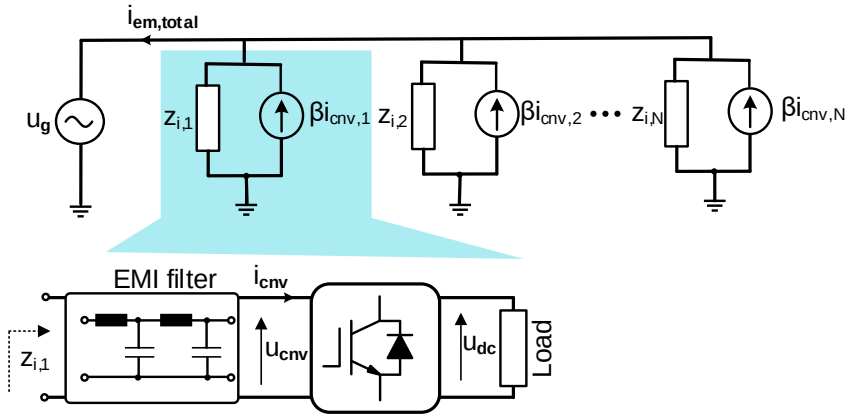

***Fig. 1.3**: The extension of developed power converter equivalent circuit model for interleaved/multi-converter modeling.*

In Fig. 1.3, the general Norton equivalent circuit model of the interleaved/multi-converter with EMI filter [J1]. PFC can be a sample for interleaved as the synchronized scenario. For EMI analysis investigation, the noise signal is derived by carrying out computer simulations of the converter with a LISN and then transferring to the frequency domain [12], [30], time-domain [31] as well as time/frequency domain [9], [26], [32]. Measurements related to voltage noise are transferred via Fourier analysis to the frequency/domain with an EMI receiver and a LISN. Regarding reports in the literature, the frequency domain process usually is faster than that its time-domain counterpart. In this thesis, the low-frequency EMI emissions related to PE-based systems via the closed-loop impedance modeling are defined within frequencies up to 150 kHz. This model is developed for both single-phase and three-phase PE converters. PFC converters have been extensively utilized in most PE applications as they obey Total harmonic distortion (THD) standards and improve power factor with acceptable energy efficiency [33]. Thus, an analytic model of a PFC converter is suggested in this thesis. It is also broadly agreed that the voltage source inverter (VSI) is in place for PE applications because of its simplicity, higher efficiency, and broad availability [34]. Hence, a single-phase inverter is selected as the second case study to analyze and achieve the analytical model. In the next step, a reduced-order model is characterized to employ the model in aggregation units.

1.1.3. Mitigation Strategies and Multi Converter System Based Analysis

As discussed earlier, developing a proper equivalent circuit model for power converters is an important stage in frequency behavior analysis and, consequently, addresses EMI issues [C1]. Thus, the prevention of noise emission through the power grid is one of the main objectives of this thesis. More importantly, finding appropriate mitigation techniques is considered as one of the main challenges in the new frequency range. One technique to reduce low-frequency emissions of EMI is the

application of passive EMI filters. Fig. 1.3 depicts an EMI filter in a grid-connected PE converter. Numerous EMI filters have been proposed in the literature for frequencies above 150 kHz [17– 19]. As such, a minimized EMI filter has been carried out for a 3-phase 3-level T-type PWM converter system. Additionally, a summary of the systematic approach for an optimized volume for a 2-stage DM and CM EMI filter was presented for a 10-kW power converter within the frequency range above 150 kHz [19]. In [35], different techniques were reported for an enhanced low-frequency duty of CM EMI filters, such as an improved equivalent parallel capacitance (EPC) and equivalent series inductance (ESL) for a CM EMI filter. In most research works, an EMI filter was suggested for a frequency range within 150 kHz– 30 MHz.

Notably, only a number of the reported works were carried out within the frequency range of 2–150 kHz. Solving the EMI emission issue only by utilizing an EMI filter within 9–150 kHz) has led to an increased EMI filter size; thus, the active mitigation technique was utilized to prevent the increased size of EMI filters[15]. Most of the references are on designing the EMI filter within a frequency above 150 kHz. However, in [15], the design of an EMI filter under 150 kHz has been reported. Further, the Fig. 1.4 is shown the considered emission limits following CISPR 15 based on QP (Quasi Peak).

Another approach to reducing the EMI emissions without significant changes in the size of an EMI filter was proposed to alter noise emission spectra. There are two techniques to propagate the noise energy over the spectra, including a variable frequency and randomized schemes. The reduced EMI for DC/DC PE converters via the randomized PWM application and neglecting an EMI filter was studied in [33, 34]. Further, compared to the PWM, [36, 37] details a study of the impacts of 4 various randomized modulation schemes, including the random pulse position modulation (RPPM), the random pulse-width modulation (RPWM), and the random carrier-frequency modulation with a fixed duty cycle (RCFMFD) or random carrier-frequency modulation with a variable duty cycle (RCFMVD) on conductive EMI for the DC/DC synchronous rectifier. In the last step, the RPWM and RCFMFD create a minimized low-frequency harmonic, and thus they are proper for DC-DC converters [36]. The frequency dithering is considered as a spectral-shaping technique to reduce an EMI emission. The effective period dithering technique operates by varying the PWM signal frequency driving the PE inverter switches for an EMI reduction in a single-phase DC/AC [38].

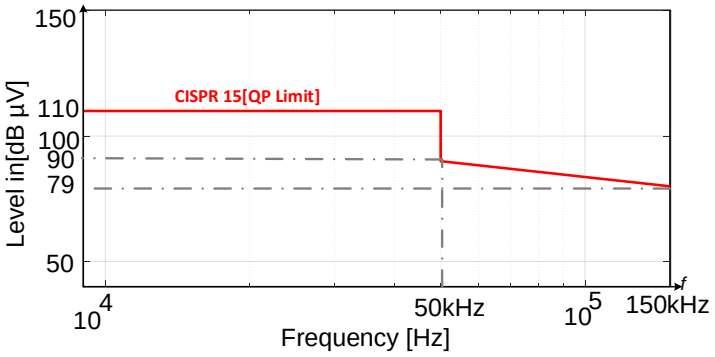

Fig. 1.4: *Considered emission limits following CISPR 15 based on QP (Quasi Peak*) [C2].

Further, the phase impact of this signal for EMI reduction was referred to [38]. In [39] the EMI level reduction in the buck converter utilizing the variable frequency is described. The triangular profile along with a high-frequency switching imposes a maximally reduced EMI spectrum; the experimental verification of the technique proposed for the buck converter. Besides, the variable spectral-shaping of a reduced EMI for high-frequency ballasts and inverters was investigated in [40]. Topologically, interleaving power converters can effectively decrease the input ripple current and DM EMI noise magnitude, leading to a smaller DM filter size [41].

By employing the obtained models, the interactions among various PE converters and their impacts on low-frequency EMI are considered as the main gap in this research field studied in this thesis. Thus, the application of PE converter models can accelerate the design processes, avoid timely trial/error processes, experimental measurements, decrease costs, and investigate large-scale systems. This is important when dealing with electric power distribution networks to which numerous PE converters are connected in a parallel fashion [C1]. The interaction among such devices becomes of interest with numerous devices connected at the same point, such as a lighting installation, a computer center, etc. When devices are launched by the same manufacturer and the same type, the situation is further complicated due to minor switching frequency variations [42]. Therefore, the factory tolerances of switching frequency for the same power converter lead to the beating in the parallel operation.

Fig. 1.3 illustrates the several units like boost PFC which are connected to the common point. There are some reports and measurement data in the low frequency range related to the units' interactions and beating effects [39– 41]. For example, [42] details a simple model to explain the high-frequency current flow through various devices and power grids. The model is also employed to demonstrate the aggregation among devices considering slight frequency differences. In addition, several measurements have been carried out on an entire-scale electric power model of an

individual house to investigate the equipment emissions and impedances under 9–95 kHz in [44]. Most equipment creates a remarkably lower impedance route than the grid itself. Based on the results, the conducted disturbances concerning this frequency range mainly propagate through the individual devices rather than both the devices and the electric power grid. Moreover, it is demonstrated that the input impedance related to the equipment may be large time-dependent when the time-scale is less than a power system frequency cycle. Hence, it is required to propose a model that can achieve the interaction current among units and aggregated EMI model.

1.2. Project Motivation

As discussed above, various challenges still exist and need to be addressed to increase the penetration level of PE converters. Recent literature and various ongoing standardization activities over the frequency range of 2-150 kHz demonstrate the significant analysis of EMI emissions for PWM converters. Interestingly, the importance of these frequency ranges as new frequency ranges are shown based on Table 1-1. 2-150 kHz is one of the critical frequency areas, which is a high number of the PE converters and MCS are operated. Hence, generated noise from the PE converter may seriously deteriorate MCS communication signals [J1]. The overall project motivation can be further divided into five sub-questions:

1) There is no report regarding general standards covering the frequency of 2-150 kHz. Hence, there is a lack of systematic perception of the noise emission through power grids within the mentioned frequency range [J1]. As a result, in order to get a better understanding of the PE converter's frequency behavior, an appropriate modeling methodology should be available to effectively estimate DM EMI noise levels in single or three-phase power converter.

2) Select an appropriate EMI mitigation technique like designing suitable DM EMI filters to comply with the standard recommendations. More importantly, the unavailability of general standards for the frequency of 9-150 kHz has resulted in the unavailability of PE converters characteristic models within this frequency range.

3) Therefore, proposing such a model may help characterize the influencing parameters employed to reduce the model in a multi-converters system analysis. Additionally, in order to achieve a reduced EMI model within the frequency range of 2-150 kHz, it is required to define important parameters to decrease the order and complexity of the model [J1]. On the other hand, the main sources of DM and CM noise of PE converters in PE-based systems should be determined. A noise emission model should be provided for each source in 1-phase and 3-phase PE converters with simulations.

4) Numerous simulation modeling techniques have already been suggested; however, the analytical modeling technique is highly demanding to enhance the computational time and modify it at the multi-converters system analysis.

5) There exists no idea or analysis for the multi-units system analysis to which many converters are connected via a common point. Thus, extending aggregated models for multi-parallel PE converters considering single-unit and multi-unit modes

are modeled and then verified via computer simulations and the obtained experimental results. This model should cover the interaction between various units and the power grid as well as LISN.
The overall study exercises in this Ph.D. project are graphically summarized in Fig. 1.5.

1.3. Research Questions and Objectives

This thesis aims to comprehensively address EMI emissions by power converters within the newly proposed frequency range of 2–150 kHz. For this purpose, the main question is

how to model and limit the low-frequency EMI emission of power converters to the electric power grids to comply with the existing standards?

Accordingly, the project assumptions are as follows: accurate DM EMI noise models are mandatory for single-phase and three-phase converters as well as aggregation multi-units, selection of the proper EMI mitigation strategies on the basis of active/passive spectral shaping techniques. Thus, solving the question mentioned above is highly facilitated. The overall question can be further divided into three sub-questions:

1) How to characterize DM noise and closed-loop input impedance for a single-phase converter within this novel frequency range?
2) How to extend the analytical equivalent circuit model in a three-phase grid-tied application?
3) Is it possible to develop aggregated analytical models for multi-parallel PE converters and choose the best EMI mitigation technique?

Based on the aforementioned research questions, three sub-objectives are defined:

1) **Develop a DM EMI emission model for the PE-based systems via a closed-loop impedance and switching function modeling for a single-phase boost PFC and VSI.**
   To better understand PE converter's frequency behavior, an appropriate modeling technique is required to estimate DM EMI noise levels and design suitable DM EMI filters to obey the standards [J1]. Further, the unavailability of typical standards for the frequency of 2–150 kHz has resulted in a lack of characteristic models for PE converters within this frequency range. Thus, the performance of the suggested time-frequency domain approach is validated experimentally through a single-phase grid-tied boost PFC and VSI.

2) **Derive and extend the DM EMI analytical model for a three-phase power converter, including the active rectifier and VSI, limiting the noise level based on the standard requirements.**

The low-frequency EMI emissions related to PE-based systems via a closed-loop impedance modeling are defined up to a frequency of 150 kHz for three-phase power converters. Furthermore, an analytical formulation between the input LISN current and the EMI receiver branch and the analytical formulation between various EMI receiver parts have been computed. A three-phase AC/DC grid-tied converter prototype and VSI are employed to confirm the suggested EMI modeling technique.

3) **Achieved reduced-order model for the single and three-phase converter to decrease time-consuming and complexity in the multi converter noise analysis and investigation.**
By employing this model, one can define the influencing parameters utilized to simplify the suggested model at the multi-converter systems study. To get a simplified EMI model within the frequency of 2-150 kHz, it is crucial to determine salient parameters to decrease the model order and complexity [J1]. Hence, it speeds up the analysis in the multi-converter system.

4) **Designed an appropriate passive EMI filter to limit the noise based on the standard specification.**
EMI filter is one of the noise mitigation techniques which is design based on the passive component, including capacitor and inductors. The performance of designed filters is validated by boost PFC in different switching frequencies with simulation and experimental results.

5) **The analysis of the interaction between the units and developed the aggregated analytical models for multi-converter systems.**
The developed models are aggregated to emulate the behavior of the multiple parallel grid-tied converters. Multi-parallel single-phase PE converters are illustrated in Fig. 1.3. Additionally, the interactions fulfilled among various PE converters and the corresponding impacts on low-frequency EMI, are studied utilizing the developed models in synchronized and unsynchronized scenarios. The EMI mitigation techniques on the basis of active and/or passive spectrum-

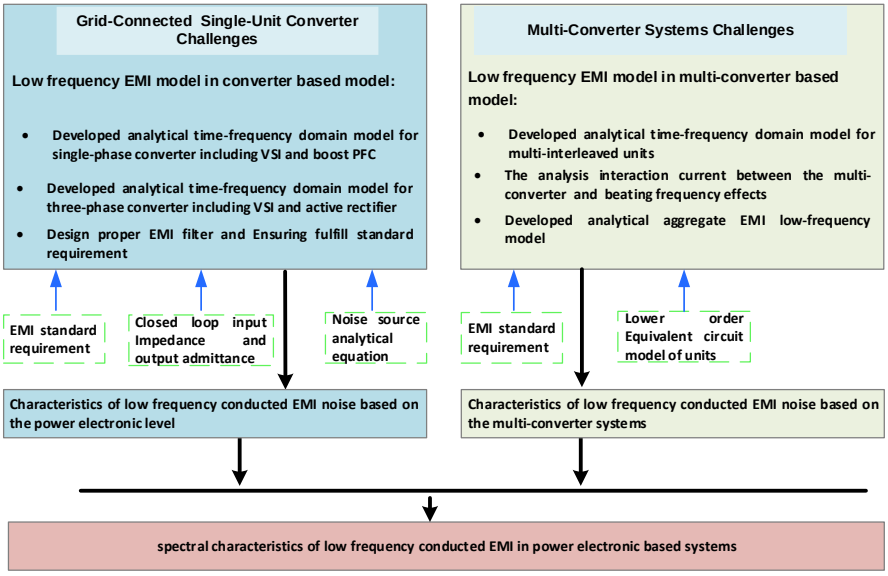

***Fig. 1.5**: Study activities in the Ph.D. outline: develop the analytical EMI model in a PE-based system.*

shaping techniques are extended, and their impact and adequacy at the multi-converter systems with numerous converters are analyzed. The suggested time-frequency domain approach's performance is verified experimentally with a single-phase interleaved boost PFC and multi-unit PV application.

1.4. Limitations

The Ph.D. project has the following limitations:

- The impact of parasitic components is neglected. The DM noise within the new frequency range is more important than CM noise because the parasitic capacitor's size is smaller for the former, limiting the EMI level subjected to standard criteria. This is verified in most applications except for a few special practices such as motor drives. Based on the assumptions above, the suggested analytical modeling technique is confirmed for the frequency of 2−150 kHz and is extended for higher frequencies if the impacts of parasites related to devices/components are considered. The majority of modeling approaches employed for high-frequency EMI modeling techniques are based on computer simulations and semi-experimental models due to the complicated behavior of various components and the EMI behavior's dependency on PE converter design [J1]. Thus, the parasitic impacts are not

considered for modeling purposes in this thesis because the related quantity is trivial.

- The analytical EMI model depends on the modulation technique, impedance /admittance, and power converter configuration. Hence the model can not cover the converter black-box due to the no access to the factory design's data.
- Grid impedance variation effect and grid abnormalities are neglected. Moreover, unsymmetrical effects in the three-phase converter operations are neglected.
- There are several converter topologies in single-phase and three-phase with different modulation. Due to the dependency of the proposed technique on the given topology and modulation, modeling all types of grid-connected converters is not possible in this work. Hence, the more common type of single-phase for boost PFC and VSI (with both bipolar and unipolar modulations) and three-phase for rectifier and VSI are selected for analysis and modeling.

1.5. Thesis Outline

The Ph.D. project outcomes are documented in this Ph.D. thesis, constituting of two main parts: report and selected publications. The report summarizes the research works conducted at the time of the Ph.D study, and partial research outcomes are included in the selected publications. The thesis frame is depicted in Fig. 1.6, suggesting a linking guideline between the report and the selected literature.

The report part is organized into five distinct chapters. Finally, the concluding remarks, major contributions, and suggested future research are summed up in Chapter 5. Chapter 1 details the Ph.D. thesis introduction in the research background, and then the project objectives are discussed. The next two chapters deal with the EMI modeling and analysis of the studied grid-tied topology using an equivalent circuit modeling. Chapter 2 is on characterizing the low-frequency EMI emissions by PE-based systems through closed-loop impedance modeling within the frequency range up to 150 kHz. Analytical EMI level estimation of boost PFC systems is discussed in detail. The estimation accuracy performance is confirmed via experiments. Comprehensive comparisons with the prior-art estimation techniques are carried out. An EMI passive mitigation technique, including the EMI filter, is employed to limit the EMI noise level based on the recommended standard requirements. In Chapter 3, the model is extended for three-phase grid-tied PE converters comprising of rectifier and inverter. A proper EMI filter is design for the three-phase active rectifier to limit noise level. In Chapter 4, Firstly, EMI analytical model is extended to multi-interleaved units by the phase shift impacts. Moreover, phase shift impacts at EMI filter design are investigated. The obtained results are verified via simulations and experiments. Secondly, the developed models are aggregated to emulate the behavior of multiple parallel grid-tied converters. Additionally, the interactions among different PE converters and their impacts on low-frequency EMI in the synchronize and unsynchronized scenarios, as the main research gap in this field, are detailed

utilizing the developed models.Notably, the aggregated EMI model is achieved for multi-converter systems. In the end, concluding remarks and main contributions of this Ph.D. thesis are summed up in Chapter 5. Future research perspectives/directions are also described in the final chapter.

1.6. List of Publications

The research outcomes during the Ph.D. study are published in journal papers and conference proceedings listed below. Furthermore, these papers are partly used in the Ph.D. thesis shown in Fig. 1.6.

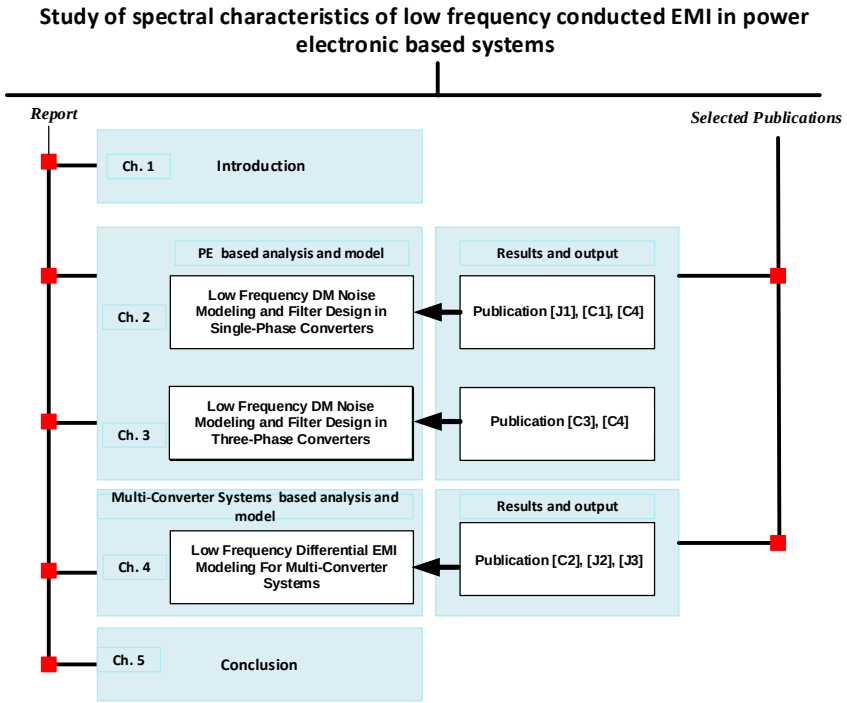

***Fig. 1.6**: Thesis framework and related key articles of each part.*

Publications in Refereed Journals

J1. **N. N. Esfetanaj**, H. Wang, F. Blaabjerg and P. Davari, " Differential mode noise prediction and analysis in single-phase boost PFC for the new frequency range of 9- 150 kHz," *IEEE Journal of Emerging and Selected Topics in Industrial Electronics (Early Access)*, 2021, doi: 10.1109/JESTIE.2021.3066320.

J2. **N. N. Esfetanaj**, H. Wang, F. Blaabjerg and P. Davari, " Differential Mode Noise Estimation and Filter Design for Interleaved Boost Power Factor Correction Converters," *Journal of Applied Sciences,2021*, https://doi.org/10.3390/app11062716.

J3. **N. N. Esfetanaj**, J. Meyer, H. Wang, F. Blaabjerg and P. Davari, " Developed aggregated EMI models and analysis for converters in the frequency range of 2- 150 kHz," *Journal of power electronics,2021*.

Publications in Refereed Conferences

C1. **N. N. Esfetanaj**, S. Peyghami, H. Wang and P. Davari, "Analytical Modeling of 9-150 kHz EMI in Single-Phase PFC Converter," IECON 2019 - 45th Annual Conference of the IEEE Industrial Electronics Society, Lisbon, Portugal, 2019, pp. 4689-4693, doi: 10.1109/IECON.2019.8927705.

C2. **N. N. Esfetanaj**, Y. Saad, O. A. Sakaria, H. Wang and P. Davari, "Differential Model EMI Filter Analysis for Interleaved Boost PFC Converters Considering Optimal Phase Shifting," *2020 22nd European Conference on Power Electronics and Applications (EPE'20 ECCE Europe)*, Lyon, France, 2020, pp. P.1-P.10, doi: 10.23919/EPE20ECCEEurope43536.2020.9215730.

C3. **N. N. Esfetanaj**, Y. Peng, H. Wang, F. Blaabjerg and P. Davari, "Analytical Modeling of 9-150 kHz EMI in Three-Phase Active Rectifiers," 2020 IEEE 21st Workshop on Control and Modeling for Power Electronics (COMPEL), Aalborg, Denmark, 2020, pp. 1-6, doi: 10.1109/COMPEL49091.2020.9265727.

C4. **N. N. Esfetanaj**, J. Meyer, H. Wang, F. Blaabjerg and P. Davari, " Differential mode noise prediction and analysis in single and three-phase grid-tied inverters for the frequency range of 9-150 kHz," *2021 23nd European Conference on Power Electronics and Applications (EPE'21 ECCE Europe), Ghent, Belgium, 2021*

Chapter 2. Low Frequency DM Noise Modeling and Filter Design in Single-Phase Converters

2.1. Introduction

PFC converters have been widely utilized in most PE applications due to their high-power factor and low current total harmonic distortion (THD) [33], [45, 46]. Moreover, VSI is more prevalent in many photovoltaic (PV) applications because it provides many benefits such as simplified control, flexibility in operation, and the possibility of connecting to the grid [47– 50]. Thus, analytical models for PFC and VSI converters are suggested in this Chapter. As discussed before, the EMI noise is generated due to the power converter's switching, and it is creating challenges for many communication systems which transmit data in the frequency range of 2-150 kHz. Recent EMI noise reports in the references show EMI noise should be further investigated on the new frequency range of 2 – 150 kHz [51–54]. For instance, in [55] the effect of EMI noise causing measurement error of smart meters (i.e., 45%) in the new frequency range of 2-150 kHz is reported. Lack of a general standard for emission level and lack of in-depth analysis of power converter frequency behavior lead to no theoretical basis to cover the EMI noise model and limit noise level based on the new standard requirement [23], [25], [56]. Hence, there is a need for developing a model to analyze and estimate the noise emission within the frequency range of interest. The suggested model is constituted based on time-frequency domain analysis; thus, presenting the behavior of a PE converter that employs its switching function as the major source of noise and the closed-loop impedance / admittance for EMI estimations [J1]. An analytical simplified-order DM EMI model is constructed within the frequency range of 2-150 kHz according to the following assumptions:

- The impacts of parasitic components are neglected.
- Rise and fall times related to switching waveforms may be neglected [J1].

In this Chapter, a suitable model order-reduction technique for the low-frequency emission ranges is proposed. The developed model can be adjusted by considering selected power converter topologies and modulation methods. The proposed technique estimates the generated emissions of the PE converter within the frequency range of 9–150 kHz by utilizing double Fourier analysis and closed-loop impedance. Although the primary goal of the developed modeling technique is to characterize the power converter emission, the estimated emission level is used for proper EMI filter design resulting in damping the emission levels below the selected standard limit within the 9-150 kHz frequency range. Notably, the conventional simplified EMI analytical technique for filter sizing [28] is utilized for comparison purposes when the

proposed technique is employed to highlight the proposed technique's accuracy and appropriateness for filter design [J1].

It is demonstrated that the suggested technique is able to simplify the estimation of all DM noises within the frequency range of 9 - 150 kHz through double Fourier analysis. Moreover, the sampling frequency and partial power impacts on input impedance are studied [J1]. Further experiments considering the EMI filter were also presented in this thesis.

2.2. Control and Parameter Selection

2.2.1. Single-Phase Boost PFC

This section focuses on the design and control of single-phase boost PFC. It is known that continuous conduction mode (CCM)[57], [58] has a lower current ripple compared to the other operation modes (Discontinuous current mode (DCM) [59], Quasi-conduction mode (QCM)[60], etc.) in boost PFC. Thus, a relatively large boost inductor is required in CCM that also reduces high frequency (HF) ripple, leading to a smaller EMI filter [61]. Fig. 2.1 shows the block diagram of a PFC converter. As it can be seen to implement CCM operation, the control block diagram is based on a double-loop control strategy. The outer loop regulates the DC-link voltage while providing reference current for the inner current control loop resulting in a sinusoidal input current waveform. As mentioned earlier in the prior section, the current control is traditionally leveraged in a single-phase PFC (CCM operation) [57]. The block diagram related to one of the systems studied, comprising the power stage related to a boost PFC, control block diagram, EMI, receiver LISN, and EMI filter is presented in Fig. 2.1. To select the needed inductor value, firstly, the inductor value should be more than that of (2-1). This amount guarantees the converter operation in CCM. Secondly, the inductance is decided based on the maximized peak-to-peak current ripple, $\Delta i_{L,max}$. The maximum current ripple happens once $u_{rec} = u_{dc/2}$ (that is, D=0.5) [57], [62]:

$$L = \frac{u_{dc}}{4 f_{sw} \Delta i_{L,\max}} \tag{2-1}$$

where $\Delta i_{L,max}$ is set regarding the average inductor current value once the maximum current ripples occur $I_{L,avg}(D=0.5)$ using the ripple factor k_{ripple} [63]:

$$\Delta i_{L,\max} = k_{ripple} . I_{L,avg(D=0.5)} \tag{2-2}$$

where k_{ripple} is typically selected in the range of 20% to 40% in CCM [62], $i_{L,avg}$ is the mean inductor current. Additionally, the mean current controller based on PI was employed. The voltage control loop regulates the output voltage by comparing the measured output voltage (u_{dc}), with the output voltage of interest (u_{dc}^*). Table 2-1 provides the applied system specifications.

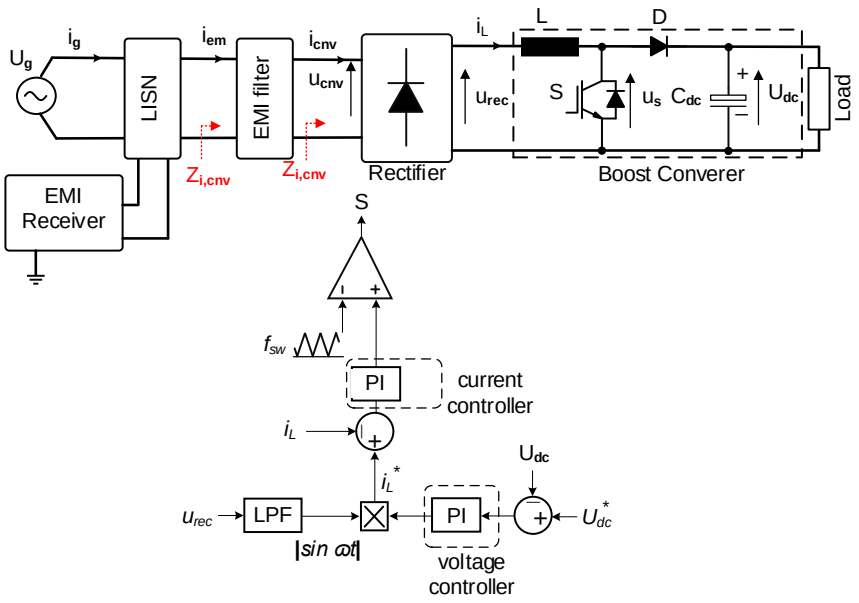

Fig. 2.1: *Block-diagram of a 1-phase boost PFC converter comprising of control block-diagram, EMI receiver, LISN, and EMI filter [J1].*

Table 2-1*: Studied case system specifications [J1],[C1]*

Symbol	Definition	Value	Unit
U_g	Grid side's voltage	230	*Vrms*
f_g	Frequency of the grid	50	*Hz*
L	Boost inductor	2,1	*mH*
f_{sw}	Frequency of switching	20,25,40	*kHz*
C_{dc}	Output capacitor	500	μF
U_{dc}	DC voltage	400	*V*
P_o	Power	1	*kW*

2.2.2. Single-Phase VSI

This subsection presents the next topology, which is considered for EMI modeling and investigation. Further, the PI controller is constituted of an inductor current as of the internal loop, and the output voltage as the external feedback loop. Thus, the external control loop of a DC-link voltage bandwidth must be limited between 1/50

and 1/10 related to the current control loop. For this case, a bandwidth of 100 Hz (10 times slower than the internal current control loop) is considered. Fig. 2.2 illustrates the diagram of a 1-phase inverter, including the current control scheme, where I_g denotes the inductor current's rated RMS value for the fundamental component, U_g denotes the RMS quantity of the grid voltage, λ_{v_Lf} is roughly fixed to 5%. Practically, λ_{c_Lf} is regulated as 20-30%. In the subsequent step, the inverter-side inductor within the bipolar single-phase inverter is obtained by (2-3)

$$\frac{U_{dc}T_{sw}}{2\lambda_{c\_Lf}I_g} \le L_f \le \frac{\lambda_{v\_Lf}U_g}{\omega_g I_g} \tag{2-3}$$

where, T_{sw} is switching period. Moreover, to select an appropriate value for the inductor in converter side for unipolar single-phase converter, L_f is calculated by (2-4)

$$L_f = \frac{U_{dc}T_{sw}}{8\lambda_{c\_Lf}I_g} \tag{2-4}$$

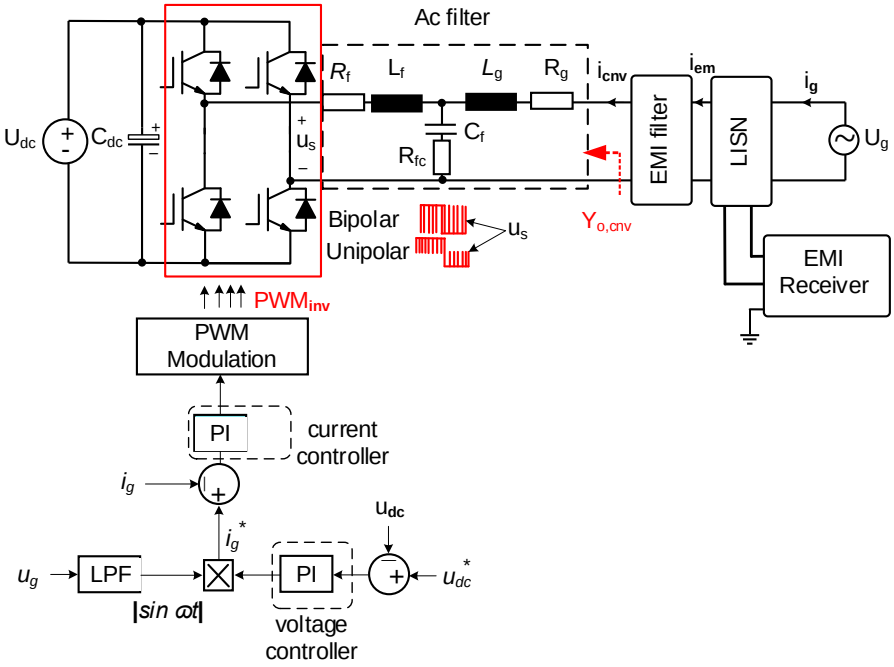

***Fig. 2.2**: Single-phase structure of grid-tied inverter including the control block diagram [C4].*

The filter capacitor leads to the production of reactive power. Thus, λ_C is defined as the ratio of the injected reactive power by capacitor related to a filter to the output active power related to the grid-connected converter [C3]. Thus, the highest value of the filter capacitance is formulated by (2-5) as [64]

$$C_f = \lambda_C \frac{P_o}{\omega_g U_g^2} \tag{2-5}$$

where *Po* is the active power output, U_g is the grid voltage. Damping resistance is achieved from (2-6) [C3]

$$R_{fc} = \frac{1}{3\omega_r C_f} \rightarrow (\omega_r = \sqrt{\frac{L_g + L_f}{L_f L_g C_f}}) \tag{2-6}$$

Further, the grid-side inductor is obtained by (2-7)

$$L_g = \frac{1}{L_g C_f \omega_h^2 - 1}(L_f + \frac{|u_s(j\omega_h)|}{\omega_h \lambda_h I_2}) \tag{2-7}$$

where ω_h denotes the angular frequency, *h* denotes the order of harmonics, $u_s(j\omega_h)$ and I_2 denote the RMS ratings of an inverter bridge voltage and the grid current, respectively. If a single-phase bipolar inverter, and single-phase unipolar inverter are utilized, $u_s(j\omega_h)$ are given in (2-19) and (2-20), respectively. For h>35, λ_h is chosen as 0.3 as recommended in [64]. Table 2-2 provides the applied system specification for single phase VSI.

2.3. Proposed Time-Frequency Domain EMI Model

This section describes the proposed modeling technique principle and its concept based on the Norton equivalent circuit model having the closed-loop impedance / admittance and the noise source [C3]. Fig. 2.3 exemplifies the equivalent circuit model of a PFC converter shown in Fig. 2.1.

Table 2-2: VSI case studies specification [C4], [C1].

Symbol	Definition	1-ph bipolar	1-ph unipolar	Unit
U_g	Grid side voltage	230	230	*Vrms*
f_g	Frequency of the grid	50	50	*Hz*
f_{sw}	Frequency of switching	20	20	*kHz*
C_{dc}	Output capacitor	1.5	1.5	*µF*
U_{dc}	Output voltage	360	360	*V*
P_o	Power	3	3	*kW*
L_f	Inductor of the converter side	2.5	0.6	*mH*
L_g	Inductor of grid side	250	20	*µH*
R_{fc}	Damping resistor	8	8	Ω
C_f	Reactive capacitor	8	8	*µF*
λ_{v_Lf}	Ripple factor of the voltage	5	-	*%*
λ_{c_Lf}	Ripple factor of the current	30	30	*%*
λ_C	Reactive power	5	5	*%*
λ_h	Factor of the harmonic	0.3	0.3	-

2.3.1. DM EMI Noise Source Model

In this subsection, the differential noise sources are modeled for single-phase boost PFC and VSI. The modeling principle is based on developing corresponding switching functions following double Fourier series analysis.

2.3.1.1 Single Phase Boost PFC

It is clear that switching is one of the main reasons behind DM noise sources considered a challenge in grid-connected PE systems. Thus, as the primary goal of

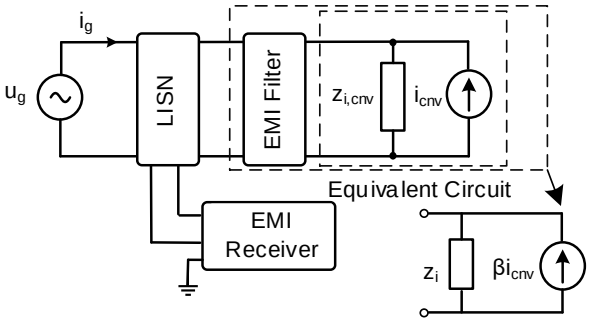

***Fig. 2.3**: Norton equivalent circuit for the reduced boost PFC converter including EMI filter [J1].*

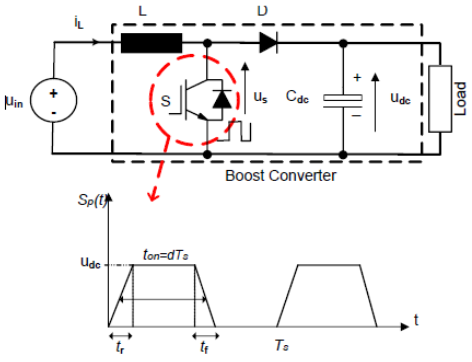

***Fig. 2.4**: Voltage waveform applied to power switch in a boost converter [J1]*

this subsection, it is tried to model DM noise voltage applied across the power switch depicted in Fig. 2.4 to analyze frequency behavior and design EMI filter related DM noise. In the frequency domain, the coefficients of the Fourier series are obtained by (2-8) assuming the ($t_r = t_f$) [65].

$$S_p(f) = 2U_{dc}d\frac{\sin(n'\pi ft_{on})}{n'\pi ft_{on}}\frac{\sin(n'\pi ft_r)}{n'\pi ft_r} \tag{2-8}$$

where U_{dc} denotes voltage amplitude, d denotes the duty cycle, n' denotes the order of harmonics, t_{on} denotes the pulse-width, f denotes system frequency, t_r denotes rise time [65]. The frequency spectrum of the aforementioned voltage with trapezoidal and ideal waveform applied to a power switch is illustrated in Fig. 2.4. As seen, the 2nd corner frequency depends on the rise and/or fall times. Therefore, to understand how the rise or fall times influence the EMI noise under 150 kHz, the transition time needs to be more than 2.15 µs [J1]. As the PE switches work fast, this transition time is not

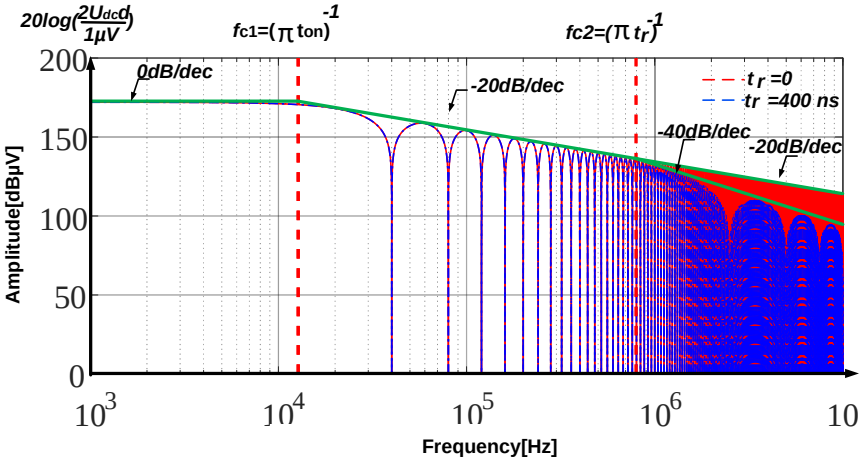

Fig. 2.5: *Frequency spectrum of the trapezoidal and ideal pulse voltage applied to a power switch, (U_{dc} =400, f_{sw} = 20 kHz, t_r = t_f = 400 ns, d = 0.5)[J1].*

generally fulfilled. An ideal pulse waveform in this thesis is considered operating on frequencies below 150 kHz. So, the related Fourier series can be represented by (2-9)

$$S_p(f) = 2U_{dc}d\frac{\sin(n'\pi ft_{on})}{n'\pi ft_{on}} \tag{2-9}$$

Mostly in grid-connected applications, including boost power factor correction (PFC), the duty cycle is not fixed since different modulation strategies are utilized. To assess the impact of modulation, a time-domain modeling technique is suggested in [28] to get the input noise current of the related converter. In this thesis, a double Fourier analysis is employed to model the effect of the modulation strategy. The modulation technique applied under CCM operation is considered to develop the switching function related to the voltage across the power switch (See Fig. 2.6)) [J1]. Hence, the voltage in the frequency domain employed across the PE switch is formulated in (2-10) [J1].

$$\begin{aligned} u_s(t) &= \frac{a_{00}}{2} + \sum_{n=1}^{\infty}[a_{0n}\cos(n\omega_g t) + b_{0n}\sin(n\omega_g t)] \\ &+ \sum_{m=1}^{\infty}[a_{m0}\cos(m\omega_{sw}t) + b_{m0}\sin(m\omega_{sw}t)] \\ &+ \sum_{m=1}^{\infty}\sum_{\substack{n=-\infty \\ n\neq 0}}^{\infty} a_{mn}\cos(\left[m\omega_{sw} + n\omega_g\right]t) + b_{mn}\sin(\left[m\omega_{sw} + n\omega_g\right]t) \end{aligned} \tag{2-10}$$

where ω_{sw} and ω_g denote fundamental frequency and carrier angular frequency, respectively; a_{0n}, b_{0n}, a_{m0}, b_{m0}, a_{mn}, and b_{mn} denote the Fourier coefficients computed through the double Fourier series of the employed voltage; *m* and *n* are the carrier and baseband indices, respectively; both appeared as integer multiples of the fundamental component [J1], [66]. Thus, (2-11) are expressed as

$$a_{mn} + jb_{mn} = \frac{1}{2\pi^2}\int_{-\pi}^{+\pi}\int_{-\pi.M.|\cos(y)|}^{\pi.M.|\cos(y)|} U_{dc} e^{j(m.x+ny)} dxdy \tag{2-11}$$

where U_{dc} denotes the dc voltage output, and *M* denotes the modulation index given by (2-12)

$$M = \frac{U_g}{U_{dc}} \tag{2-12}$$

For simplicity, rising or falling time effects in-between 2-150 kHz are neglected considering (2-8) and (2-9). Thus, the pulse voltage across the power switch is simplified to an ideal pulse having a variable duty cycle. Accordingly, the rising or falling time effects are omitted from (2-11) , and the Fourier coefficients are recalculated. Considering the modulation scheme depicted in, the integral domain of double Fourier is defined. The selected values for the index variables *m* and *n* are evaluated by (2-11) and considering the integer multiples and fundamental Frequency of modulation. Thus, the dc component is obtained with regard to $m = n = 0$ put in (2-11) [J1] as

$$a_{00} + jb_{00} = \frac{a_{00}}{2} = \frac{2MU_{dc}}{\pi} \tag{2-13}$$

So, baseband and fundamental harmonics are achieved through putting $m = 0$ into (2-11) as

$$a_{0n} + jb_{0n} = \frac{MU_{dc}}{\pi}(-ni + 2e^{\frac{n\pi i}{2}} + ine^{n\pi i})\frac{-e^{-n\pi i}(1+e^{n\pi i})}{n^2-1} \tag{2-14}$$

Further, carrier harmonics are obtained by putting $n = 0$ into (2-11) [J1] as

$$a_{m0} + jb_{m0} = \frac{8U_{dc}}{\pi^2}\frac{1}{m}\sum_{\substack{k=1\\k=odd}}^{\infty}\frac{J_k(m\pi M)}{k} \tag{2-15}$$

Then, by considering the index variables as $m \neq 0$, $n \neq 0$ in (2-11), sideband harmonics are determined for each side of the main carrier harmonics as [J1]

$$a_{mn} + jb_{mn} = \frac{2U_{dc}}{\pi^2}\frac{1}{jm}\times\sum_{k=1}^{\infty} J_k(m\pi M)(j^k - j^{-k})\left(\frac{(\sin(\frac{k-n}{2})\pi)}{k-n} + \frac{(\sin(\frac{k+n}{2})\pi)}{k+n}\right) \tag{2-16}$$

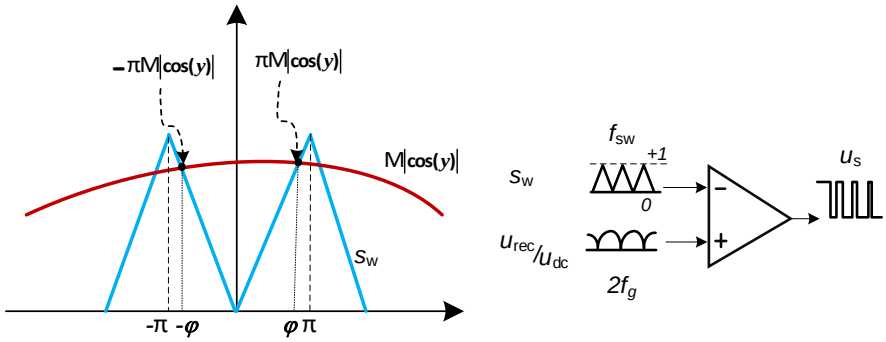

***Fig. 2.6**: Modulation scheme of single-phase boost PFC presented in **Fig. 2.1** under CCM operation [J1]*

Next, the frequency spectrum related to the noise source is achieved considering (2-14) -(2-16). Hence, u_s is updated considering the full-bridge diode rectifier impact to get the noise source at the input side of the converter. Thus, Fourier frequency analysis related to the full-bridge rectifier is fulfilled regarding a square waveform signal of the switching function [J1]. Moreover, the frequency spectrum related to a full-bridge diode rectifier is given by

$$u_{fd}(t) = \sum_{\substack{h=1 \\ h=odd}}^{\infty} \frac{2}{h\pi} \sin(\frac{h.\pi}{2}) \cos(\omega_g h t) \tag{2-17}$$

Thus following (2-16), the Thevenin voltage (or Norton current) modeled as the noise voltage source shown in Fig. 2.3 is given by (2-18)

$$u_{cnv}(t) = u_{fd}(t) u_s(t) \tag{2-18}$$

Finally, once the converter closed-loop input impedance is achieved, the Norton current can be obtained.

2.3.1.2 Single-Phase VSI

The noise source model of VSI can be obtained based on the same principle applied to the PFC converter using double Fourier analysis illustrated in (2-9). Notably, for a VSI, line-to-neutral voltage is modeled (denoted as u_s in Fig. 2.2). Further details on expanding the frequency-domain function are elaborated in [66, 67]. Regarding single-phase VSI, two modulation types are commonly considered (See Fig. 2.2). As illustrated in Fig. 2.2, u_s only operates in two voltage levels denoted by $+U_{dc}$ and, $-U_{dc}$ bipolar SPWM. The frequency-domain function related to the noise considering bipolar modulation with Fourier coefficients is expressed by (2-19) as

$$u_s = MU_{dc}\sin\omega_g t + \frac{4u_{dc}}{\pi}\sum_{m=1,3,5,..}^{\infty}\sum_{n=\pm1,\pm3,...}^{\infty}\frac{J_n(mM\pi/2)}{m}\sin\frac{m\pi}{2}e^{jm\theta}\cos(m\omega_{sw}t+n\omega_g t)+.. \quad (2\text{-}19)$$
$$..+\frac{4u_{dc}}{\pi}\sum_{m=2,4,6,..}^{\infty}\sum_{n=\pm1,\pm3,...}^{\infty}\frac{J_n(mM\pi/2)}{m}\cos\frac{m\pi}{2}e^{jm\theta}\sin(m\omega_{sw}t+n\omega_g t)$$

where $J_n(x)$ denotes the first type Bessel function, U_{dc} is the output dc voltage. In (2-19), the first term denotes the fundamental term, the second one denotes the sideband harmonics expanded over odd-multiples related to the carrier frequency, and the third one represents the sideband harmonics expanded over even-multiples related to the carrier frequency. As already defined by the second and third terms, '*m*' and '*n*' denote the carrier and baseband indices, respectively. Evidently, '*m*' and '*n*' also define the harmonics distribution. Fig. 2.7. (a) depicts the frequency behavior related to a noise source model based on (2-19) , and accordingly, simulations are carried out in PLECS. As seen in Fig. 2.7. (a), DM noise source model estimates the DM peak noise with high accuracy by simulations. In addition, the DM noise behavior is illustrated for a 1-phase VSI having the unipolar modulation. It should be noted that the unipolar SPWM has three levels for $u_{s,}$ including + U_{dc}, - U_{dc}, as well as zero. And, the frequency domain function related to a noise source with unipolar modulation taking into account the Fourier coefficients is expanded by (2-20) [C4]

$$u_s = -MU_{dc}\sin\omega_g t + \frac{4u_{dc}}{\pi}\sum_{m=2,4,6,..}^{\infty}\sum_{n=\pm1,\pm3,...}^{\infty}\frac{J_n(mM\pi/2)}{m}\cos\frac{m\pi}{2}e^{jm\theta}\sin(m\omega_{sw}t+n\omega_g t) \quad (2\text{-}20)$$

Comparing (2-19) and (2-20) reveals that only the even-numbered hamonic orders available for the unipolar modulation; by contrast, odd- and even-order harmonics available for the bipolar modulation. The estimated noise model, along with computer simulations, is depicted in Fig. 2.7 (b)**.**

2.3.2. Closed Loop Input Impedance and Output Admittance

2.3.2.1 Input Impedance of Single-Phase Boost PFC

In this section, it is attempted to model the closed-loop input impedance of PFC converter. Interested readers are invited to read more details on the modeling of closed-loop input impedance and the corresponding frequency behavior in [68]. The closed-loop block diagram of a single-phase boost PFC converter is illustrated in Fig. 2.8. Since the focus of this thesis is on frequencies below 150 kHz, it is not required to consider the high-frequency behavior impact of the layout and the related components [J1]. Now, the closed-loop impedance is modeled based on a large signal model through (2-21)

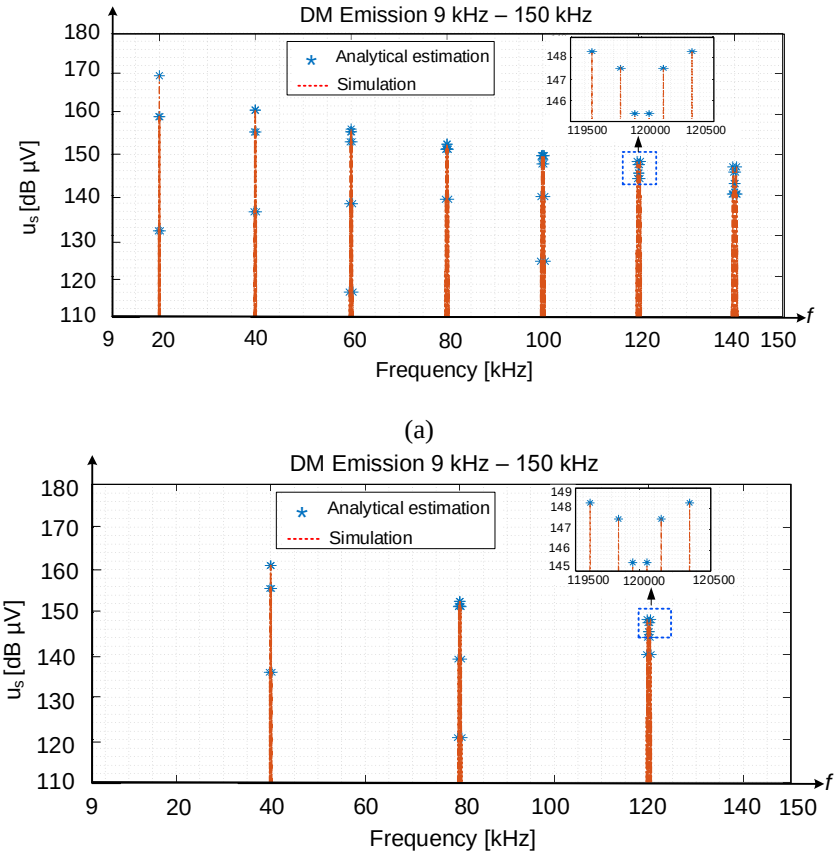

Fig. 2.7: *Frequency spectrum of the noise source model: (a) single-phase VSI with bipolar modulation, (b) single-phase VSI with unipolar modulation. system specification is based on Table 2-2 [C4].*

$$Z_{i,cnv}(s)=\frac{u_{cnv}(s)}{i_{cnv}(s)}=\frac{sL+\dfrac{R_s}{u_{mo}}\left(U_{dc}G_{ci}(s)\right)}{1+\dfrac{1}{u_{mo}}\left(gU_{dc}G_{ci}(s)\right)} \tag{2-21}$$

where u_{mo} denotes PWM signal's peak-to-peak amplitude, and g stands for a fixed value (obtained by $g = p_g/U_g^2$ with p_g and U_g (i.e., the input power and input voltage), respectively). Additionally, it is required to integrate a low-pass filter into current reference to ensure system stability for total operating conditions [68] while zero-crossing distortion is suppressed [69]. The impact of a low-pass filter on current reference is not marginal at high-frequency range and, thus, must be employed on the

input impedance model [J1], [68]. Hence, i_{ref} illustrated in Fig. 2.8 is substituted by $i_{ref} = g.Q./u_{cnv}/.$ As a result, the transfer function related to the low-pass filter is formulated by:

$$Q(s) \approx \frac{1}{1+\frac{s}{\omega_z}} \tag{2-22}$$

It is worthnoting that the control parameters are a function of the related bandwidth. And, as the bandwidth is commonly constrained up to 9 kHz, they can be simply neglected. Thus, the input impedance can be achieved by(2-23)[J1]

$$Z_{i,cnv}(s) = \frac{sL + \frac{R_s}{u_{mo}}\left(U_{dc}G_{ci}(s)\right)}{1+\frac{1}{u_{mo}}\left(g\,Q(s)U_{dc}\,G_{ci}(s)\right)} \approx sL \tag{2-23}$$

Fig. 2.9 depicts the low-pass filter impacts on closed-loop input impedance behavior. The low-pass filter leads the impedance behavior to match the boost inductor characteristics for higher frequency ranges [J1]. That is appropriate for the frequency range of interest (i.e., 9 – 150 kHz). To assess the microcontroller sampling impact on the obtained model, its transfer function, G_d is given by (2-24). So, the transfer function should be put into the closed-loop impedance model.

$$G_d = e^{-sT_d}, (T_d = 1.5T_{sw}/k, k = T_{sw}/T_s) \tag{2-24}$$

where T_{sw}, T_s, and T_d denote switching time, sampling time, and time delay in the control loop, respectively; k denotes the ratio of switching time to sampling time. Thus, the closed-loop impedance model with regard to sampling time can be given by (2-25)[J1]

$$Z_{i,cnv} = \frac{u_{cnv}(s)}{i_{cnv}(s)} = \frac{sL + \frac{R_s}{u_{mo}}\left(U_{dc}G_d(s)G_{ci}(s)\right)}{1+\frac{1}{u_{mo}}\left(gQ(s)U_{dc}G_{ci}(s)G_d(s)\right)} \approx sL \tag{2-25}$$

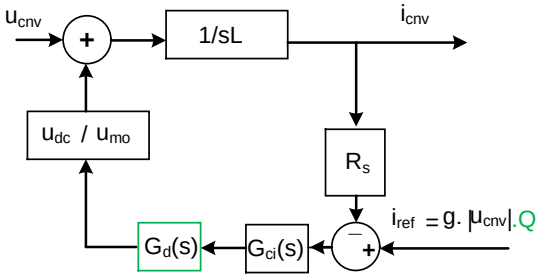

***Fig. 2.8**: Block diagram of input current dynamics related to single-phase boost PFC converter [J1].*

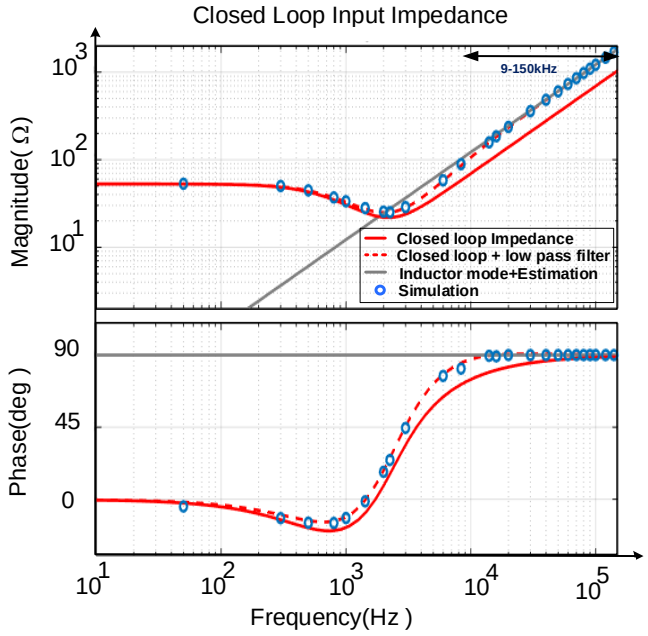

***Fig. 2.9**: Closed-loop impedance behavior considering the impact of low-pass filter against boost inductor model and simulation results [J1].*

Concerning the above equation, when $f > 9$ kHz, then $Z_{i,cnv}(s)$ is roughly sL. Fig. 2.10 shows the behavior of a closed-loop input impedance regarding the impacts of sampling task and low-pass filter in the model depicted in Fig. 2.8 [J1]. Further, the impedance model regarding sampling frequency of $2f_{sw}$ and $5f_{sw}$ with compensating low-pass filter ($Q(s)$) is shown in Fig. 2.9. The closed-loop is verified via simulation results (by PLECS) when the low-pass filter and sampling frequency of $2f_{sw}$ are taken into account.

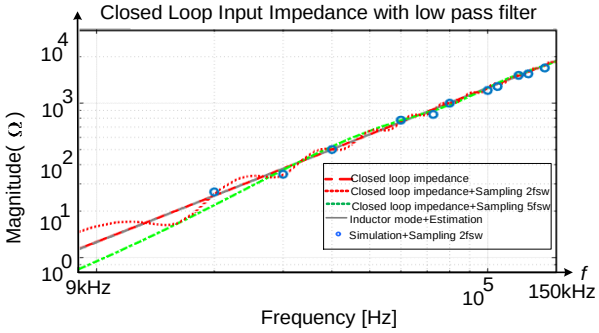

Fig. 2.10: *Closed-loop impedance behavior on the basis of a simplified boost inductor model given by sampling frequencies of $2f_{sw}$ and $5f_{sw}$ [J1].*

This would increase the estimation error on the EMI levels. Thus, Fig. 2.11 shows the simulated low-frequency EMI by considering the sampling frequency for a case study regarding the frequency equal to 10 kHz. As shown in this figure, the obtained error difference between these two simulation cases is raised to 1.8 dB. As a result, the sampling transfer function must be considered in the input impedance modeling process if the selected sampling frequency is less than 20 kHz [J1]. In the next step, the impact of output power variations on the input impedance is studied. Thus, considering (2-21), the impedance depends upon the rating power with *g* and can be modified in the operation mode of the converter. But, as depicted in Fig. 2.12, loading conditions may be ignored in the impedance behavior when operated above controller bandwidth (i.e., > 9 kHz). Thus, the input impedance is estimated only by the inductor impedance within the frequency of 9-150 kHz, which is commonly higher than the current controller bandwidth [J1] (see Fig. 2.9, Fig. 2.10 and Fig. 2.12).

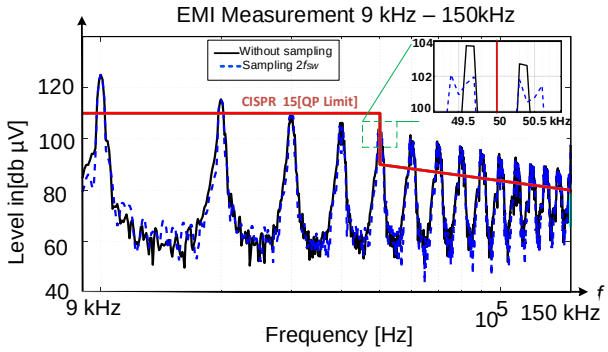

Fig. 2.11*: EMI simulation with frequency in between 9 kHz - 150 kHz with regard to the sampling transfer function($2f_{sw}$)and f_{sw}=10 kHz [J1].*

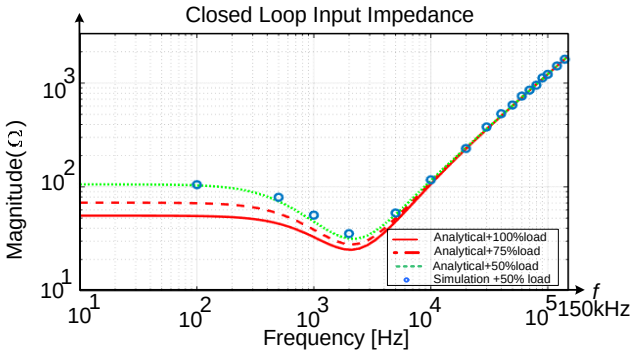

Fig. 2.12: *The impact of output power level on closed-loop impedance behavior[J1].*

2.3.2.2 Output Admittance Single-Phase Inverter

The single-phase grid-tied VSI with a current control is depicted in Fig. 2.13.(a). For modeling the output admittance of inverter, the mean switching model is utilized as depicted in Fig. 2.13.(b). In addition, there are a filter and/or a current controller (G_c) within the control loop, and a time delay caused by the computations and pulse-width modulation (G_d). The gain of a modulator, K_{PWM}, is determined by (2-26):

$$G_c(s)=K,\ G_d(s)=e^{-1.5T_s s},K_{PWM}=1 \tag{2-26}$$

where K is the current controller's proportional gain, T_s is the inverter's sampling time [70]. The input-output relationships of the filter considering Fig. 2.2 and ignoring the parasitic resistances related to the passive components is obtained by:

$$Y_O(s)=\frac{-i_g}{u_g}\bigg|u_s=0=\frac{L_fC_fs^2+R_{fc}C_fs+1}{s(L_fC_fL_gs^2+R_{fc}C_f(L_g+L_f)s+(L_g+L_f))} \tag{2-27}$$

$$Y_M(s)=\frac{i_g}{u_s}\bigg|u_g=0=\frac{R_{fc}C_fs+1}{s(L_fC_fL_gs^2+R_{fc}C_f(L_g+L_f)s+(L_g+L_f))} \tag{2-28}$$

In the end, the VSI's output closed-loop admittance is as (2-29):

$$Y_C(s)=\frac{i_g}{u_g}\bigg|i_g^*=0=\frac{Y_O(s)}{1+G_c(s)G_d(s)Y_M(s)} \tag{2-29}$$

where, i_g denotes the grid current; u_g and u_s and are the grid and modulator voltage, respectively. Hence, Y_O is an open-loop admittance of VSI. Thus, the output

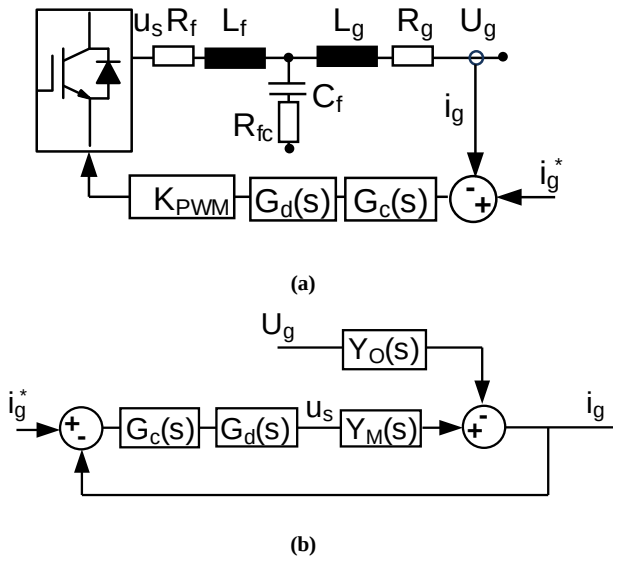

Fig. 2.13*: (a) Single-phase LCL-filtered inverter including grid current control (b) mean switching model of the grid inverter [C4].*

admittance is verified by applying numerous sinusoidal perturbations and, then, checking its impacts on the given variable. Next, a Fourier analysis is carried out to get the amplitude/phase of the frequency of the sinusoidal perturbations. Fig. 2.14 depicts the behavior of an output 1-phase admittance for single-phase grid-tied by (2-29) and simulation results by PLECS (that is, switching model).

2.3.3. Norton current model

2.3.3.1 Boost PFC

Equivalent Norton current modeled as a noise source is obtained from the equivalent Thevenin voltage divided further by a closed-loop input impedance as:

$$i_{cnv} = \frac{u_{cnv}}{Z_{i,cnv}} \tag{2-30}$$

The equivalent Norton circuit model for a single-phase boost PFC converter is depicted in Fig. 2.3 by a Norton current source and a closed-loop input impedance. Moreover, The EMI filter for noise level constraint must be coupled with the Norton model [J1].

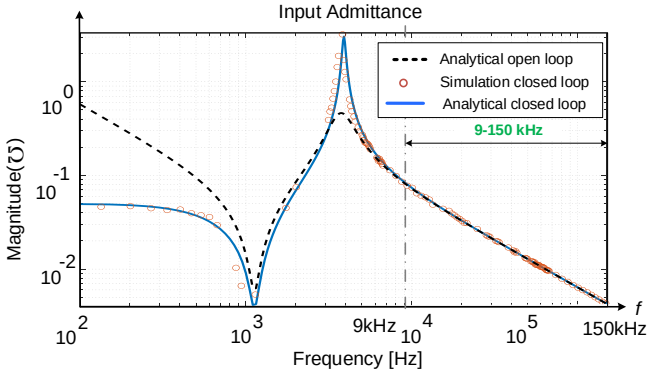

Fig. 2.14: *Single-phase illustrations of the output closed-loop admittance behavior including the magnitude and phase of a single-phase grid-tied inverter and simulation results by PLECS[C4].*

2.3.3.2 VSI

Finally, the model for an output noise source is reformulated through the voltage division in the LCL filter via (2-31):

$$u_s' = u_s . \frac{1/Y_{Cf}(s)}{1/Y_{Cf}(s) + 1/Y_{Lf}(s)} \tag{2-31}$$

Hence, the Norton current is obtained by (2-32)

$$i_{cnv} = Y_C u_s' \tag{2-32}$$

where Y_{Cf} and Y_{Lf} denote the amount of capacitor and converter-side inductor admittance related to an LCL filter.

2.4. Inclusion of EMI Filter in the Power Converter DM EMI Model

The structure of an EMI filter is illustrated in Fig. 2.15. The equivalent circuit, including the EMI filter, is modified via the Middlebrook extra-element theory [71]. In this section, an equivalent circuit model including EMI filters and a converter is presented to simplify the low-frequency EMI model [J1]. Thus, firstly, the boost PFC converter's closed-loop input impedance is considered as an extra component

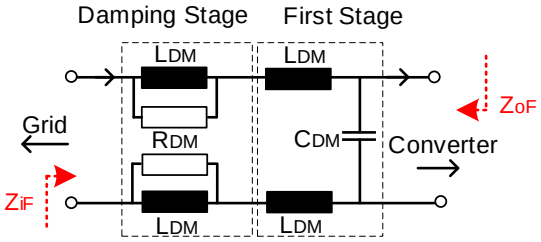

***Fig. 2.15**: Block diagram of a single stage DM EMI filter with a parallel RL damping stage [J1].*

connected to the EMI filter's secondary point. Therefore, the new input impedance obtained at the grid-side having an EMI filter is obtained by (2-33)

$$Z_i = Z_{iF} \cdot \frac{1 + \dfrac{Z_{oFo}}{Z_{i,cnv}}}{1 + \dfrac{Z_{oF\infty}}{Z_{i,cnv}}} \tag{2-33}$$

where, Z_{iF} denotes the EMI filter input impedance with output port open. It is given by (2-34)

$$Z_{iF}(s) = Z_{C_{DM}}(s) + 2(Z_{L_{DM}} + \frac{R_{DM}.Z_{L_{DM}}(s)}{R_{DM} + Z_{L_{DM}}(s)}) \tag{2-34}$$

The readers are referred to [J1] for more detail's information. Z_{oFo} is the EMI filter output impedance with input port shorted, which is obtained as

$$Z_{oFo}(s) = 2(Z_{L_{DM}}(s) + \frac{R_{DM}.Z_{L_{DM}}(s)}{R_{DM} + Z_{L_{DM}}(s)}) \| Z_{C_{DM}}(s) \tag{2-35}$$

Next, $Z_{oF\infty}$ is the EMI filter output impedance with input port open, which is determined as

$$Z_{oF\infty} = Z_{C_{DM}}(s) \tag{2-36}$$

Fig. 2.16 depicts a closed-loop impedance model with / without an EMI filter. Additionally, simulation results validate Middlebrook output. In the next step, a modified Norton current having an EMI filter must be evaluated. The relationship between Norton current in conditions without/ with of EMI filter is obtained by (2-37) [J1],

$$\frac{i_{em}(s)}{i_{cnv}(s)} = \beta \tag{2-37}$$

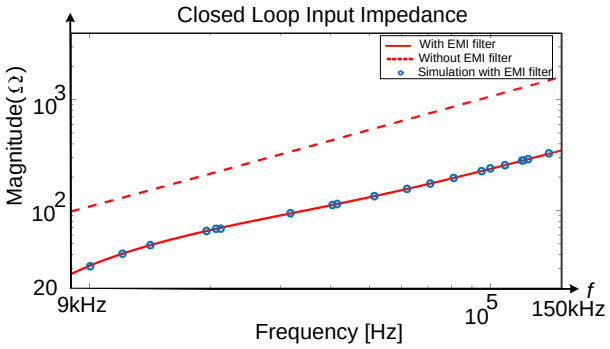

***Fig. 2.16**: Closed-loop input impedance model with/without EMI filter[J1].*

where i_{cnv} denotes Norton current neglecting the EMI filter, i_{em} denotes Norton current with EMI filter, and β is calculated by (2-37). The relationship between EMI filter input current and Norton current is obtained by (2-38)[J1]

$$\frac{i_1(s)}{i_{cnv}(s)} = \frac{Z_{i,cnv}(s)}{Z_{i,cnv}(s) + Z_{oFo}(s)} \tag{2-38}$$

So, the relationship between the input and output currents related to an EMI filter is obtained by (2-39)

$$\frac{i_{em}(s)}{i_1(s)} = \frac{Z_{C_{DM}}(s)}{2(Z_{L_{DM}}(s) + \frac{R_{DM}.Z_{L_{DM}}(s)}{R_{DM} + Z_{L_{DM}}(s)}) + Z_{C_{DM}}(s)} \tag{2-39}$$

where i_{em} denoted final Norton current that is determined by substituting (2-38) and (2-39) into (2-37)

$$\beta = \frac{Z_{C_{DM}}(s)}{2(Z_{L_{DM}}(s) + \frac{R_{DM}.Z_{L_{DM}}(s)}{R_{DM} + Z_{L_{DM}}(s)}) + z_{C_{DM}}(s)} \cdot \frac{Z_{i,cnv}(s)}{Z_{i,cnv}(s) + Z_{oFo}(s)} \tag{2-40}$$

where β denotes the relationship between Norton current in conditions without/ with the EMI filter. In the end, the equivalent circuit model with an EMI filter, depicted in Fig. 2.3, is available to investigate the EMI model [J1].

2.5. Differential EMI Filter Designing Procedure

Here, the process of designing an EMI filter is investigated. The main goal is to design an appropriate filter that can limit the recommended EMI standard level. It should be noted that an EMI filter's performance depends upon its passive components, including capacitors and inductors[J1]. The general prototype of a single-stage EMI filter is depicted in Fig. 2.15. So, the leakage inductance of a CM choke, i.e., L_{DM}, is

commonly utilized to realize frequencies above 150 kHz that are recommended frequency standards in the practical design of an EMI filter [72]. The CM choke leakage inductance may not be sufficient to eliminate the noise emissions below 150 kHz. So, an extra DM inductor should be designed for DM filter to mitigate frequencies below 150 kHz. Additionally, the filter design depends upon the filter attenuation requirements, Att_{req}. This is obtained by investigating the detected QP voltage (U_{max}) within the CISPR QP limits represented by (2-41)[J1]

$$A_{tt_{req}}(f)[dB] = U_{\max}(f)[dB\mu V] - CISPR_{\lim it}(f)[dB\mu V] + M\arg in[dB] \quad (2\text{-}41)$$

where Att_{req} denotes the noise value that must be damped by filters, U_{max} denotes the highest value of the spectrum obtained from the suggested analytical model; $CISPR_{limit}$ is obtained from the standards [20– 22]. Furthermore, 6 dB margin is considered to cover the component tolerances and parameter shifts caused by degradation. But, for a 1-stage EMI filter size of inductor and capacitor is calculated by (2-42) [J1]

$$A_{tt}(f_{sweep}) \geq \frac{2L^2_{DM}C_{DM}(j2\pi f)^3 + 4L_{DM}R_{DM}C_{DM}(j2\pi f)^2 + L_{DM}(j2\pi f) + R_{DM}}{R_{DM} + L_{DM}(j2\pi f)} \quad (2\text{-}42)$$
$$= A_{tt_{EMI\_Filter}(f_{sweep})}$$

2.6. EMI receiver and LISN Modeling

Regarding CISPR 16 standard [11], LISN is put in between the power converter and the grid (See Fig. 2.1) [J1]. LISN guarantees the measurement reproducibility, fixes the impedance of the EMI receiver, and decouples the under-test equipment from the grid. In addition, the EMI receiver is connected to LISN due to measurement noise level. More details on EMI receiver and LISN are reported in [J1]. As already explained, Norton noise current flows into the LISN, and then the EMI receiver is able to get noise emission measurements as a voltage signal [C1]. Thus, the EMI receiver and LISN model have to be integrated into the analytic models to estimate the EMI noise level. Fig. 2.17.(b) depicts the transfer function between EMI receiver voltage and LISN input current. It should be mentioned that the transfer function must be integrated in analytical form into the proposed technique. Moreover, the relation between the input current's LISN and EMI receiver branch regarding the EMI filter is expressed by (2-43) [J1]

$$i_{rec} = \frac{C}{D} i_{em} \quad (2\text{-}43)$$

where C and D are determined by (2-44) and (2-45), respectively.

$$C = L_1L_2C_1C_2s^4 + R_2C_1C_2(L_2 + L_1)s^3 + C_1(L_2 + L_1)s^2 \quad (2\text{-}44)$$

$$D = C_1C_2(R_2L_1 + L_2L_1)s^4 + C_1C_2(L_2R_1 + L_2)s^3 + (L_1C_1 + L_2C_2 + L_2C_1 + R_1R_2C_2C_1)s^2 + (R_1C_1 + R_2C_2)s + 1 \quad (2\text{-}45)$$

Here, i_{cnv} is employed instead of i_{em} in (2-43) for measuring the EMI level having no EMI filter. Further, the voltage noise of an EMI receiver is represented by

$$U_{meas} = R_1 i_{rec} \quad (2\text{-}46)$$

The bandwidth of an EMI receiver filter must be set to 200 Hz with regard to CISPR 16 standard for Band A. In addition, a fourth-order Butterworth filter is applied to model this filter, and the EMI is defined by sweeping the RBW filter within the frequency of Band A. By employing the EMI peak measurements [J1], the EMI receiver model is obtained by (2-47) [C1, 28]

$$U_{\max}[dB\mu V] = 20\log[1/\mu V \sum_{f=MB-\frac{BW}{2}}^{f=MB+\frac{BW}{2}} U_{meas}(f)\cdot RBW(f)] \quad (2\text{-}47)$$

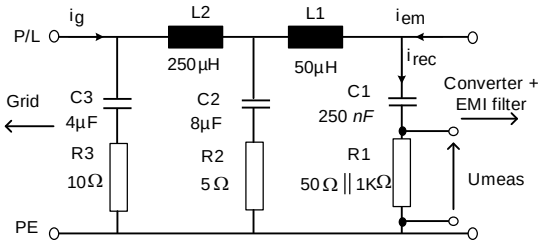

(a)

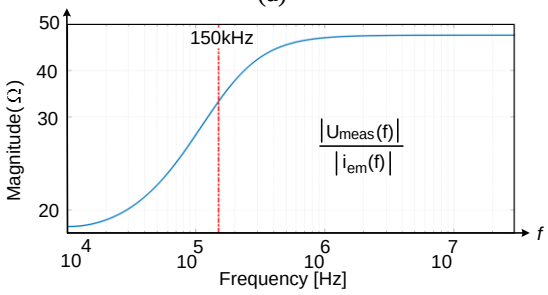

(b)

***Fig. 2.17**. LISN recommended by CISPR for Band A: a) per-phase circuit diagram, b) per-phase DM mode transfer function [C1],[J1].*

2.7. Results

In this step, more simulation and experimental validation are presented to show the accuracy and efficiency of the proposed techniques.

2.7.1. Boost PFC Case Study

A single-phase boost PFC converter having one stage DM EMI filter was considered to validate the proposed modeling approach. In order to assess the effectiveness of the proposed modeling technique, a traditional analytical technique explained in [J1] is considered for a comparative analysis. The switching model runs in PLECS. The employed sampling frequency for simulations and experimental results is set to 100 kHz. Notably, the boost inductor is sized for both case studies with frequencies of f_{sw} = 20 kHz, 25 kHz, and 40 kHz in a way to guarantee the CCM operation of the converter. Two simulation cases are studied to verify PFC rectifier's EMI measurement of 9–150 kHz within various switching frequencies. For assessing the analytical time-frequency domain estimation, simulation results representing the converter's real switching model are obtained in PLECS. Thus, besides two case studies with various switching frequencies, DM noise estimation is studied without/ with EMI filter impact. Fig. 2.18 depicts DM noise's comparative results for a single-phase boost PFC working at f_{sw} = 20 kHz and having no EMI filter [J1]. The results obtained by the proposed analytical technique demonstrate an appropriate agreement with experimental results; however, the conventional technique gets a reasonable estimation only for the first peak. This implies that the traditional analytical technique is effective for a filter design and not proper for the converter characterization within the complete frequency ranges in between 9–150 kHz [J1]. The suggested analytical model entirely matches the experimental ones, and, thus, the highest error value in the frequency of 9–150 kHz is under the 1.8 dB, 1.25 dB, and 1.7 dB for case studies with switching frequencies 20, 25, 40 kHz without EMI filter. Further details regarding comparing the different methods can be founded on the [J1], [C1]. Even though the conventional technique has a lower error for the first peak, which is sufficient for designing an EMI filter, the error raises extremely after the first peak. Fig. 2.18 shows that the estimated and measured levels of the noise breaches the standard limits of CISPR 15. Thus, the EMI filter is devised by following and with regard to the recommended standards, i.e., CISPR 15. Table 2-3 presents the parameters of a DM filter computed for both frequencies. Fig. 2.19 shows the comparative results obtained by the suggested approach when f_{sw} = 20 kHz. The designed EMI filter properly damps the noise level under the standard limits. The suggested analytical model good compatibility the experimental ones and, thus, the highest error value in the frequency of 9–150 kHz is under the 1.8 dB and 1.7 dB for case studies with switching frequencies 20, 40 kHz with EMI filter. The test setup for Boost PFC converter is depicted in the Fig. 2.20.

***Table 2-3**: Specifications of 1-stage EMI filter and 1-stages damping [J1].*

f_{sw}	C_{DM}	R_{DM}	L_{DM}
20 kHz	1.7 µF	22 Ω	180 µH
40 kHz	1.3 µF	22 Ω	180 µH

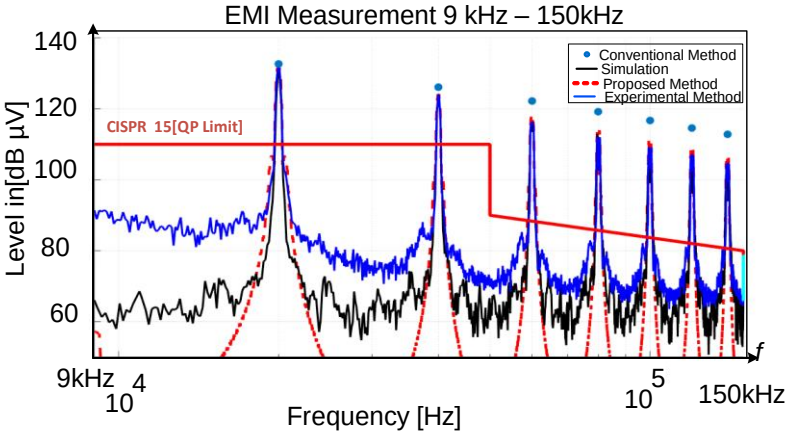

***Fig. 2.18 :** DM noise results for 1-phase boost PFC regarding f_{sw} = 20 kHz without EMI filter [J1].*

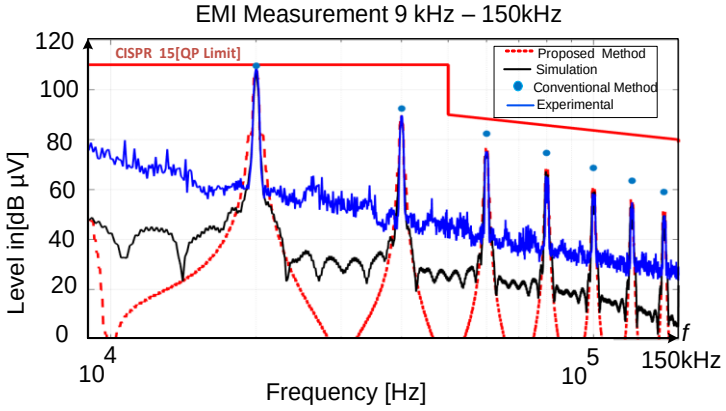

***Fig. 2.19:** The DM noise results for a 1-phase boost PFC with f_{sw} = 20 kHz and EMI filter [J1].*

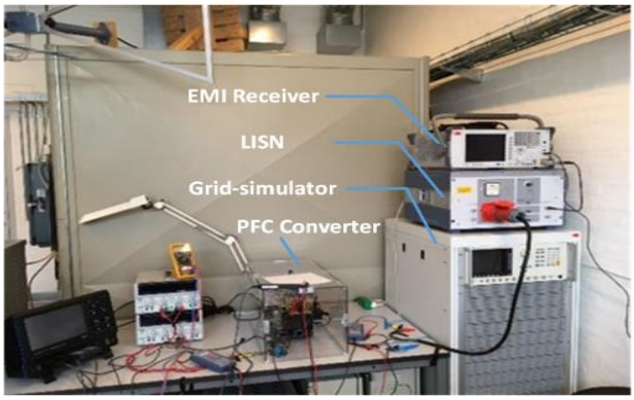

***Fig. 2.20**:Test setup for the studied single-phase Boost PFC converter [C1].*

2.7.2. VSI Case Study

In order to substantiate the performance of the proposed technique, a simulation technique is detailed. As declared earlier, the suggested technique is based on the equivalent circuit model, including the output admittance and a noise source. Additionally, the suggested analytical noise source is verified by PLECS simulation. It should be mentioned that the filter component sizes are obtained based on (2-3)-(2-7). Table 2-4 presents the comparitive DM EMI results related noise for two cases, including bipolar and unipolar grid-tied VSI by switching frequency of 20 kHz to compare in Band A. It can be seen that the errors for all DM EMI estimations related to noise are below 1.3 dB and 0.8 dB for single-phase bipolar and unipolar grid-tied VSI, respectively. The suggested technique is employed for the EMI level estimations related to all DM carier harmonics, particularly at the first carrier harmonics remarkable in the EMI filter design.

2.8. Summary

In this Chapter, the analytical time-frequency modeling technique was proposed to predict a low-frequency differential mode EMI noise. The suggested technique was studied on single-phase PFC and VSI converters. Then, the effectiveness of the proposed approach was evaluated via simulations and experiments under different modes of operation. Furthermore, the effectiveness of this technique was compared to the conventional simplified DM noise analytical technique. According to the obtained results by simulations and experiments, the suggested and conventional approaches would be effectively used in designing an EMI filter; because low-estimation errors

***Table 2-4**: The obtained comparative results of DM noise for case neglecting EMI filter (f_{sw}=20 kHz)[C4].*

(Bipolar) Frequency [kHz]							
Technique [dBµV]	20 kHz	40 kHz	60 kHz	80 kHz	100 kHz	120 kHz	140 kHz
Proposed	119.67	107.15	99.07	92.97	88.6	84.3	80.7
Simulated	119.26	107.55	99.85	92.92	87.6	83.2	79.6
E_{P-S}	0.4	0.4	0.77	0.05	1	1.1	1.3
(Unipolar) Frequency [kHz]							
Technique [dBµV]/	40 kHz	80 kHz	120 kHz	-	-	-	-
Proposed	127.62	114.3	105.3	-	-	-	-
Simulated	127.58	113.5	105.1	-	-	-	-
E_{P-S}	0.04	0.8	0.2	-	-	-	-

E_{P-S}: Error between proposed and simulation

were observed in the first peak level of the noise. A suitable EMI filter was designed to make the converter comply with the selected standard. However, the proposed method revealed an appropriate estimation accuracy for the entire frequency range of 9 – 150 kHz, suggesting it as an appropriate candidate for system-level study. Notably, based on the studied power converters, it is viable to determine remarkable characteristics for further reducing model order and far less model dependency on the employed control parameters via the proposed modeling scheme [J1].

Chapter 3. Low Frequency DM Noise Modeling and Filter Design in Three-Phase Converters

3.1. Introduction

Three-phase converters are equally important as single-phase converters and they play a major role in generating emissions, especially for the new frequency range. Moreover, three-phase power converters are more adopted in the industrial environment. Similar to the previous chapter modeling of three-phase converters and EMI filter design are discussed in this Chapter.

All previous efforts related to modeling and analysis of the EMI are based on simulations and experiments due to the model's dependency on the design and high-frequency behavior of the converter's component. For instance, designing the EMI filter for a 1-MHz, 10-kW 3-phase/level PWM rectifier was reported in [20]. According to the models proposed for the frequency up to 30 MHz, experimental validation of the designed EMI filter was provided by measuring the impedance and conducted emission (CE) taken from a 10-kW prototype. Viable routes for CM noise in a three-phase PWM level rectifier were investigated in [20], where parasitic capacitances with respect to the heat sink and earth were considered. In addition, in [73], a 3-terminal CM EMI model was extended for an uninterruptible power supply (UPS). Based on the reduced CM model, EMI production, emission, and mitigation strategies of the full SiC UPS module were studied.

This Chapter focuses majorly on identifying the effective parameters to reduce the model of EMI via the frequency behavior analysis of the three-phase grid-tied converter. Moreover, the three-phase active rectifier and inverter are chosen to validate the proposed method due to the commonly applied industrial PE. In addition, the analytical model of DM EMI based on the closed-loop is extended to a system-level EMI and proper design of EMI filters to meet the standard requirements [C3].

3.2. Three-Phase Grid-Connected Converter and Control Schemes

3.2.1. Three-Phase Active Rectifier

Fig. 3.1 shows a general configuration of a three-phase active rectifier based on the SPWM modulation, including LISN, *L*, *LC* filter, and EMI receiver [C3]. In addition, the inductor and capacitor of an LC filter calculated by the (2-3) and (2-5), respectively. In order to get an enhanced performance of the active rectifier, an external control loop should be included in the control scheme. This external control

loop operates as an internal current controller; however, the external loop is based on voltage control. Thus, the external voltage control loop can regulate the DC-link voltage by providing an appropriate reference current for the current controller [57].

3.2.2. Three-Phase VSI

A general structure of a three-phase VSI with an LCL filter type constituting of a LISN, an EMI receiver, and an EMI filter was depicted in Fig. 3.2. AC filter component design is presented comprehensively in Chapter 2. Inverter-side inductor size and grid-side inductor size were calculated by (2-3) and (2-6), respectively. In addition, the capacitor size is achieved by (2-5).

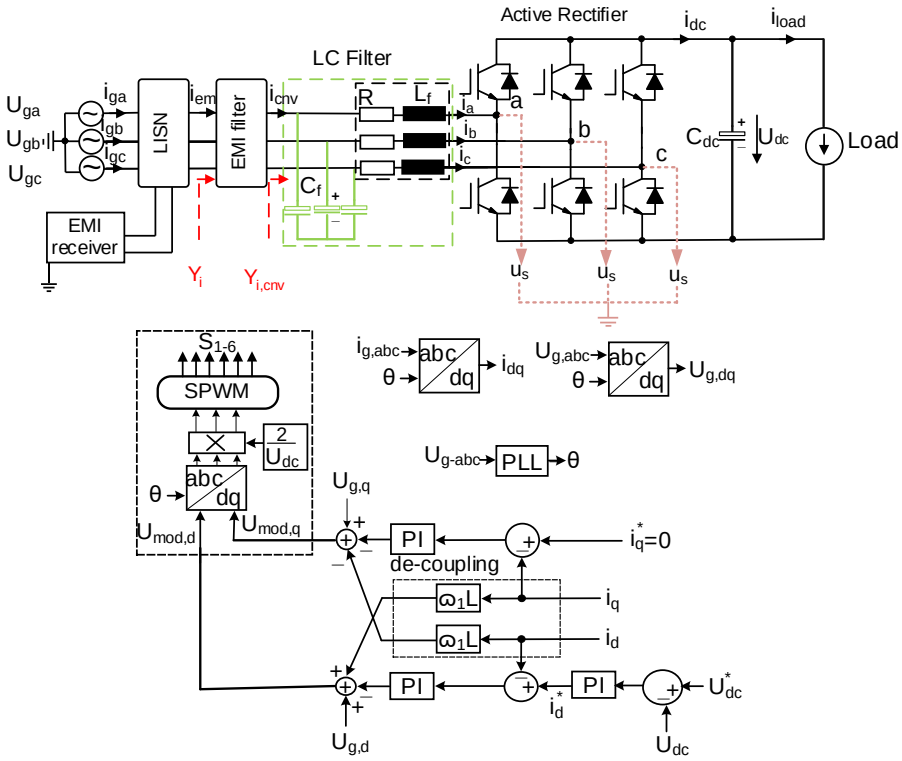

Fig. 3.1: *Block diagram of a typical three-phase grid-connected active rectifier with L/LC filter configuration including EMI testing structure comprising of LISN and EMI receiver[C3].*

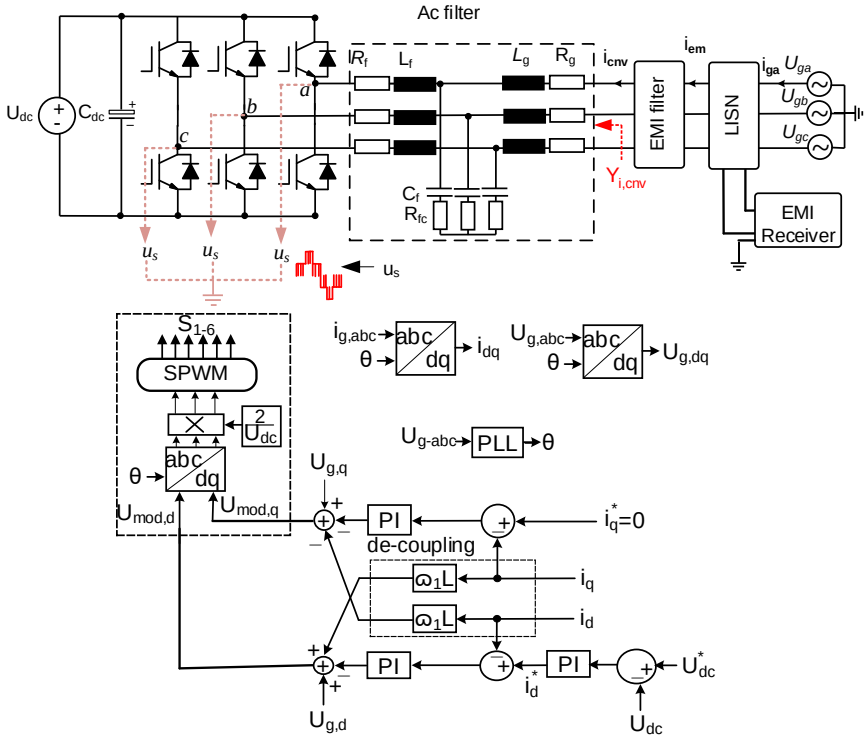

Fig. 3.2: *Typical structure of three-phase VSI with LCL filter type including LISN, EMI receiver and EMI filter[C4].*

3.3. Proposed Time-Frequency Domain EMI Model

Fig. 3.1 shows the general structure of the three-phase active rectifier. In order to obtain the equivalent model of the circuit, a typical converter is modeled considering its DM noise source and the closed-loop impedance, depicted in Fig. 3.3. Thus, this Chapter details DM EMI's model regarding an input closed-loop admittance and a noise source by applying the double Fourier analysis [C3]. Notably, this section's main purpose is to achieve the converters' equivalent circuit model shown in Fig. 3.11 to provide the analysis and the related frequency behavior.

3.3.1. DM EMI Noise Source Model

The first step to get an equivalent circuit model is modeling the emission noise. Hence, in this subsection, the DM noise source model is presented for the three-phase rectifier and inverter by employing the double Fourier analysis. On the other hand, the frequency behavior of the noise emission and its modeling are presented.

3.3.1.1 Three-Phase Active Rectifier

The fundamental idea behind the suggested time-domain frequency-domain technique is established based on the converter's developed equivalent circuit model for the converter (See Fig. 3.3). Thus, developing the suggested technique, the noise source and the related close-loop impedance need to be modeled. To this end, power switches' common points can be differentiated from the noise source frequency behavior. So, Fig. 3.4 shows the obtained simulation waveform of u_s in PLECS. Thus, the noise source frequency behavior is computed by applying a double Fourier technique over u_s waveform. Therefore, the frequency-domain noise spectrum function as a model of source noise needs to be included. Detailed explanations on the

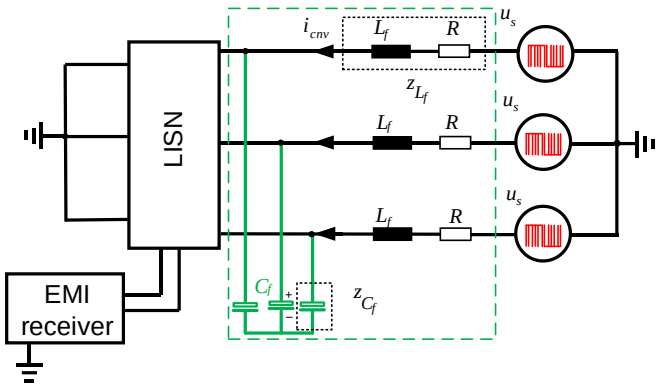

***Fig. 3.3**: Conducted equivalent circuit of noise in a three-phase PWM rectifier system comprising of EMI receiver and LISN[C3].*

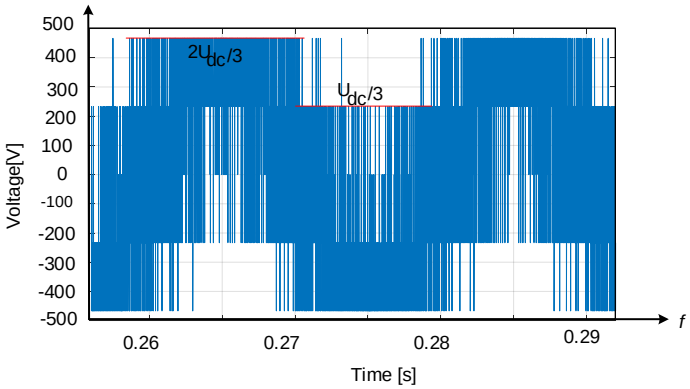

***Fig. 3.4**: Simulation result of DM voltage waveform (u_s) of the three-phase active rectifier system operating at P_o = 9 kW carried out in PLECS[C3]*

function in frequency-domain were reported in [C3]. A general function of frequency-domain related to the noise source model, including the baseband spectrum, carrier group spectrum, dc offset value, and side-band spectrum, is represented (2-10). Ultimately, the switching noise function in frequency-domain considering the double Fourier analysis is expressed as [C3]

$$\begin{aligned} u_s &= \frac{MU_{dc}}{2}\sin\omega_0 t + \ldots \\ &\frac{2U_{dc}}{\pi}\sum_{m=1,3,5,..}^{\infty}\sum_{n=\pm2,\pm4,...}^{\infty}\frac{4}{3}\frac{J_n(mM\pi/2)}{m}\sin\frac{m\pi}{2}\sin^2\frac{n\pi}{3}\cos(m\omega_{sw}t+n\omega_0 t)+\ldots \\ &\frac{2U_{dc}}{\pi}\sum_{m=2,4,6,..}^{\infty}\sum_{n=\pm1,\pm3,...}^{\infty}\frac{4}{3}\frac{J_n(mM\pi/2)}{m}\cos\frac{m\pi}{2}\sin^2\frac{n\pi}{3}\sin(m\omega_{sw}t+n\omega_0 t) \end{aligned} \quad (3\text{-}1)$$

M denotes the modulation index as $M=2U_g/U_{dc}$. So, the frequency-domain function includes side-bands related to carrier components (m = 1, 2…) and base-bands related to the first carrier component (n=1) [C3]. So, U_{dc} is denoted by the dc voltage output. Fig. 3.5(a) illustrates the noise source frequency behavior model via (3-1)and simulations carried out in PLECS. As seen in Fig. 3.5, the simulation model verified the noise source model of DM analytically with regard to (3-5). Furthermore, to get a clarified comparison by the proposed method in simulations, Fig. 3.5 (b) is illustrated in the zoomed-in parts of Fig. 3.5(a) [C3]. Regarding Fig. 3.5, it should be mentioned that the noise source of DM is modeled as a Thevenin equivalent circuit voltage.

3.3.1.2 Three-Phase VSI

Fig. 3.2 depicts the three-phase grid-tied VSI configuration. To obtain its simplified noise source model, voltage points a, b, and c is defined as the voltage noise source. Applying a double Fourier over the noise source voltage, the frequency-domain switching function of the noise source is obtained by (3-2)[C3]

$$\begin{aligned} u_s &= \frac{MU_{dc}}{2}\sin\omega_g t + \frac{2u_{dc}}{\pi}\sum_{m=1,3,5,..}^{\infty}\sum_{n=\pm2,\pm4,...}^{\infty}\frac{4}{3}\frac{J_n(mM\pi/2)}{m}\sin\frac{m\pi}{2}\sin^2\frac{n\pi}{3}\cos(m\omega_{sw}t+n\omega_g t)+\ldots \\ &\frac{2u_{dc}}{\pi}\sum_{m=2,4,6,..}^{\infty}\sum_{n=\pm1,\pm3,...}^{\infty}\frac{4}{3}\frac{J_n(mM\pi/2)}{m}\cos\frac{m\pi}{2}\sin^2\frac{n\pi}{3}\sin(m\omega_{sw}t+n\omega_g t) \end{aligned} \quad (3\text{-}2)$$

The modulation index is represented as $M=2U_{ga}/U_{dc}$. The three-phase VSI operation is assumed symmetrical in this thesis. Thus, Fig. 3.6 depicts an analytical approach and simulation for the three-phase grid-tied VSI noise. Additionally, the proposed method has a high accuracy due to the application of a double Fourier.

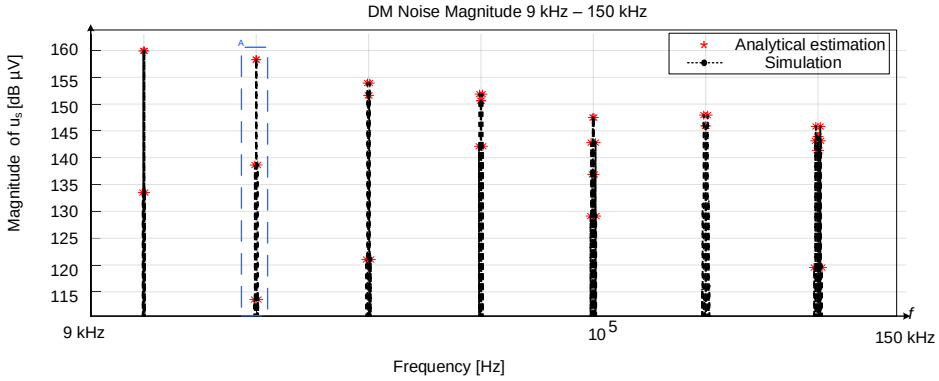

(a)

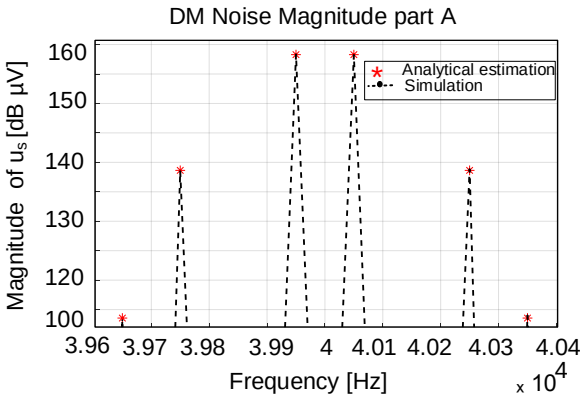

(b)

Fig. 3.5*: Comparative results of the noise source frequency spectrum regarding the proposed analytical approach and simulation result in PLECS, a) frequency-range of 9-150 kHz, b) frequency-range within 40 kHz[C3].*

3.3.2. Closed Loop Input/output admittance

The second step to get an equivalent circuit model is modeling the admittance or impedance model, as shown in Fig. 3.3. Thus, based on the converter type, the input and output admittance are modeled in this subsection.

3.3.2.1 Input Admittance of Three-Phase Active Rectifier

Fig. 3.7 depicts the single-phase LCL-filtered rectifier, including grid current-control and mean switching model of the three-phase grid-connected converter. Fig. 3.8 depicts the equivalent behavior of a single-phase input admittance, including magnitude and phase for three-phase rectifiers, comprising of boost inductor, L_f, (3-3)

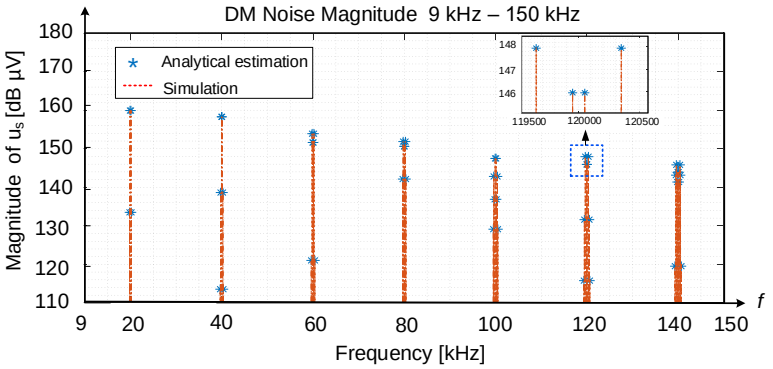

Fig. 3.6: *Comparative results of the noise source frequency spectrum for a three-phase VSI in with regard to (3-2) proposed analytical model, and simulation results in PLECS[C4].*

and simulations carried out in PLECS. With regard to the validated model, it is obvious in Fig. 3-6 that the suggested model of an input impedance considering (3-3) within 9–150 kHz is verified by simulations.

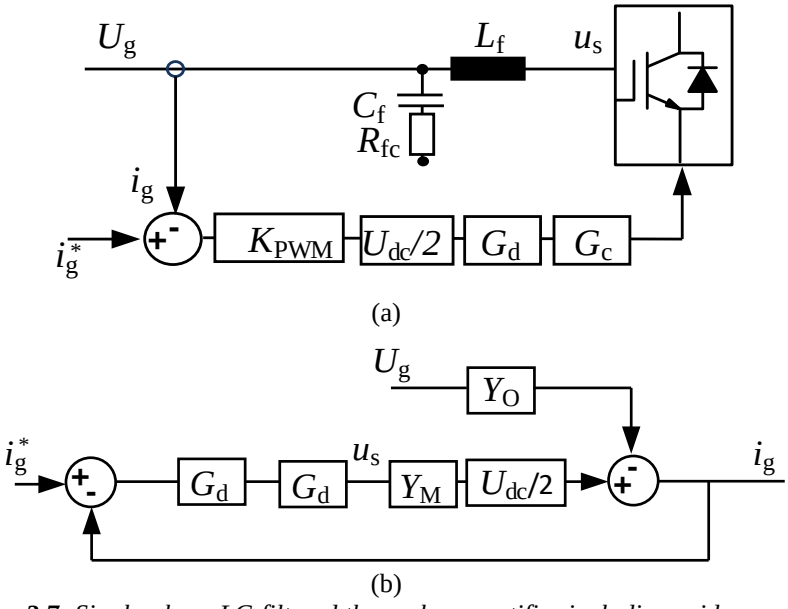

Fig. 3.7*: Single-phase LC-filtered three phase rectifier including grid current control including grid current control (b) average switching model of the rectifier* [C3].

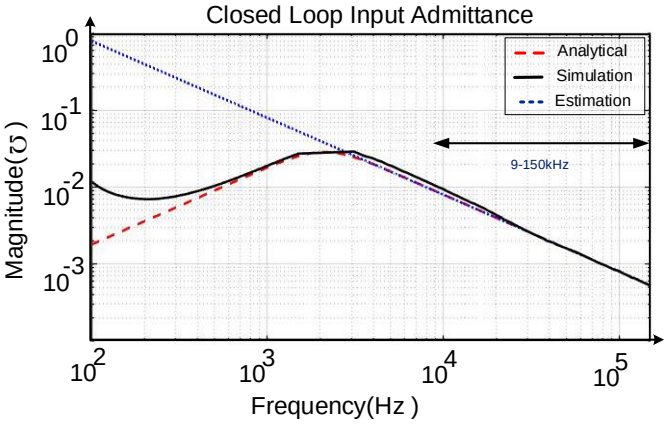

(a)

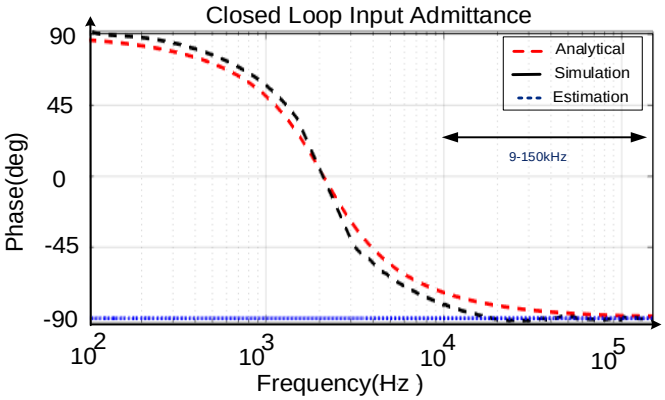

Fig. 3.8*: Input single-phase admittance magnitude and phase behavior for three-phase active rectifier including L as boost inductor regarding (3-3) and simulation results from PLECS (i.e., switching model) [C3].*

$$Y_C(s) = \frac{i_g}{u_g}\bigg|_{i_g^* = 0} = \frac{Y_O}{1 + \frac{U_{dc}}{2} G_c G_d Y_M} \tag{3-3}$$

where G_d and G_c are obtained from the(2-26), Y_o and Y_M can be calculated by (3-4) and (3-5) for the boost inductor L_f.

$$Y_O(s) = \frac{-i_g}{u_g}\bigg|_{u_s = 0} = \frac{1}{L_f s} \tag{3-4}$$

$$Y_M(s) = \frac{i_g}{u_s}\bigg|_{u_g=0} = \frac{1}{L_f s} \tag{3-5}$$

Further, Y_o and Y_M can be calculated by (3-6) and (3-7) for the $L_f C_f$ case studies.

$$Y_O(s) = \frac{-i_g}{u_g}\bigg|_{u_s=0} = \frac{L_f C_f s^2 + 1}{L_f s} \tag{3-6}$$

$$Y_M(s) = \frac{i_g}{u_s}\bigg|_{u_g=0} = \frac{1}{L_f s} \tag{3-7}$$

As seen in Fig. 3.8, it is found that the closed-loop admittance is matched with inductor admittance. So, it is an excellent estimation to use it in the system-level EMI analysis. It should be noted that many converters are connected to the same point. For more analysis and obtaining the characteristics of the influencing parameters on the closed-loop model, the effects of sampling the admittance should be analyzed via investigating G_d. Hence, Fig. 3.9 shows the analysis of the sampling effects on the input admittance based on the (2-26). As it is clear from Fig. 3.9, the sampling effects are not significant on the input admittance above 150 kHz. Fig. 3.10 shows the load changing effect on the EMI simulation for L_f filter configuration [C3]. Notably, load changing does not affect the EMI simulation result.

3.3.2.2 Output Admittance of Three-Phase Voltage Source Inverter

The three-phase inverter is modeled similarly to the single-phase counterpart described in Chapter 2 by assuming the symmetrical operation. On the other hand, (2-29) can present the output admittance of the three-phase grid-connected inverter.

3.3.3. Norton current model

The main purpose of this subsection is to present the Norton current as shown in the Fig. 3.11.

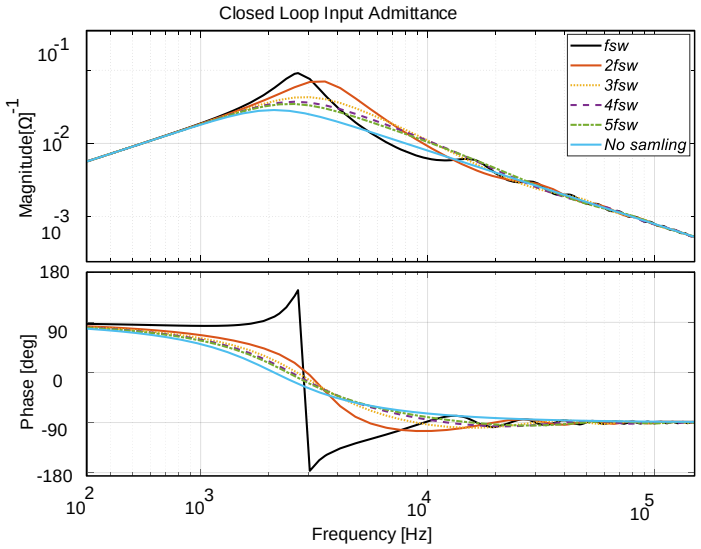

Fig. 3.9: *Analysis of the sampling effects on the input admittance based on the (2-26) with f_{sw} is 20 kHz.*

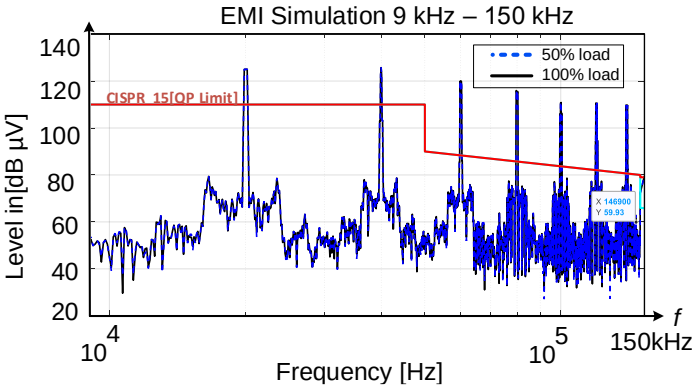

Fig. 3.10*: Analysis of the load changing on the EMI simulation in the case of L_f with f_{sw} = 20 kHz.*

3.3.3.1 Norton Model of Three-Phase Active Rectifier

The noise source model is updated via a voltage division rule obtained in the case study of $L_f C_f$. Thus, Norton current is obtained by (3-8) [C3]

$$i_{cnv}(s) = u_s Y_C . \frac{z_{C_f}}{z_{C_f} + z_{L_f}} \tag{3-8}$$

Moreover, it can be found for the L_f case study by

$$i_{cnv}(s) = u_s Y_C \tag{3-9}$$

3.3.3.2 Norton Model of Three-Phase VSI

The three-phase inverter is modeled similar to its single-phase counterpart described in Chapter 2 in subsection 2.3.3.2.

3.3.4. Three-phase LISN Modeling

In this subsection, the relationship between the noise current and EMI receiver should be modeled. Hence, the relationship between LISN input current and EMI receiver measurement branch can be presented as (3-10)

$$\frac{i_{rec}(s)}{i_{cnv}(s)} = \frac{(L_2 s \| \frac{1}{C_2 s} + R_2) + L_1 s}{(L_2 s \| \frac{1}{C_2 s} + R_2) + L_1 s + (\frac{1}{C_1 s} + R_1)} \tag{3-10}$$

Also, the receiver voltage noise of EMI depicted in Fig. 3.11 is computed as

$$U_{meas}(s) = R_1 . i_{rec} \tag{3-11}$$

By applying the EMI peak detection, it can be obtained by (2-47). Based on the CISPR-16 standard, the filter bandwidth related to the EMI receiver needs to be set to 200 Hz for Band A and 9 kHz for Band B [24], [C3].

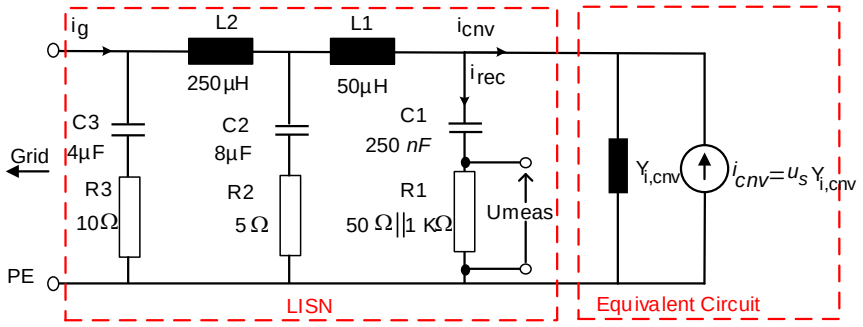

***Fig. 3.11**: Single-phase Norton equivalent circuit in a three-phase grid-connected converter with out EMI filter considering LISN [C3].*

3.3.5. Inclusion of EMI Filter into the Model

The structure of the two-stage EMI filter is shown in Fig. 3.12. Filter required attenuation is achieved based on (2-41). Further, the component size, including the inductor and capacitor, is calculated by the (3-12) [15]

$$A_{tt}(f_{sweep}) \geq \left\{ A_{tt_{EMI\_Filter}(f_{sweep})} = \left| ((j2\pi f)^2 . L_{DM} . C_{DM} + 1)^2 + (j2\pi f)^2 . L_{DM} . C_{DM} \right| \right\} \quad (3\text{-}12)$$

Damping resistor is calculated as [74]

$$R_{DM} = \sqrt{\frac{L_{DM}}{C_{DM}}} \cdot \frac{1+n}{n} \cdot \sqrt{\frac{(2+n)(4+3n)}{2(1+n)(4+n)}} \quad (3\text{-}13)$$

where n denotes the number of the filter stages where the equivalent circuit model should be updated by the EMI filter's effects because it is part of the converter [C3]. The Middlebrook extra element theory updates the equivalent circuit model, including the admittance and Norton current [71]. Hence

$$Y_i(s) = Y_{iF} \frac{1 + \frac{Y_{i,cnv}}{Y_{oF\infty}}}{1 + \frac{Y_{i,cnv}}{Y_{oFo}}} \quad (3\text{-}14)$$

where Y_{iF} is EMI filter input admittance. Input admittance of the two-stages EMI filter can be determined from

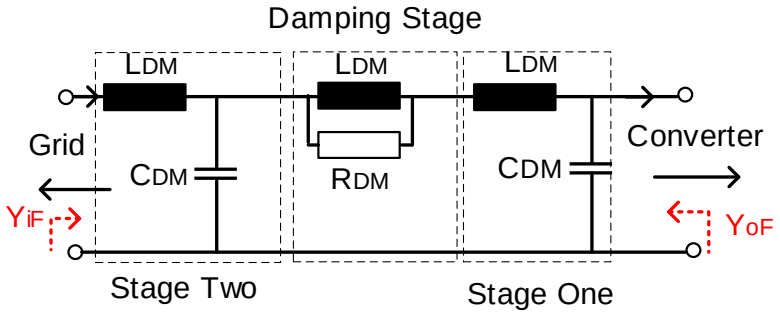

***Fig. 3.12**: Single-phase representation of DM EMI filter configuration with two filtering stages and one damping stage[C4].*

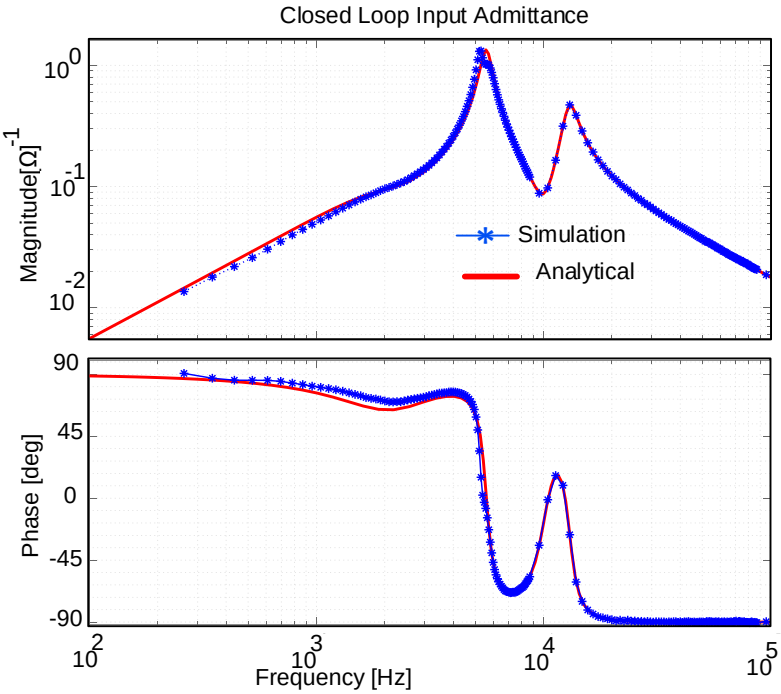

***Fig. 3.13**: Closed Loop input admittance for three-phase rectifier with two-stage EMI filter based on (3-14) and simulation validation by the PLECS simulation.*

$$Y_{iF}(s) = ((Y_{C_{DM}} + Y_{L_{DM}} + \frac{Y_{L_{DM}} Y_R}{Y_{L_{DM}} + Y_R}) \| Y_{C_{DM}} + Y_{L_{DM}}) \tag{3-15}$$

Y_{oFo} is defined as

$$Y_{oFo}(s) = ((Y_{L_f} + Y_{C_f}) \| Y_{L_f}) + Y_{C_f} \tag{3-16}$$

Also, $Y_{oF\infty}$ is defined by the (3-17),

$$Y_{oF\infty}(s) = ((Y_{L_f} + Y_{C_f}) \| Y_{L_f}) + Y_{C_f} \tag{3-17}$$

Fig. 3.13 shows the closed-loop input admittance with a two-stage EMI filter based on (3-14) and simulation validation by the PLECS simulation. Moreover, in the next step, the Norton current is updated by the EMI filter's effects. Hence, the relationship between Norton current with and without of EMI filter is obtained from (2-37). The relation between input EMI filter current and Norton current can be calculated from (3-18) [J1]

$$\frac{i_1(s)}{i_{cnv}(s)} = \frac{Y_{oFo}}{Y_{oFo} + Y_{i,cnv}} \tag{3-18}$$

The relation between input and output current of the EMI filter can be calculated by (3-19) , and finally, the β is calculated by the (3-21) [J1]

$$\frac{i_{em}(s)}{i_1(s)} = \frac{Y_{L_{DM}} Y_1}{(2Y_1 + Y_{C_{DM}})(Y_{L_{DM}} + Y_{C_{DM}}) - Y_{L_{DM}} Y_1} \tag{3-19}$$

$$Y_1(s) = (R_{DM} + Y_{L_{DM}}) \Big\| Y_{L_{DM}} \tag{3-20}$$

$$\frac{i_{em}(s)}{i_{cnv}(s)} = \beta = \left(\frac{Y_{L_{DM}} Y_1}{(2Y_1 + Y_{C_{DM}})(Y_{L_{DM}} + Y_{C_{DM}}) - Y_{L_{DM}} Y_1}\right) . \frac{Y_{oFo}}{Y_{oFo} + Y_{c,inv}} \tag{3-21}$$

3.4. Results

In order to investigate the proposed analytical approach, a three-phase AC/DC grid-connected converter depicted in Fig. 3.1 is designed and the related parameters are provided in Table 3-1. Two case studies are considered for active rectifier to validate the proposed modeling approach, including effect of different input filters. To verify the proposed analytical technique, simulations have been run in PLECS. Here, the obtained models are coalesced to get the EMI results that are highly important for designing the EMI filter [C3].

***Table 3-1**: Case Study Specification with Including Two Different Cases[C3].*

	C_{dc}	U_{dc}	U_g	f_{sw}	P_O
case	[µF]	[V]	[V]	[kHz]	[KW]
studies	500	700	230	20	9
	L_f	Ripple current	--	--	--
L	[mH]	%			
	2	15	--	--	--
	L_f	Ripple current	C_f	Ratio of the	
LC	[mH]	%	[µF]	reactive power	
				%	
	2	15	5	3	

So, Fig. 3.14 illustrates the analytical model obtained regarding (3-11) and (2-47) model of simulations based on the obtained results in PLECS for peak detection EMI (Band A) having a just (L_f). The analytical model appropriately matches the model of switching simulations. The obtained is less than 1.2 dB (detailed in Table 3-2 and Fig. 3.14). It is demonstrated that the suggested technique can simply determine DM noises within 9−150 kHz with high accuracy by employing a double Fourier analysis. Then, Fig. 3.15 illustrates the effectiveness of the suggested technique and model of simulations with an input filter $L_f C_f$. The resulting error for $L_f C_f$ case study appeared for all noise estimations related to DM is less than 1.2 dB[C3].

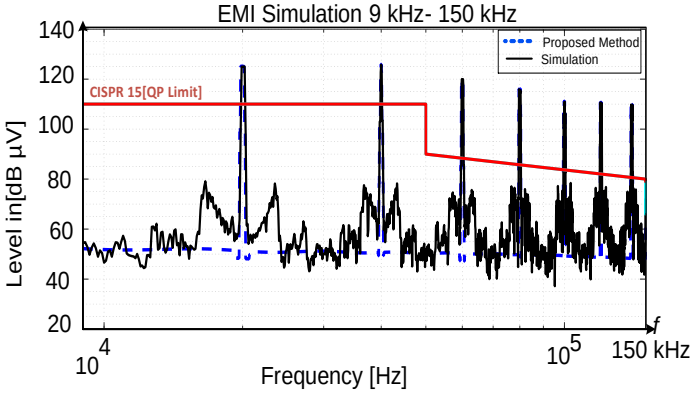

***Fig. 3.14**: The DM noise results for the three-phase active rectifier, including L_f as boost inductor with f_{sw} = 20 kHz, based on the suggested analytical model (3-9) and* (2-47) *and PLECS [C3].*

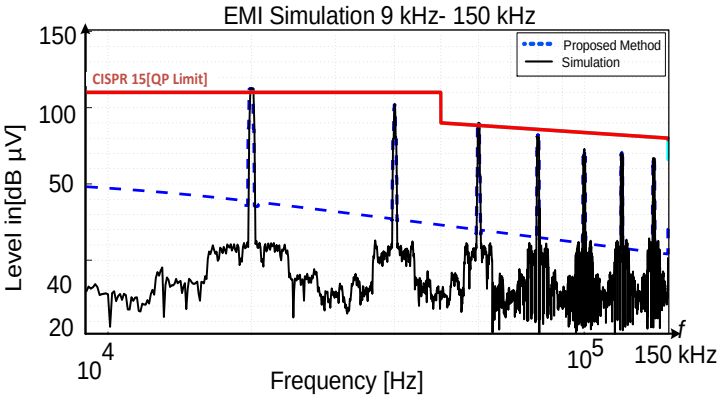

***Fig. 3.15**: The DM noise results for a three-phase active rectifier by including $L_f C_f$ filter with f_{sw} = 20 kHz based on the suggested analytical model* (2-47) *and (3-8), and PLECS[C3].*

It is demonstrated that the suggested technique is able to simply estimate DM noises within the frequency range of 9–150 kHz with higher accuracy. As depicted in Fig. 3.15 and Fig. 3.14, the EMI level is higher than the standard limits of EMI [C3]. So, the EMI filter should meet the standard requirements. Next, a simulation approach is presented to verify the proposed analytical method for three-phase VSI . As mentioned earlier, the proposed method is based on the equivalent circuit model comprising an output admittance and a noise source. Thus, the output admittance can be confirmed by applying several sinusoidal perturbations and, then checking the resulting impacts on the considered variables. Next, a Fourier analysis is employed to get the amplitude and phase related to the frequency of the sinusoidal perturbations.

Moreover, the proposed analytical noise source is verified via simulation results depicted in Fig. 3.2. In order to confirm the proposed modeling approach efficiency, a three-phase grid-tied inverter having an $L_fC_fL_g$ filter is considered.
provides the applied system specifications. To verify the efficacy of the suggested approach, a simulation model was carried out in PLECS. Therefore, Fig. 3.16 depicts DM EMI for a three-phase grid-tied VSI. As seen from Fig. 3.16, the forecasted EMI noise levels from the proposed modeling approach are in good agreement with the simulation results, and the resulting error is below 1 dB at different modes[C4]. Obviously, based on the [C4], the resulting errors for all DM EMI noise estimations are less than 1 dB for three-phase grid-tied VSI, respectively. The proposed method can be utilized to estimate the EMI level for all DM carrier harmonics, particularly at the first carrier harmonics, which is important in the EMI filter designing.

***Table 3-2**: Obtained Comparative Results for DM Noise in Rectifier Case Study (L_f) Carried Out At 20kHz Switching Frequency[C3].*

Method[dBµV] /Frequency	**20 [kHz]**	**40 [kHz]**	**60 [kHz]**	**80 [kHz]**	**100 [kHz]**	**120 [kHz]**	**140 [kHz]**
Proposed analytical model	125.2	129.9	120.1	117.5	111.1	111.7	109.8
Simulation	125.1	125.7	120	116.4	110.9	110.6	109.7
Error	0.1	0.2	0.1	1.1	1.2	1.1	0.2

***Table 3-3**: Three-phase Inverter Specification Required for EMI Analysis[C4].*

Symbol	Parameter	3-ph	Symbol	Parameter	3-ph
U_g	Grid phase voltage (v)	230	C_{dc}	DC link capacitor (mF)	2
f_g	Grid frequency (Hz)	50	U_{dc}	Output voltage (v)	700
f_{sw}	Switching Frequency (kHz)	20	P_o	Output power (kW)	9
C_f	Reactive capacitor (µF)	8	L_f	Converter side inductor (mH)	2.5
λ_{v_Lf}	Voltage ripple factor (%)	5	L_g	Grid side inductor (µH)	250
λ_{c_Lf}	Current ripple factor (%)	30	R_{fc}	Damping resistor (Ω)	8
λ_{h}	Harmonic factor	0.3	λ_{C}	Reactive power (%)	5

In the end, for the EMI experiments to investigate the suggested technique, a three-phase grid-connected converter, depicted in Fig. 3.17 is designed. Finally, experimental measurements related to EMI are carried out through A Keysight N9010A spectrum analyzer and ESH2-Z5 LISN backed by CISPR measurement requirements. Fig. 3.18 illustrates the comparative results of DM noise obtained for a three-phase converter operating at f_{sw} = 20 kHz without considering the EMI filter. The results obtained demonstrate an acceptable agreement between the proposed analytical technique and experiments [C3].

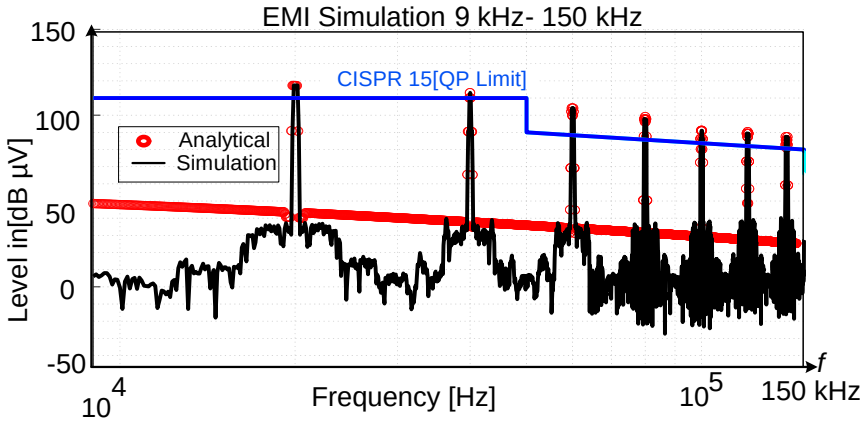

***Fig. 3.16**: Obtained DM noise for a three-phase grid-tied inverter comprising of LCL filter with a frequency of f_{sw} = 20 kHz based on the suggested analytical model* (2-47) *and* (3-9) *and simulations in PLECS[C4].*

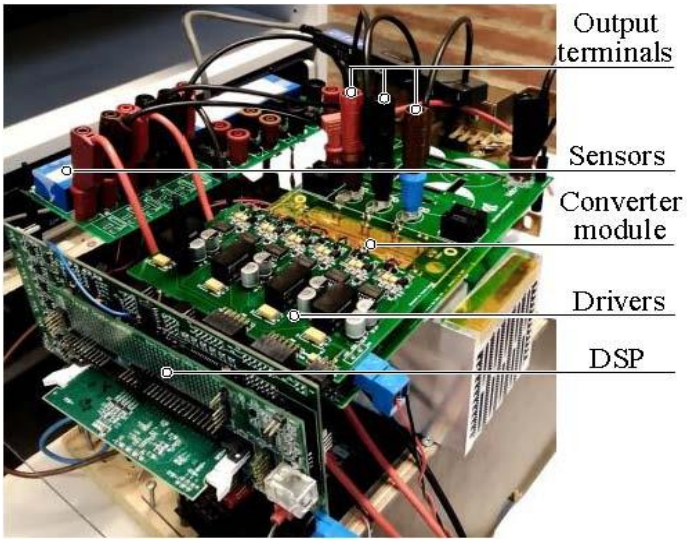

***Fig. 3.17**: A picture of the three-phase power converter experimental prototype [C3].*

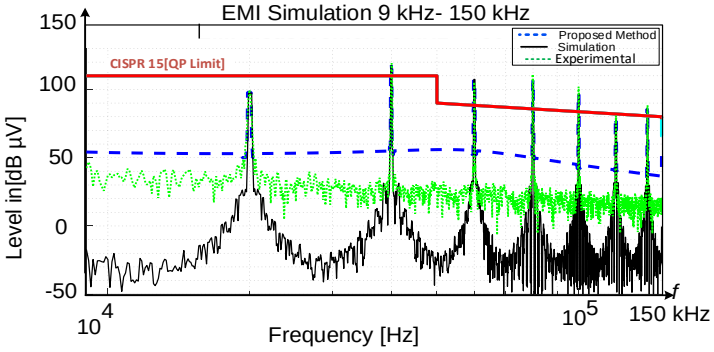

***Fig. 3.18**: Obtained DM noise for the three-phase converter, including LC filter with f_{sw} = 20 kHz based on the proposed analytical model* (2-47) *and (3-8) and including PLECS simulation and experimental results.(L_f = 1.8 (mH), C_f = 150 (nF), U_{ga} = 25 (V), U_{dc} = 125 (V), P_o = 40 (W), C_{dc} =1000) [C3].*

3.5. Summary

In this Chapter, an analytical time-frequency modeling technique was proposed to predict various modes of conducted EMI noise in three-phase grid-connected power converters. For this purpose, typical three-phase active rectifier and voltage source inverter topologies were considered and modeled. The proposed analytical approach demonstrated an acceptable estimation accuracy with a maximum resulting error below 1.2 dB. Moreover, the frequency behavior of the inverter output admittance and rectifier input admittance revealed the effective parameters to employ in the system-level studies and EMI filter design. Thus, the proposed technique obtained high accuracy in DM EMI noise analysis considering a simplified model and decreased computation time [C3]. The performance of the suggested technique was verified via simulations and experiments on a three-phase converter. Notably, the EMI filter to meet standard requirements is more capable and effective.

Chapter 4. Low Frequency Differential EMI Modeling For Multi-Converter Systems

4.1. Introduction

The multi-converter configuration has many applications to provide some advantages, for example, in PFC converters in synchronized scenarios. Notably, they are not synchronized in many cases[42], [75], for instance, PV applications. Hence, in this thesis, to study the pros and cons of synchronized or unsynchronized scenarios on the new frequency range of 9 – 150 kHz, two applications are considered.
As discussed in chapter 2, boost PFC configurations are developed to reach an enhanced power factor very close to one (unity) in order to comply with harmonic standards as well as power factor requirements. Moreover, in order to improve the performance of PFC converters from power rating, overall design volume, input ripple current, interleaving is typically applied. By employing an interleaved topology, depicted in Fig. 4.1, a remarkable decrease in switching frequency ripples can be obtained [41], [61], [76]. Following the objective of the Ph.D. thesis, the analytical EMI modeling is conducted considering the effect of phase shift in the analytical equation. Furthermore, EMI filter design in order to damp emissions below 150 kHz is performed as well.

Interleaving power converters can effectively reduce input current ripples leading to reduced noise magnitude of DM EMI as well as the filter attenuation requirements [41]. The effect of phase shift for above 150 kHz frequency range on the filter size and the generated emission have been well studied before [77]. However, considering the new coming requirement for below 150 kHz frequency range there is a lack of understanding regarding the effect of interleaving approach and applied phase-shift on the DM filter size and generate emission.

From an EMI point of view, obtaining proper phase-shift angles is highly important for optimum filter volume [76, 77]. Thus, the optimum design of DM EMI filters for applications of the boost PFC is a critical issue, in particular within the low-frequency range of EMI, 2-150 kHz. This thesis aims at proposing the estimation of a proper analytical-based DM EMI noise as well as suitable EMI filter design. Further, the analytical noise approach includes the number of interleaved units as well as the corresponding various phase-shift types. Therefore, the unconventional phase-shift is obtained on the basis of estimating the EMI for harmonics in Band-B.

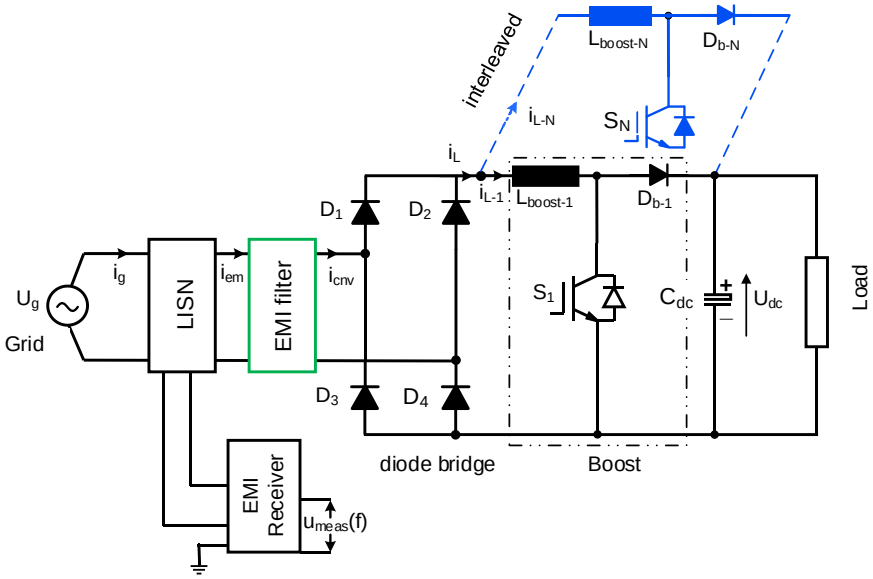

***Fig. 4.1**: Block-diagram of a so-called interleaved boost PFC converter considering EMI receiver, LISN, and EMI filter [J2].*

Considering the new paradigm to shift to more renewable energies PV converters are going to be penetrated more and more. To achieve more power, the many PVs units connected to the same point. But, there are not unsynchronized due to the factory switching tolerance. Further, the importance of studying their effect on EMI in the < 150 kHz that it was the intention of this chapter. In recent years, many authors have interested in parallel operation for delivering high amount of power to the load center/point satisfying power quality (PQ) levels, e.g., minimum total harmonic distortion (THD) regarding the specified power grid requirements [33]. Additionally, the parallel operation of various PE converters within similar power switching frequencies has led to unprecedented emissions within high frequencies, including a beating frequency and EMI under 150 kHz. Even though numerous investigations have previously reported measuring/supervising the interference issues, there exists no basic perceptions of the noise emissions and related suppressing techniques within 2-150 kHz. Thus, it is mandatory to develop a systematic technique in order to model multi-parallel converters and investigate possible interactions, such as their frequency behavior and the interaction with power grids. The interaction among different devices becomes of great importance when numerous PE inverters are connected to a similar point, including lighting installations, computer centers, etc. Moreover, the situation is far complicated because of small variations in switching frequency if the devices are provided by an individual manufacturer and type [42], [75]. So, factory tolerances related to switching frequency for the same PE converter may result in beating in the parallel operation. This research purpose is to suggest the aggregated models developed to demonstrate high-frequency behavior as well as the interactions made between PE converters and the power grid impedance and/or LISN impedance.

At the end, various topologies related to the EMI filter are suggested for the interaction current circulating around the power grid as well as different units.

4.2. DM EMI analytical approach For Interleaved Units

4.2.1. Analytical Approach Model

In order to estimate DM EMI noise generated from interleaved PFC converter, here the proposed analytical EMI modeling approach in Chapter 2 is updated considering the effect of phase-shift (θ). Notably, the equivalent closed loop impedance calculation is modified as well by considering the total parallel input impedance of interleaved converters. More details with regard to modeling of DM noise, input impedance, as well as the resulting frequency behavior were studied in [J2] for a non-interleaved boost PFC. And, the DM noise spectrum related to each switch is provided by (2-18), including a DC-offset value, carrier group harmonics, baseband harmonics, and sideband harmonics. In addition, it should be stated that the carrier harmonics would be refreshed by phase-shift impacts as (4-1)

$$A_{mo} + jB_{mo} = \frac{8U_{dc}}{\pi^2}\frac{1}{m}e^{jm\theta}\sum_{\substack{k=1\\k=odd}}^{\infty}\frac{J_k(m\pi M)}{k} \tag{4-1}$$

At the end, side-band harmonics are achieved by phase-shift impacts in interleaved units provided as (4-2) [J2]

$$A_{mn} + jB_{mn} = \frac{2U_{dc}}{\pi^2}\frac{1}{jm}e^{jm\theta}\sum_{k=1}^{\infty}J_k(m\pi M)(j^k - j^{-k})\left(\frac{(\sin(\frac{k-n}{2})\pi)}{k-n} + \frac{(\sin(\frac{k+n}{2})\pi)}{k+n}\right) \tag{4-2}$$

where θ denotes the phase-shift of an interleaved unit chosen by the phase selection techniques. For example, with 2 interleaved units, the phase-shift of the first and second units are equal to zero and θ, respectively. The topology of a simple studied case regarding Norton equivalent circuit is depicted in Fig. 4.2. The current flowing through N units is obtained from (4-3) [J2]

$$i_L(s) = \sum_{n'=1}^{N}\frac{u_s\{(n'-1)\theta\}}{z_{in}(n')} \tag{4-3}$$

where *(n'-1)* θ is the phase-shift related to unit # *n'*. And, the input impedance related to a PFC converter is achieved by (2-21) [J2]. As the switching function related to a diode rectifier is in the form of a square wave signal, the Fourier transform is achieved via (4-4)

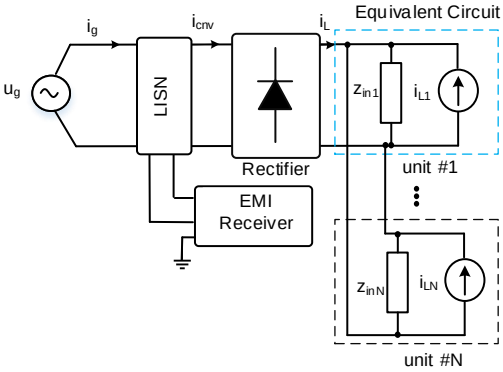

***Fig. 4.2**: Norton equivalent circuit diagram of interleaved boost PFC converter [J2].*

$$i_d(t) = \sum_{\substack{h=1 \\ h=odd}}^{\infty} \frac{2}{h\pi} \sin(\frac{h.\pi}{2}) \cos(\omega_0 ht) \tag{4-4}$$

where *h* denotes the order of harmonics. Thus, the input current related to LISN is achieved by

$$i_{cnv}(s) = i_d(s) i_L(s) \tag{4-5}$$

As the final step, the relation between EMI receiver voltage and LISN input current must be considered. Therefore, the relation between EMI receiver branch and the input current LISN regarding the EMI filter is obtained by (2-43). Furthermore, the voltage noise of an EMI receiver can be represented by (2-46) where comparative studies are performed which shows high accuracy of the proposed modeling technique[J1].

4.2.2. Two-Stage DM EMI Filter Design

An EMI filter is usually utilized to protect the utility against probable high-frequency noises. For this purpose, they need to comply with the given EMI standard requirements. Thus, a symmetrical design for a two-stage filter, illustrated in Fig. 4.3, is considered. Selecting filter components depends on the filter's given attenuation requirements, Att_{req}, computed by (4-7) [J2]. Hence, Att_{req} for a symmetric 2-stage EMI filter, regarding the size of inductor and capacitor is obtained by (4-6):

$$Att_{req}(f) = \left| ((j2\pi f)^2 . (2L_{DM}) . C_{DM} + 1)^2 + (2\pi f)^2 . (2L_{DM}) . C_{DM} \right| \tag{4-6}$$

As mentioned previously, the reduction of input current ripples leads to a reduced noise magnitude of a DM EMI (U_{max}) which can be calculated from the (2-48) and Fig. 4.1, and consequently to smaller EMI filter size with higher corner frequency

requirement. One of the main objectives of this thesis is to investigate possibility of obtaining optimum corner frequency through interleaving converters applying suitable phase-shift for frequency range of below 150 kHz.

4.2.3. Suitable Phase-Shift Selection

In order to investigate effect of suitable phase-shift following analysis are performed. More analysis and investigation have been done in [C2] regarding the filter's attenuation requirements and filter corner frequency for 1-unit non-interleaved and 2-unit and 3-unit with a conventional phase-shift as shown in Fig. 4.4. Therefore, the interleaving technique has no superiority at specific switching frequencies like 75–150 kHz for 2-unit interleaved compared to 1-unit interleaved in Band-B. So, carrier frequency harmonics' behavior is necessarily observed to obtain the optimum phase-shift in a given frequency. Importantly, the analysis-based EMI approach is forecasted on the noise level of an EMI for all orders of carrier frequency harmonics according to the chosen phase-angle. Hence, an optimum phase-shift may be chosen regarding the behavior of the first appeared carrier harmonics for various phases in Band-B. As a result, it gives an optimum phase-shift obtained by an analytical approach in order to get a lower attenuation requirement of filter on the basis of switching frequency as well as the number of the interleaved units.

Moreover, the first carrier harmonics are removed by an appropriate phase-shift selection technique. By eliminating the first peak of noise, that is critical in designing an EMI filter in Band-B, the filter design frequency changes (shifts) to a higher frequency. Thus (4-8) expressing unconventional phase-shift formulations are achieved from Table 4-1 by evaluation of the relationship between N, k, and θ [J2].

$$\theta = \frac{360^o}{N} \qquad if\ k\ is\ not\ a\ multiple\ of\ N \tag{4-7}$$

$$\theta = \frac{360^o}{\min\{\, factor(N).k \,\}} \qquad if\ k\ is\ a\ multiple\ of\ N \tag{4-8}$$

where k is the harmonics- order related to switching frequency, which is the first peak of a noise in Band-B.

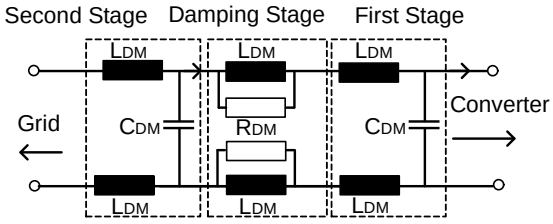

Fig. 4.3: *A symmetric topology of a 2-stage DM EMI filter [J2].*

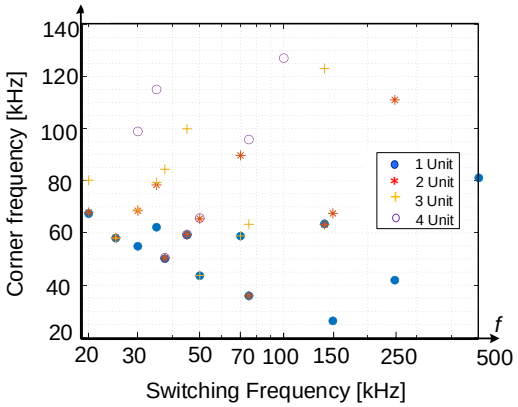

***Fig. 4.4**: The relationship between a corner frequency and switching frequency (up to four units interleaved). The conventional phase shift is considered based on the (4-7) [J2].*

***Table 4-1**: The optimum phase-shift angles within the frequency range (20–150 kHz) up to 4 interleaved units [J2].*

Frequency (kHz)	**Harm. order (*k*):**	**Number of interleaved units (*N*) and optimum phase-shift**		
		2	**3**	**4**
20	8th	22.5°	120°	22.5°
25	6th	30°	20°	90°
30	5th	180°	120°	90°
35	5th	180°	120°	90°
37.5	4th	45°	120°	45°
45	4th	45°	120°	45°
50	3rd	180°	40°	90°
70	3rd	180°	40°	90°
75	2nd	90°	120°	90°
140	2nd	90°	120°	90°
150	1st	180°	120°	90°

4.2.4. Filter Volume Optimization

Using the filter sizing equations and the proposed analytical modeling the optimization can be done relatively easy in an automated way. Here, the main goal of this section is optimizing the size of an EMI filter with regard to the selected phase-shift. An EMI filter volume is computed on the basis of [62], [78, 79] in order to investigate the effectiveness of the suggested technique. Ultimately, Fig. 4.5

illustrates a flowchart providing the design steps for the optimum size of a filter on the basis of the analytical-based EMI noise approach. The flowchart is majorly utilized to compute the components of an EMI filter only with few equations regarding appropriate phase shifts. As mentioned earlier, the symmetrical 2-stage EMI filter, illustrated in Fig. 4.3, was considered for studies in this research work. So, the volume size of the capacitor related to an EMI filter is achieved from (4-9) [J2]

$$V_C = k_{C1} C_{DM} u_g^2 + k_{C2} \tag{4-9}$$

Where, V_c is capacitor volume size, u_g is peak value, the factor k_{C1} is the proportionality of a capacitance to the energy storage; and k_{C2} is a voltage-dependent factor. In addition, the inductor value is achieved via (4-10) [J2]

$$V_L = k_{L1} L_{DM} I_g^2 + k_{L2} L_{DM} + k_{L3} I_g \tag{4-10}$$

V_L is capacitor volume size, I_g is average value, k_{L1} denotes a fixed factor representing the ratio of the energy storage, $E_L = 1/2 \cdot L_{DM} \cdot I_g^2$, to the size of an inductor. These factors may be obtained similarly to k_{L1}, k_{L2}, and k_{L3} through the provided data by the manufacturer via the use of Magnetics toroid cores, presented in [J2]. Thus, the totally, the size of a 2-stage symmetric EMI filter is obtained by (4-11)

$$V_{tot} = 2(n_f + 1) V_L + n_f V_C \rightarrow \min \tag{4-11}$$

where V_{tot} is EMI filter volume, n_f denotes the counts of filter stages. By solving(4-9) – (4-10) and (4-6), one can obtain an optimized component parameters of the filter for a specified counts of filter stages, n_f. In order to reduce the computational analysis, relation (4-6) is simplified for 2-stage filter of an EMI as

$$Att_{req}(f) = (j2\pi f)^{2n_f} . (2L_{DM})^{n_f} . C_{DM}{}^{n_f} \tag{4-12}$$

At the end, components of an EMI filter are computed by:

$$C_{DM} = \sqrt{\frac{(n_f + 1)(k_{L1} . I_g^2 + k_{L2}) . \sqrt[n_f]{Att_{req}}}{2n_f . k_{C1} . u_g^2 . (2\pi f_D)^2}} \tag{4-13}$$

$$L_{DM} = \sqrt{\frac{n_f . k_{C1} . u_g^2 . \sqrt[2]{Att_{req}}}{2(n_f + 1) . (k_{L1} . I_g^2 + k_{L2}) . (2\pi f_D)^2}} \tag{4-14}$$

The components of an EMI filter can be computed only with few equations regarding appropriate phase shifts. Moreover, two cases are provided with various phase-shifts, such as conventional case, 180o, and unconventional case, 45o, selected from Table 4-1 according to f_{sw} = 37.5 kHz for 2-unit interleaved. And, Table 4-2 gives the obtained results of the two cases that include the attenuation requirements and corner frequency [J2]. The phase-shift of '45º' is required to get a reduced filter attenuation in Band-B, and a phase-shift of '180º' requires a larger filter attenuation. As given Table 4-2 in the unconventional/conventional phase-shifts have numerous

advantages, including the reduced size of EMI filter in Band-B and Band-A, respectively [J2].

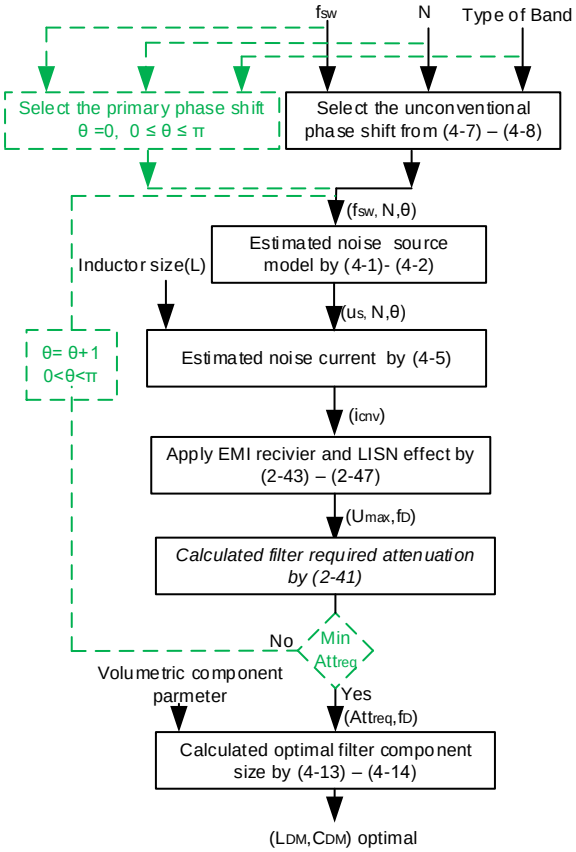

***Fig. 4.5**: Flowchart of an optimum boxed-volume related to DM EMI filter [J2].*

***Table 4-2:** EMI Filter Design in Band-A and B on the basis of Simulations Carried Out in PLECS for Standard Case (180º) and Unconventional Phase-Shift (45º) [J2].*

Type of the Band	Phase shift	L_{boost} [mH]	Δi_L [%]	f_D [kHz]	Att_{req} [dB]	L_{DM} [µH]	C_{DM} [nF]	V_{tot} [cm^3]
B	180º			150	41.5	40	150	41.5
	45º	4.3	22	187.5	30.4	23	90	**34.86**
A	180º			75	39.77	75	293	**54.4**
	45º			37.5	21.6	90	350	59.7

***Table 4-3**: Detailed Specifications for experimental Case Studies [J2].*

Symbol	Definition	Value	Unit
u_g	Grid side's voltage	230	Vrms
f_g	Grid side's frequency	50	Hz
L	Boost inductor	2	mH
f_{sw}	Switching frequency	20	kHz
C_{dc}	Output capacitor	500	µF
U_{dc}	Output voltage	400	V
P_o	Power	2	kW
$\Delta V_{dc,max}$	Ripple output voltage	20	V
$\Delta i_{L,max}$	Ripple of inductor current	20	%
θ	Phase shift	0,90,180	degree (°)

4.2.5. Results for Interleaved Units

In order to validate the simulation results, a 2-unit interleaved boost PFC rectifier operating in CCM is regarded as an experimental case, shown in Fig. 4.1. The needed data are provided briefly in Table 4-3. A lab setup comprising of a LISN, an EMI receiver, and the 2-unit interleaved converter, is regarded to substantiate theories with practical implementations. A reduced single-phase interleaved boost PFC converter prototype, shown in Fig. 4.7, is employed to validate the suggested technique. Moreover, the simulation model is implemented in PLECS. Moreover, the sampling frequency for computer simulations and experiments is 100 kHz [J2]. Fig. 4.6 illustrates the obtained computer simulation and experimental results comparatively for a 2-unit interleaved having $\theta = 0°, 90°, 180°$ [C2], [J2]. Obviously, from Fig. 4.6(b), the results obtained by experiments are validated via simulations with regard to the conventional phase-shifts between different units. The 1st order harmonics occur in $2f_{sw}$ in comparison with the case of $\theta = 180°$ within higher frequencies. Evidently, the suggested analytical model is able to accurately match with the experiments, and the highest error values in Band-A and Band-B are below 1.3 dB[J2] for all phase-shifts. So, the analytical modeling technique is verified for various phase-shifts and is applied by numerous interleaved parts.

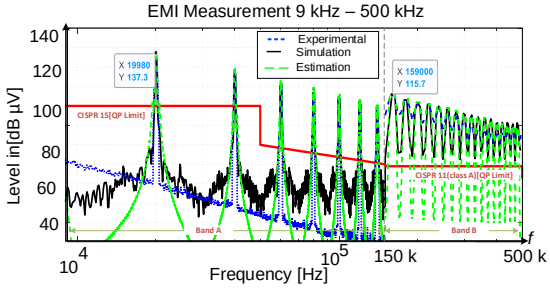

(a) θ = 0°

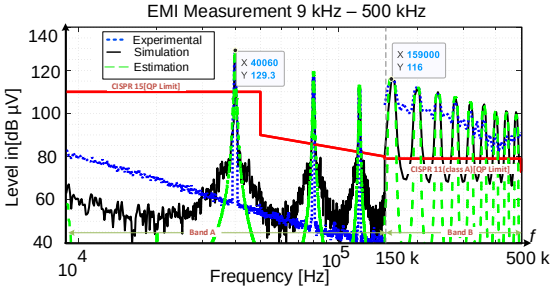

(b) θ = 180°

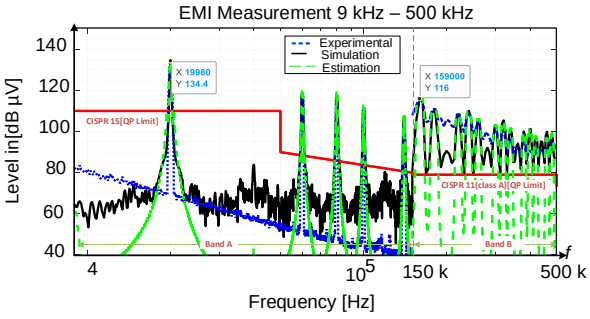

(c) θ = 90°

***Fig. 4.6**: EMI measurements for 2-unit interleaved boost PFC converter [C2], [J2].*

4.3. The Aggregated Noise Model for Unsynchronized Multi-Converters System

4.3.1. Interaction Noise Current

Fig. 4.8 (a) shows a block-diagram related to the system of study, comprising of a single-phase bipolar VSI, an EMI receiver, a LISN, and an EMI filter. In order to investigate the interaction among various aggregated PV inverters, an analytical model is explained for a single-phase inverter. The major concept of the presented

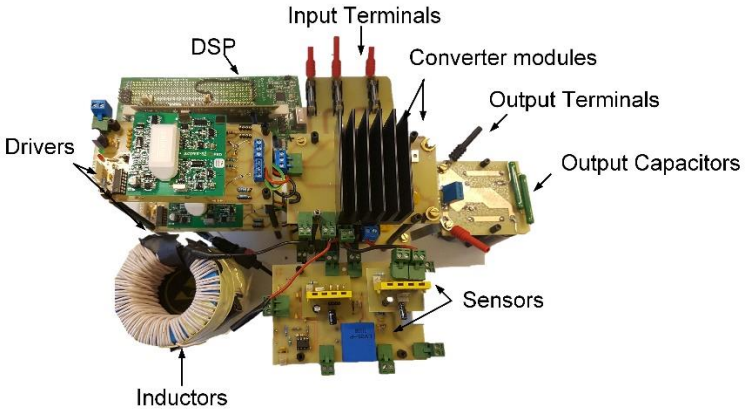

***Fig. 4.7**: Experimental prototype related to two single phase interleaved boost PFC converters [J2].*

technique is developing a Norton equivalent circuit model for PE converters. Thus, the models of a noise source as well as the related closed-loop admittance are presented to get an equivalent circuit for the PE converter for frequency behavior studies. The model is presented for the PV single phase application by the (2-19) and (2-29). When numerous converters produced by the similar manufactures are integrated into one point, there would typically be negligible differences among the switching frequencies that is due to fluctuations at the time of production and under different environmental conditions. It may lead to a remarkable influence on the behavior of a noise current at PCC for the PE converters. Thus, the suggested model is employed to investigate the frequency interaction among various aggregated units. This model is developed to cover the frequency behavior of N units. Fig. 4.9 depicts the Norton equivalent circuit related to N-unit VSI considering the EMI receiver and LISN. According to the standard requirements, a LISN is necessary for DM EMI noise measurements (Fig. 4.9). Because it is able to present a constant impedance and decouple the device under test (DUT) from the power grid. Obviously, Fig. 4.9 depicts the highly effected LISN impedance by the noise measurement with regard to the current division among various units. The noise current related to each unit is shared between the LISN and other units considering the corresponding impedances. So, the relation (4-15) represents the current flowing into the LISN originating from all various units that is important in EMI measurements and may be computed as:

$$i_{cnv} = \sum_{j=1}^{j=N} \frac{\dfrac{1}{Y_{o,cnv}}}{\dfrac{1}{Y_{o,cnv}} + \left(\dfrac{1}{Y_{o,cnv}(N-1)} \| Z_{LISN}\right)} \frac{\dfrac{1}{Y_{o,cnv}(N-1)}}{Z_{LISN} + \dfrac{1}{Y_{o,cnv}(N-1)}} i_{cnv(j)} \quad (4\text{-}15)$$

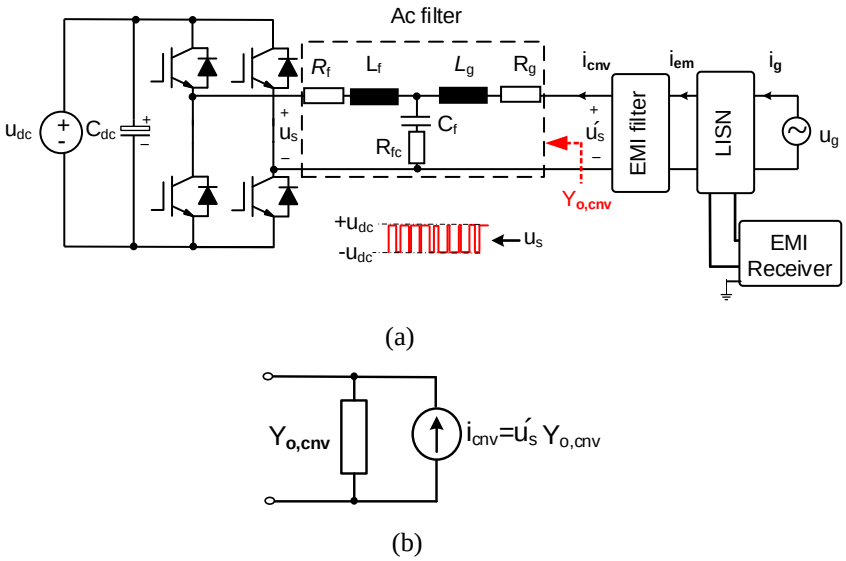

Fig. 4.8*: VSI structure and its model a) General topology of a single-phase VSI comprising of an EMI receiver, LISN and an EMI filter. b) VSI Norton equivalent circuit model [J3].*

where, Z_{LISN} denotes the LISN input impedance, N denotes the number of units, $i_{cnv(j)}$ denotes the current model of a noise related to unit # *j*. An analytical formulation related to input impedance (Z_{LISN}) of a LISN is calculated by:

$$Z_{LISN(IN)} = (2(L_2 s \| R_2 + \frac{1}{C_2 s}) + 2L_1 s) \| 2(R_1 + \frac{1}{C_1 s}) \tag{4-16}$$

The consideration of the LISN in noise measurement creates circulating currents among various units. The LISN impedance may be substituted by power grid impedance once the LISN is removed. However, the LISN or grid impedance results in some reverse current flowing back into units. In this research, the LISN impedance considered as a worst case in the units' interaction is taken into account for analysis. The LISN impedance is high and influences the current flowing to network as well as interaction current regarding (4-15) and (4-17). So, the circulating current among various units is obtained by:

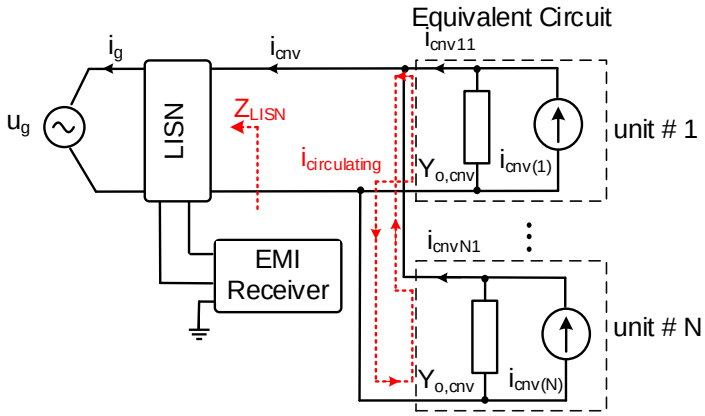

***Fig. 4.9**: Norton equivalent circuit related to N-unit VSI considering LISN and EMI receiver [J3].*

$$i_{\text{circulating}} = \frac{\dfrac{1}{Y_{o,cnv}}}{\dfrac{1}{Y_{o,cnv}} + \left(\dfrac{1}{Y_{o,cnv}(N-1)} \| Z_{LISN}\right)} i_{cnv(1)} - \sum_{\substack{j=1 \\ j\neq n}}^{j=N} \frac{\dfrac{1}{Y_{o,cnv}}}{\dfrac{1}{Y_{o,cnv}} + \left(\dfrac{1}{Y_{o,cnv}(N-1)} \| Z_{LISN}\right)} \frac{Z_{LISN}}{Z_{LISN} + \dfrac{1}{Y_{o,cnv}(N-1)}} i_{cnv(j)} \quad (4\text{-}17)$$

As the suggested technique is on the basis of analytical equations, a study regarding the impact of the beating frequency as well as unsynchronized switching frequency on the aggregated PVs is needed. The aggregated model is verified via simulation results given schematically in Fig. 4.10. Fig. 4.11 depicts the obtained results of modeling the interaction current regarding (4-16) and (4-17) obtained by simulations implemented for a two-unit mode provided in the Table 4-4. The switching frequency tolerance of converter influences the harmonics' RMS currents in an emission band named a beat. Thus, the beating effects may reduce the harmonic currents circulating around the grid by addition of units. So, the switching frequency tolerance is modeled via a continuous uniform random number in the interval of [-10 to +10] in order to analyze the beating effects.

***Table 4-4**: Practical Specifications of a Case Study for an PV inverter [J3].*

Symbol	Definition	Values
U_g	Grid side voltage (V)- peak vlaue	230
f_g	Grid side's frequency (Hz)	50
f_{sw}	Switching Frequency (kHz)	20
f_s	Sampling Frequency (kHz)	100
U_{dc}	Dc-Link Voltage (V)	360
P_o	Power (kW)	3
L_f	Converter-side inductor (mH)	2.5
L_g	Grid-side inductor (µH)	250
R_{fc}	Damping resistance (Ω)	8
C_f	Reactive capacitor (µF)	8
λ_{h}	Harmonic factor	0.3

Accordingly, Table 4-5 presents the switching frequency tolerance obtained for each unit. The frequency switching related to each unit should be sum of the obtained tolerances in order to get the primary frequency switching. Thus, there exist various noise voltage sources with regard to different frequencies for f_{sw}. Fig. 4.11 shows the RMS current of the noise flowing into the LISN (or, network current) and circulating current between the units. It should be mentioned that; the reversed current value is on the basis of the number of units. The obtained results are based upon the resulting analytical model. The measurement bandwidth is 400 Hz for the first emission band (i.e., 20 kHz). Clearly, the beating effects results in a decreased current flowing into the network that is critical for designing an EMI filter. Thus, the current flowing among *N* units would likely raises by an increase in the number of units.

***Table 4-5**: Frequency switching tolerance for a 10-unit single-phase VSI inverter [J3].*

Unit No.	1	2	3	4	5	6	7	8	9	10
Frequency deviation (Hz)	0	6	-4	1	-7	2	-5	3	4	5

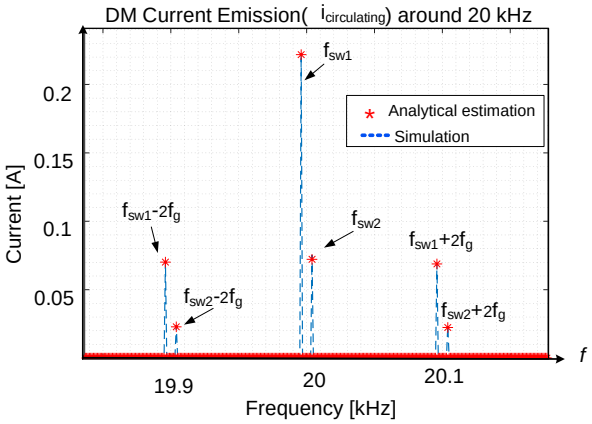

***Fig. 4.10**: Circulating current between the two units VSI ($i_{circulating}$) (f_{sw1}=19996 & f_{sw2}=20004) [J3].*

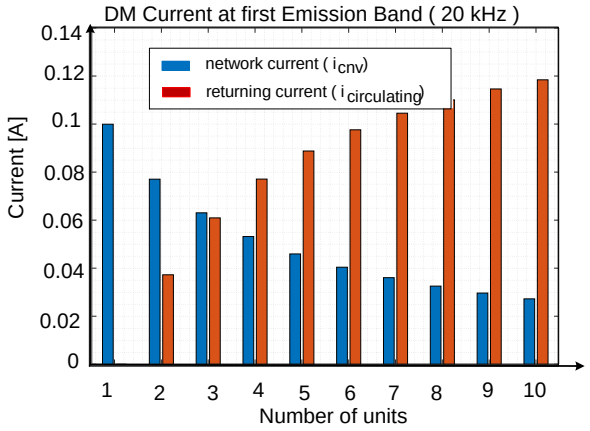

***Fig. 4.11**: RMS current of the Noise flowing into LISN and reversed current based upon the number units within the first emission band [J3].*

4.3.2. EMI Filter Effects on the Noise Current Interaction

As we discussed before, the major goal of design is to structure a valid filter that is able to constrain the EMI level within the recommended standards. In the next step, the EMI filter effects on interaction current between the units should be investigated. Fig. 4.12 shows CL and π topologies of a symmetrical DM EMI filter with regarding a damping stage and a filter stage. The design process of a CL and π filters is explained in [81], respectively. The required attenuation of a filter, denoted by A_{ttreq}, is obtained from [J1]

$$A_{tt_{req}}(f)[dB] = U_{\max}(f)[dB\mu V] - CISPR_{\lim it}(f)[dB\mu V] + M\arg in[dB] \quad (4\text{-}18)$$

where U_{max} is the noise peak voltage estimated via the suggested analytical model. The value of $CISPR_{limit}$ is computed from the standards reported in [23], [25], [56]. The value of 6 dB is considered as a margin for designing an EMI filter. Moreover, the size of components related to one-stage LC EMI filter is obtained by

$$A_{tt}(f_{sweep}) \geq \frac{2L^2_{DM}C_{DM}(j2\pi f)^3 + 4L_{DM}R_{DM}C_{DM}(j2\pi f)^2 + L_{DM}(j2\pi f) + R_{DM}}{R_{DM} + L_{DM}(j2\pi f)} \quad (4\text{-}19)$$

$$= A_{tt_{EMI\_Filter}(f_{sweep})}$$

Afterwards, designing a π filter is similar to that of the CL filter. However, the attenuation value with network capacitor (C_{DM2}) is considered in combination with an input impedance of the LISN (4-16) and it should present the attenuation quantity of $A_{ttCDM2}[dB] = A_{ttreq}[dB] - A_{ttsec1}[dB]$ at the frequency of 20 kHz. Hence, this characterizes C_{DM2} straightforwardly. Once the EMI filter is added, the Norton current needs to be updated via Middlebrook extra element theory. More information with regard to the updated modeling via the Middlebrook extra element theory are reported in [71]. So, the Norton current utilizing the CL EMI filter is computed by

$$i_{em}(s) = \frac{Z_{C_{DM}}}{2(Z_{L_{DM}} + \frac{R_{DM}.Z_{L_{DM}}}{R_{DM} + Z_{L_{DM}}}) + Z_{C_{DM}}} \cdot \frac{Y_{oFo}}{Y_{oFo} + Y_{o,cnv}} . i_{cnv} \quad (4\text{-}20)$$

where Y_{oFo} with CL filter is obtained by

$$Y_{oFo}(s) = 1 \Big/ Z_{C_{DM}} \quad (4\text{-}21)$$

The input admittance employing the CL EMI filter is obtained via the Middlebrook theory by

$$Y_i(s) = Y_{iF} \cdot \frac{1 + \frac{Y_{o,cnv}}{Y_{oF\infty}}}{1 + \frac{Y_{o,cnv}}{Y_{oFo}}} \quad (4\text{-}22)$$

Here, $Y_{oF\infty}$ with CL filter is given by

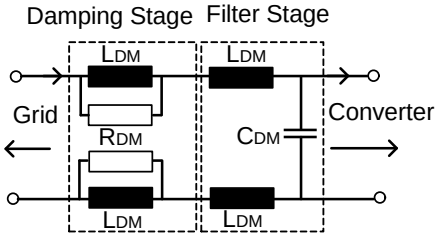

(a) CL

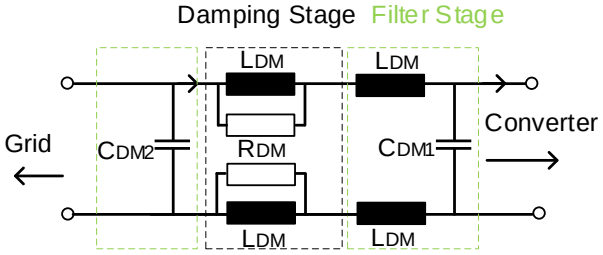

(b) π filter

***Fig. 4.12**: Considering single-stage DM EMI filter configuration including a damping stage [J3].*

***Table 4-6**: Specifications of one-stage CL and π EMI filters [J3].*

Type	A_{ttreq} [dB]	C_{DM1} [µF]	R_{DM} [Ω]	L_{DM} [µH]	C_{DM2} [nF]
CL	18.5	0.8	29.3	180	-
π (CLC)	18.5	0.68	29.3	180	130

$$Y_{oF\infty}(s) = \frac{1}{2(Z_{L_{DM}} + \frac{R_{DM}.Z_{L_{DM}}}{R_{DM} + Z_{L_{DM}}}) \| Z_{C_{DM}}} \tag{4-23}$$

where, Y_{iF} denotes the CL EMI filter's input admittance that can be presented by

$$Y_{iF}(s)=\frac{1}{2(Z_{L_{DM}}+\frac{R_{DM}.Z_{L_{DM}}}{R_{DM}+Z_{L_{DM}}})+Z_{C_{DM}}} \tag{4-24}$$

The Norton current utilizing the π EMI filter is achieved by

$$i_{em}(s)=\frac{Z_{C_{DM1}}}{2(Z_{L_{DM}}+Z_{C_{DM2}}+\frac{R_{DM}.Z_{L_{DM}}}{R_{DM}+Z_{L_{DM}}})+Z_{C_{DM1}}}.\frac{1/Y_C}{1/Y_C+1/Y_n}.i_{cnv} \tag{4-25}$$

For analyzing the interaction current in relations (4-15) and (4-17), $i_{conv(j)}$ needs to be substituted by i_{em} regarding the EMI filter. The input admittance utilizing the π EMI filter is computed by (4-22). Yet, Y_{oFo} for the π EMI filter is similar to the case of CL filter; however, $Y_{oF\infty}$ for π EMI filter would be updated by

$$Y_{oF\infty}=\frac{1}{2(Z_{L_{DM}}+Z_{C_{DM2}}+\frac{R_{DM}.Z_{L_{DM}}}{R_{DM}+Z_{L_{DM}}})\|Z_{C_{DM1}}} \tag{4-26}$$

The π EMI filter's input admittance is computed by

$$Y_{iF}(s)=\frac{1}{(2(z_{L_{DM}}+\frac{R_{DM}.z_{L_{DM}}}{R_{DM}+z_{L_{DM}}})+z_{C_{DM1}})\|z_{C_{DM2}}} \tag{4-27}$$

By substituting Y_i in (4-15) and (4-17) instead of the $Y_{o,\mathrm{cnv}}$, the interaction current along with the current flowing through the network via EMI filter is computed. On the other hand, EMI filter's various topologies considering varying quantity of admitance may influence the interaction current among the units.

4.3.3. Results for multi converter system

In order to validate the suggested modeling approach, totally 10 PV inverters are integrated to a similar PCC (See Fig. 4.9). Table 4-4 gives the specifications of applied system for each unit. Additionally, the switching frequency is obtained via including the tolerance of factory frequency presented in Table 4-5. Simulations are implemented in PLECS to investigate the effectiveness of modeling technique. Fig. 4.13 depicts the RMS current value related to the noise flowing through LISN (network current) for both unsynchronized and synchronized cases with regard to the number of units in the first emission band via the analytical model. Clearly from Fig. 4.13, the noise current

flowing into the network decreases in unsynchronized case considering the beating effects; however, it increases in synchronized case. It is revealed that the analytical model is able to estimate/analyze the super-harmonic emission and the given interaction among various units within the frequency range of 2–150 kHz [J3]. Moreover, beating effects are increasing by addition of units. Additionally, the first emission band includes the switching frequency with regard to the bandwidth '400 Hz.' Thus, the beating impacts lead to a decreased level of noise current flowing through the network and reversing back to the converter by addition of units in the synchronized case. More importantly, Fig. 4.14 depicts the EMI estimation for both unsynchronized and synchronized cases with regard to the number of units available in the first emission band. As seen in Fig. 4.14, the EMI level declines by the addition of units in the unsynchronized case study because of beating effects. On the other hand, the attenuation required by the filter declines due to lower EMI levels.

As mentioned earlier, the interaction current depends upon the LISN input admittance and output converter admittance. Thus, EMI filter design may have an impact on the interaction current due to variation in the behavior of admittance frequency and noise source. So, two types of EMI filters (i.e., CL and π) are devised with regard to the same attenuation requirements for the converter of interest. Fig. 4.15 illustrates the RMS current value related to the noise flowing into the power grid based upon the number of units for both π and CL filters in an unsynchronized case. As illustrated in Fig. 4.15 , the current flow into the grid is larger for the π case study compared to the CL filter.

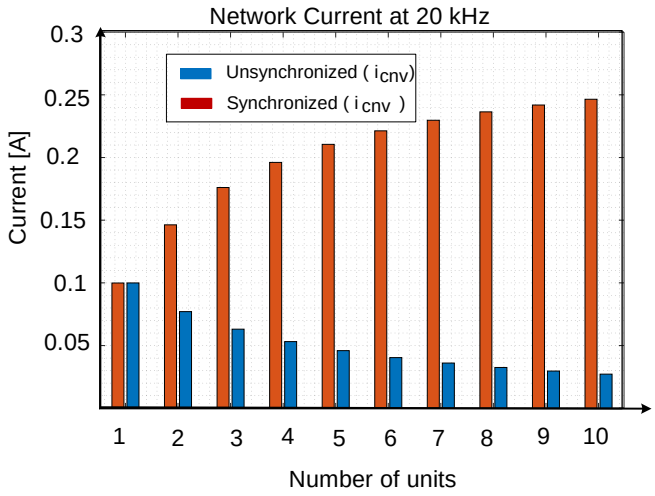

***Fig. 4.13**: RMS current of the Noise flowing into LISN and unsynchronized /synchronized based upon the number of units in the first emission band [J3].*

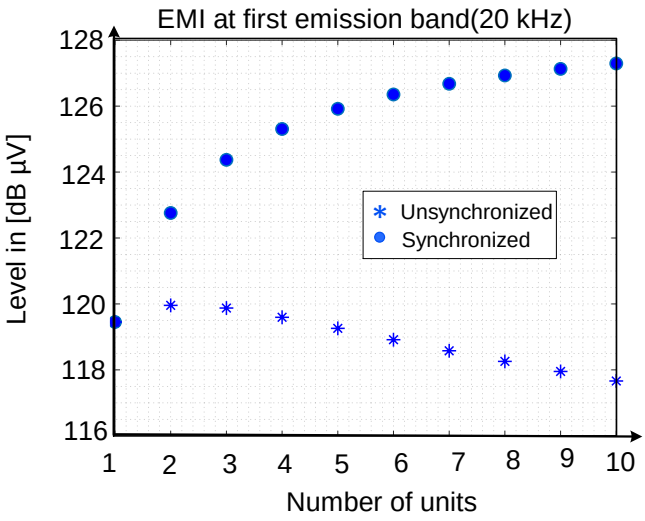

***Fig. 4.14**: EMI estimation for both case studies based upon the number of units existing in the first emission band 20 kHz [J3].*

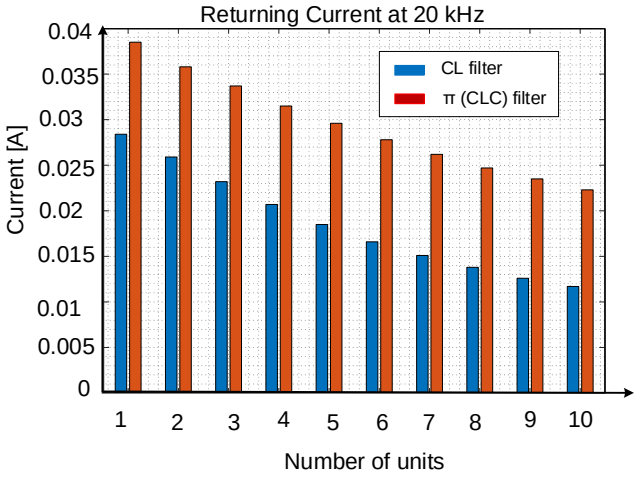

***Fig. 4.15**: RMS noise current through to the network side for unsynchronized based on the number units in first emission band for π and CL filter. Results are based on the analytical model [J3].*

Accordingly, the interaction current may fall in between different units by varying the filter topology. At the end, the obtained results demonstrated that the interaction impacts on the aggregated units are related to the topology of an EMC filter.

4.4. summary

This chapter investigated the effect of unconventional selective phase-shift on optimized EMI filter for two frequency bands of Band-A (i.e., 9-150 kHz) and Band-B (i.e., >150 kHz). The obtained results within Band-A demonstrated that the presented interleaved configuration has numerous advantages, leading to the likelihood of using no filter for frequencies beyond 75 kHz, 50 kHz, and 37.5 kHz for two-, three-, and four-unit modes. Moreover, in Band-B, the conventional phase-shifts between different units were not much effective for all frequencies. So, various phase-shifts (unconventional) were utilized to obtain a larger corner frequency and a smaller size for filters in Band-B [J3]. Interestingly, the suggested technique was employed in order to model the level of noise considering higher accuracies at various phase-shifts in order to design a DM EMI filter. Moreover, this research work highlighted the merits of employing the conventional phase-shifts in Band-A to eliminate the odd harmonics in order to get optimized attenuation requirements for designing an EMI filter [J3]. Ultimately, filter volume optimization was employed to minimize component size via an analytical approach and phase-shifts selection. So, a general technique on the basis of the analytical equation regarding the phase-shift was utilized to get an optimized EMI filter volume. Results of experiments validated the EMI analytical approach regarding various phase shifts in Band-A and Band-B, and the related maximized errors are less than 1 dB. Moreover, in this research, a single-phase VSI estimation related to DM EMI noise was detailed based upon an analytical model, the EMC receiver, and the LISN. The obtained model was developed to include N number of units. However, it also presented the likelihood of investigating the interaction currents flowing through the units. The analytical technique defines the effective parameters for reduction of the system-level analysis. The model was obtained for two he unsynchronized / synchronized cases among various units. In addition, it was determined that beating effects decreased the current flowing through the grid in unsynchronized case. In the unsynchronized case, good performance was achieved to reduce the EMI level in comparison to the synchronous case. In order to meet the standard requirements and decrease the interaction, various EMI filter topologies were investigated based upon the attenuation requirements of the filter. The π EMI filter was able to lower the interaction current compared to CL EMI filter. Ultimately, a proper design of EMI filter to obtain a reduced interaction among different units and, thus, the LISN impedance is viable through the interaction analysis.

Chapter 5. Conclusion

This chapter outlines the main conclusions and finding in this Ph.D. thesis. The main contributions presented in this thesis are highlighted, and the future research work and perspectives are discussed.

5.1. Summary

In this Ph.D. project, the main focus is modeling and characterizing the low-frequency EMI within the frequency range of 2-150 kHz [J1]. The EMI modeling in single and three-phase power converters has been developed. Mitigation techniques by EMI filter design have also been presented to fulfill relevant standard requirements. Multi-converter systems noise propagation analysis based on an aggregated model for a multi-parallel connected converter system has been discussed. A brief summary of this Ph.D. thesis is as follows.

In Chapter 1, the research background and the importance of low-frequency range emission in PE- based system have been identified. In low-frequency EMI, the noise propagation issue is one of the major concerns, which needs to be addressed. Many simulation-based models and mitigation techniques have presented above 150 kHz considering the complex behavior of noise propagation. Moreover, important EMI issues in the new frequency range are addressed in this chapter. There is no systematic study in the literature about noise propagation in low frequency range.

Chapter 2 provided a complete analytical time-frequency domain technique which estimates single-phase PE converter generated emission. The proposed analytical approach estimated the generation low-frequency emission on the basis of double Fourier analysis combined with closed loop impedance/admittance of power converter. Closed-loop impedance and admittance's behavior are analyzed to characterize the shunting effect of power converter impedance on the generated emissions. Consequently, a simplified estimation of a closed-loop impedance and admittance in order to use in the multi-converter systems analysis is achieved. A proper one-stage DM EMI filter is designed to fulfill standard requirements, and Middlebrook's extra element theorem [71] is utilized to incorporate the effect of EMI filter on the developed model. Conventional analytical estimating techniques, simulation, and experimental results are considered for a comparative analysis to assess the proposed modeling technique's effectiveness. An analytical method is implemented on the single-phase boost PFC and voltage source inverter.

In Chapter 3, the DM EMI analytical approach is extended to the three-phase application, including active rectifier and voltage source inverter. An accurate and computationally efficient model capable of characterizing a low-frequency EMI model for three-phase converters is presented. Simplified estimation for the closed-loop input impedance in an active rectifier and the closed-loop output admittance in a voltage source inverter above 9 kHz is achieved. A proper two-stage EMI filter is designed for the three-phase active rectifier to limit the noise level under the standard limitation.

Finally, the efficiency of the proposed method is validated by experiment and simulation in a three-phase inverter.

Up to this point, all the models and analysis presented consider only a single power converter with either single-phase or three-phase structure. Chapter 4 comprises of two parts, focused on multi-converter configuration considering the effect of synchronized and unsynchronized operation of power converters on the generate emissions below 150 kHz frequency range. The first part extends the time-frequency DMI EMI approach for the interleaving boost PFC units (i.e., synchronized operation). The proper selection of switching frequency and the number of interleaved units to have lower filter attenuation are discussed. Experimental results validate the noise propagation relationship with phase shift in two interleaved units. The DM EMI filter volume optimization is done by considering the phase shift effects on the interleaved units. The second part analyzes the interaction current among the power converter units. Analytical aggregated noise models for multi-parallel unsynchronized/synchronized converters are presented. The effect of the EMI filter topologies on the interaction current between units is investigated.

5.2. Main Contributions of Thesis

The main contributions of this Ph.D. project are summarized as follows:

- **Proposed a time-frequency analytical modeling approach for DM EMI noise of single-phase power converters for the frequency range of 2-150 kHz [J1]**.
  - A computationally efficient model capable of characterizing a DM noise in single-phase boost PFC and inverter with two kinds of modulation, including bipolar and unipolar was proposed [J1], [C1].
  - Developed and analyzed the influencing parameter on input closed-loop impedance for boost PFC and output closed-loop admittance for the inverter to get the simplified model to use in the multi-converter systems analysis.
  - Proper single-stage EMI filters to fulfill the standard requirement were designed and the influence of the EMI filter in the proposed analytical model was included using Middlebrrok extra element theorem.
  - A comprehensive comparison between the prior-art and the proposed method is implemented and validated by simulation and experimental results
- **Proposed time-frequency analytical modeling approach for DM EMI noise of three-phase power converters [C3].**
  - Achieved the accurate analytical DM EMI proposed approach to estimate the DM EMI noise in the frequency range under 150 kHz.
  - Closed-loop input impedance for the rectifier and output admittance for the inverter can be estimated by the ac filter input impedance and output admittance in the frequency range above 9 kHz, respectively.

- Designed the two-stage three-phase EMI filter to limit the peak noise level under the standard requirement for the three-phase active rectifier.

❖ **Analysis and modeling of EMI noise in multi-converter Systems and interleaved units**

- Extended the analytical DM EMI noise analytical approach to the interleaved units by considering the phase shift effects.
- Different phase shift effects on the EMI filter volume optimization are investigated. DM EMI filter size can be reduced by interleaving the units.
- Aggregated EMI models under 2-150 kHz for multi-converter Systems.
- The interaction model between the units was obtained for two unsynchronized/synchronized cases among various units.

5.3. Research Perspectives and Future Work

This Ph.D. project suggested the new analytical differential mode noise estimation in different single-phase and three-phase applications to improved EMI filter designing and characterizing the influence parameter to use in the system-level analysis. However, there are still some other challenges that are worth researching, as noted in the following.

- This Ph.D. project focuses on DM mode noise analytical approach and design DM EMI filter. It could be extended to CM noise modeling and the corresponding filter design.
- The PhD research is limited to the case studies of single-phase and three-phase converters with typical SPWM modulation methods. The proposed modeling approaches can be extended to other topologies and modulation methods.
- One of the Ph.D. project's purposes is using the analytical DM EMI noise approach on the EMI filter designing to fulfill the standard requirement. But the EMI filter designed for the new frequency range (i.e., < 150 kHz frequency range) increase the filter size due to shifting the filter corner frequency to lower frequency ranges [C3]. Therefore, it is worth looking at other mitigation methods, such as the dithering technique to reduce the EMI noise and consequently EMI filter size.
- EMI performance degradation due to filter component aging is not considered in this study. It is worth studying the impact of inductance and capacitance reduction of the filter components on the EMI noise level.
- This Ph.D. project focuses on the interaction between the units. Therefore, by applying the developed model, the interactions between various PE converters and the corresponding effects on a low-frequency EMI are studied as the main focus of this research. Moreover, it is found that design of the proper EMI

filter can be affected by the interacting currents. Currently, no solution is proposed for the system-level mitigation techniques. Hence, it is worth investigating to find the EMI filter design guideline for all units regarding the worst-case scenario.

References:

[1] G. F. Bartak and A. Abart, “EMI of emissions in the frequency range 2 kHz–150 kHz,” in *22nd International Conference and Exhibition on Electricity Distribution (CIRED 2013)*, 2013, pp. 1–4.

[2] M. Kasper, D. Bortis, and J. W. Kolar, “Classification and Comparative Evaluation of PV Panel-Integrated DC–DC Converter Concepts,” *IEEE Trans Power Electron*, vol. 29, no. 5, pp. 2511–2526, May 2014.

[3] J. Deng, S. Li, S. Hu, C. C. Mi, and R. Ma, “Design Methodology of LLC Resonant Converters for Electric Vehicle Battery Chargers,” *IEEE Trans Veh Technol*, vol. 63, no. 4, pp. 1581–1592, May 2014.

[4] B. Lee, J. Kim, S. Kim, and J. Lee, “A PWM SRT DC/DC Converter for 6.6-kW EV Onboard Charger,” *IEEE Trans Ind Electron*, vol. 63, no. 2, pp. 894–902, Feb. 2016.

[5] IEC. T.-E. 61000-3-10, “Emission limits in the frequency range 2 ... 9 kHz,” 2023.

[6] IEC 61000-6-3:2020, “Electromagnetic compatibility (EMC) - Part 6-3: Generic standards - Emission standard for equipment in residential environments,” p. 52, 2020.

[7] IEC. 61000-2-2:2002, “Electromagnetic compatibility (EMC) - Part 2-2: Environment - Compatibility levels for low-frequency conducted disturbances and signalling in public low-voltage power supply systems,” vol. Part 2-2, p. 57, 2002.

[8] IEC. 61000-2-4, “Electromagnetic compatibility (EMC) - Part 2-4: Environment - Compatibility levels in industrial plants for low-frequency conducted disturbances,” vol. Part 2-4, p. 75, 2002.

[9] E. O. A. Larsson, M. H. J. Bollen, M. G. Wahlberg, C. M. Lundmark, and S. K. Rönnberg, “Measurements of High-Frequency (2–150 kHz) Distortion in Low-Voltage Networks,” *IEEE Trans Power Deliv*, vol. 25, no. 3, pp. 1749–1757, Jul. 2010.

[10] S. Schöttke, J. Meyer, P. Schegner, and S. Bachmann, “Emission in the frequency range of 2 kHz to 150 kHz caused by electrical vehicle charging,” in *2014 International Symposium on Electromagnetic Compatibility*, 2014, pp. 620–625.

[11] D. Heirman, “EMC standards activity,” *IEEE Electromagn Compat Mag*, vol. 9, no. 2, p. 78, 2020.

[12] IEC TS 62578, “Power electronics systems and equipment - Operation conditions and characteristics of active infeed converter (AIC) applications including design recommendations for their emission values below 150 kHz.” p. 240, 2015.

[13] Cigre, “Assessment of conducted disturbances above 2 kHz in MV and LV power systems, Reference: 799,.” p. 86, 2020.

[14] S. R. C. 50627 Irish Standard Recommendation, “No Title,” *Study Rep Electromagn Interf between Electr Equipment/Systems Freq Range Below 150kHz*, p. 88, 2015.

[15] P. Davari, F. Blaabjerg, E. Hoene, and F. Zare, “Improving 9-150 kHz EMI Performance of Single-Phase PFC Rectifier,” in *CIPS 2018; 10th International Conference on Integrated Power Electronics Systems*, 2018, pp. 1–6.

[16] I. Fernandez *et al.*, “Characterization of non-intentional emissions from distributed energy resources up to 500 kHz: A case study in Spain,” *Int J Electr Power Energy Syst*, vol. 105, pp. 549–563, 2019.

[17] H. Bishnoi, A. C. Baisden, P. Mattavelli, and D. Boroyevich, “Analysis of EMI Terminal Modeling of Switched Power Converters,” *IEEE Trans Power Electron*, vol. 27, no. 9, pp. 3924–3933, 2012.

[18] J. Espina, J. Balcells, A. Arias, C. Ortega, and N. Berbel, “EMI model of an AC/AC power converter,” in *2010 IEEE Vehicle Power and Propulsion Conference*, 2010, pp. 1–6.

[19] D. O. Boillat, F. Krismer, and J. W. Kolar, “EMI Filter Volume Minimization of a Three-Phase, Three-Level T-Type PWM Converter System,” *IEEE Trans Power Electron*, vol. 32, no. 4, pp. 2473–2480, Apr. 2017.

[20] M. Hartmann, H. Ertl, and J. W. Kolar, “EMI Filter Design for a 1 MHz, 10 kW Three-Phase/Level PWM Rectifier,” *IEEE Trans Power Electron*, vol. 26, no. 4, pp. 1192–1204, Apr. 2011.

[21] F. Yang, X. Ruan, Q. Ji, and Z. Ye, “Input Differential-Mode EMI of CRM Boost PFC Converter,” *IEEE Trans Power Electron*, vol. 28, no. 3, pp. 1177–1188, Mar. 2013.

[22] H. Huang, L. Deng, B. Hu, and G. Wei, “Techniques for Improving the High-Frequency Performance of the Planar CM EMI Filter,” *IEEE Trans Electromagn Compat*, vol. 55, no. 5, pp. 901–908, Oct. 2013.

[23] C.I.S.P.R., “Electromagnetic compatibility - Requirements for household appliances, electric tools and similar apparatus - Part 1: Emission,” vol. 14, p. 112, 2020.

[24] C.I.S.P.R., “Specification for radio disturbance and immunity measuring apparatus and methods - Part 1-1: Radio disturbance and immunity measuring apparatus - Measuring apparatus,” vol. 16, no. 195, 2021.

[25] C.I.S.P.R., “Limits and methods of measurement of radio disturbance characteristics of electrical lighting and similar equipment Interference,” vol. 15, p. 300, 2018.

[26] P. Kotsampopoulos *et al.*, “EMC Issues in the Interaction Between Smart Meters and Power-Electronic Interfaces,” *IEEE Trans Power Deliv*, vol. 32, no. 2, pp. 822–831, Apr. 2017.

[27] S. P. Klatt. M, Stiegler.P, Meyer.J, “Generic frequency-domain model for the emission of PWM-based power converters in the frequency range from 2 to 150 kHz,” vol. 13, no. 24, pp. 5478–5486, 2019.

[28] K. Raggl, T. Nussbaumer, and J. W. Kolar, “Guideline for a Simplified Differential-Mode EMI Filter Design,” *IEEE Trans Ind Electron*, vol. 57, no. 3, pp. 1031–1040, Mar. 2010.

[29] A. Ganjavi *et al.*, “Common-Mode Current Prediction and Analysis in Motor Drive Systems for the New Frequency Range of 2–150 kHz,” *IEEE J Emerg Sel Top Power Electron*, p. 1, 2020.

[30] S. Johnson and R. Zane, “Custom spectral shaping for EMI reduction in high-frequency inverters and ballasts,” *IEEE Trans Power Electron*, vol. 20, no. 6, pp. 1499–1505, Nov. 2005.

[31] J. Biela, A. Wirthmueller, R. Waespe, M. L. Heldwein, K. Raggl, and J. W. Kolar, “Passive and Active Hybrid Integrated EMI Filters,” *IEEE Trans Power Electron*, vol. 24, no. 5, pp. 1340–1349, May 2009.

[32] S. Tan *et al.*, “Switched-capacitor converter configuration with low EMI emission obtained by interleaving and its large-signal modeling,” in *2009 IEEE International Symposium on Circuits and Systems (ISCAS)*, 2009, pp. 1081–1084.

[33] IEC. 61000-3-2, “Electromagnetic compatibility (EMC) - Part 3-2: Limits - Limits for harmonic current emissions (equipment input current ≤16 A per phase),” vol. Part 3-2, p. 73, 2018.

[34] V. Madonna, G. Migliazza, P. Giangrande, E. Lorenzani, G. Buticchi, and M. Galea, “The Rebirth of the Current Source Inverter: Advantages for Aerospace Motor Design,” *IEEE Ind Electron Mag*, vol. 13, no. 4, pp. 65–76, Dec. 2019.

[35] A. Elrayyah, K. MPK Namburi, Y. Sozer, and I. Husain, “An Effective Dithering Method for Electromagnetic Interference (EMI) Reduction in Single-Phase DC/AC Inverters,” *IEEE Trans Power Electron*, vol. 29, no. 6, pp. 2798–2806, Jun. 2014.

[36] F. Mihali and D. Kos, “Reduced Conductive EMI in Switched-Mode DC–DC Power Converters Without EMI Filters: PWM Versus Randomized PWM,” *IEEE Trans Power Electron*, vol. 21, no. 6, pp. 1783–1794, Nov. 2006.

[37] F. Mihalic and D. Kos, “Conductive EMI reduction in DC-DC converters by using the randomized PWM,” in *Proceedings of the IEEE International Symposium on Industrial Electronics, 2005. ISIE 2005.*, 2005, vol. 2, pp. 809–814 vol. 2.

[38] A. Elrayyah, K. Mpk Namburi, Y. Sozer, and I. Husain, “An effective dithering method for electromagnetic interference (EMI) reduction in single-phase DC/AC inverters,” *IEEE Trans Power Electron*, vol. 29, no. 6, pp. 2798–2806, 2014.

[39] J. Balcells, A. Santolaria, A. Orlandi, D. Gonzalez, and J. Gago, “EMI reduction in switched power converters using frequency Modulation techniques,” *IEEE Trans Electromagn Compat*, vol. 47, no. 3, pp. 569–576, Aug. 2005.

[40] S. Johnson and R. Zane, “Custom spectral shaping for EMI reduction in high-frequency inverters and ballasts,” *IEEE Trans Power Electron*, vol. 20, no. 6, pp. 1499–1505, 2005.

[41] X. Zhang, D. Boroyevich, and R. Burgos, “Impact of interleaving on common-mode EMI filter weight reduction of paralleled three-phase voltage-source converters,” in *2013 IEEE Energy Conversion Congress and Exposition*, 2013, pp. 1669–1675.

[42] M. B. and J. S. S. Rönnberg, A. Larsson, “A simple model for interaction between equipment at a frequency of some tens of kHz,” *CIRED Conf*

Proceedings, vol. ISSN 2032-, 2011.

[43] T. Slangen, T. van Wijk, V. Ćuk, and S. Cobben, "The Propagation and Interaction of Supraharmonics from Electric Vehicle Chargers in a Low-Voltage Grid," *Energies*, vol. 13, no. 15, 2020.

[44] S. K. Ronnberg, M. Wahlberg, E. O. A. Larsson, M. H. J. Bollen, and C. M. Lundmark, "Interaction between equipment and power line Communication: 9-95 kHz," in *2009 IEEE Bucharest PowerTech*, 2009, pp. 1–5.

[45] D. D. Reljić, V. V Vasić, and D. V. Oros, "Power factor correction and harmonics mitigation based on phase shifting approach," in *2012 15th International Power Electronics and Motion Control Conference (EPE/PEMC)*, 2012, p. DS3b.12-1-DS3b.12-8.

[46] Y. Onal and Y. Sozer, "Bridgeless SEPIC PFC converter for low total harmonic distortion and high power factor," in *2016 IEEE Applied Power Electronics Conference and Exposition (APEC)*, 2016, pp. 2693–2699.

[47] P. Chaudhary and M. Rizwan, "A predictive current control for solar PV fed VSI in distribution system," in *2017 IEEE International Conference on Environment and Electrical Engineering and 2017 IEEE Industrial and Commercial Power Systems Europe (EEEIC / I CPS Europe)*, 2017, pp. 1–7.

[48] A. Yadav, J. Patra, N. Pal, and H. Gupta, "Performance analysis of VSI based standalone PV generation system connected to induction motor," in *2018 4th International Conference on Recent Advances in Information Technology (RAIT)*, 2018, pp. 1–6.

[49] F. H. M. Rafi, J. Hossain, and J. Lu, "PV microgrid islanded operation analysis with the designed smart VSI," in *2015 IEEE 10th Conference on Industrial Electronics and Applications (ICIEA)*, 2015, pp. 632–637.

[50] S. Samerchur, S. Premrudeepreechacharn, Y. Kumsuwun, and K. Higuchi, "Power control of single-phase voltage source inverter for grid-connected photovoltaic systems," in *2011 IEEE/PES Power Systems Conference and Exposition*, 2011, pp. 1–6.

[51] E. O. A. Larsson, M. H. J. Bollen, M. G. Wahlberg, C. M. Lundmark, and S. K. Rönnberg, "Measurements of High-Frequency (2–150 kHz) Distortion in Low-Voltage Networks," vol. 25, no. 3, pp. 1749–1757, 2010.

[52] S. Schöttke, J. Meyer, P. Schegner, and S. Bachmann, "Emission in the frequency range of 2 kHz to 150 kHz caused by electrical vehicle charging,"

IEEE Int Symp Electromagn Compat, pp. 620–625, 2014.

[53] A. A. Gerhard F. BARTAK, “EMI OF EMISSIONS IN THE FREQUENCY RANGE 2 kHz - 150 kHz,” *22nd Int Conf Electr Distrib*, 2013.

[54] P. D. ; F. B. ; E. H. ; F. Zare, “Improving 9-150 kHz EMI Performance of Single-Phase PFC Rectifier,” pp. 512–517, 2018.

[55] P. Kotsampopoulos *et al.*, “EMC Issues in the Interaction between Smart Meters and Power-Electronic Interfaces,” *IEEE Trans Power Deliv*, vol. 32, no. 2, pp. 822–831, 2017.

[56] C.I.S.P.R, “Specification for Radio Interference Measuring Apparatus and Measurement Methos,” vol. 16.

[57] F. . A. Davari, P.; Zare, “Active Rectifiers and Their Control, Control of Power Electronic Converters and Systems,” 2018, pp. 3–52.

[58] H. Luo, J. Xu, D. He, and J. Sha, “Pulse Train Control Strategy for CCM Boost PFC Converter With Improved Dynamic Response and Unity Power Factor,” *IEEE Trans Ind Electron*, vol. 67, no. 12, pp. 10377–10387, 2020.

[59] L. Ping and K. Yong, “Design and performance of an AC/DC voltage source converter,” in *INTELEC. Twenty-Second International Telecommunications Energy Conference (Cat. No.00CH37131)*, 2000, pp. 419–423.

[60] D. C. Morais, F. J. M. de Seixas, L. C. Souza, L. S. C. e Silva, and J. C. P. Júnior, “Three-phase Half-controlled Boost Converter Operating in Quasi-critical Conduction Mode,” in *2018 13th IEEE International Conference on Industry Applications (INDUSCON)*, 2018, pp. 811–816.

[61] C. Wang, M. Xu, F. C. Lee, and B. Lu, “EMI Study for the Interleaved Multi-Channel PFC,” in *2007 IEEE Power Electronics Specialists Conference*, 2007, pp. 1336–1342.

[62] K. Raggl, T. Nussbaumer, G. Doerig, J. Biela, and J. W. Kolar, “Comprehensive Design and Optimization of a High-Power-Density Single-Phase Boost PFC,” *IEEE Trans Ind Electron*, vol. 56, no. 7, pp. 2574–2587, 2009.

[63] N. Mohan, *Power Electronics: A First Course*. 2011.

[64] X. R. · X. Wang, D. P. · D. Yang, and W. L. · C. Bao, *Control Techniques for LCL-Type Grid- Connected Inverters*. 2018.

[65] F. Costa and D. Magnon, “Graphical analysis of the spectra of EMI sources in power electronics,” *IEEE Trans Power Electron*, vol. 20, no. 6, pp. 1491–1498, 2005.

[66] T. A. L. D. G. Holmes, *Pulse Width Modulation for Power Converters: Principles and Practice*. 2003.

[67] C. Ruan, X., Wang, X., Pan, D., Yang, D., Li, W., Bao, “Design of LCL Filter,” in *Control Techniques for LCL-Type Grid-Connected Inverters*, Springer, 2018, p. 3015.

[68] J. Sun, “Input impedance analysis of single-phase PFC converters,” *IEEE Trans Power Electron*, vol. 20, no. 2, pp. 308–314, 2005.

[69] G. Spiazzi and J. A. Pomilio, “Interaction between EMI filter and power factor preregulators with average current control: analysis and design considerations,” *IEEE Trans Ind Electron*, vol. 46, no. 3, pp. 577–584, 1999.

[70] C. Yoon, H. Bai, R. N. Beres, X. Wang, C. L. Bak, and F. Blaabjerg, “Harmonic Stability Assessment for Multiparalleled, Grid-Connected Inverters,” *IEEE Trans Sustain Energy*, vol. 7, no. 4, pp. 1388–1397, 2016.

[71] R. D. Middlebrook, “Null double injection and the extra element theorem,” *IEEE Trans Educ*, vol. 32, no. 3, pp. 167–180, 1989.

[72] M. Hartmann, H. Ertl, J. W. Kolar, M. Hartmann, H. Ertl, and J. W. Kolar, “EMI Filter Design for a 1 MHz, 10 kW Three-Phase/Level PWM Rectifier,” *IEEE Trans Power Electron*, vol. 26, no. 4, pp. 1192–1204, 2011.

[73] S. Ohn *et al.*, “Three Terminal Common-Mode EMI Model and EMI Mitigation Strategy for Full SiC UPS,” in *2018 IEEE Energy Conversion Congress and Exposition (ECCE)*, 2018, pp. 2094–2101.

[74] R. W. Erickson, “Optimal single resistors damping of input filters,” in *APEC ’99. Fourteenth Annual Applied Power Electronics Conference and Exposition. 1999 Conference Proceedings (Cat. No.99CH36285)*, 1999, vol. 2, pp. 1073–1079 vol.2.

[75] S. Ronnberg, M. Wahlberg, M. Bollen, A. Larsson, and M. Lundmark, “Measurements of interaction between equipment in the frequency range 9 to 95 kHz,” in *CIRED 2009 - 20th International Conference and Exhibition on Electricity Distribution - Part 1*, 2009, pp. 1–4.

[76] M. A. Alharbi, M. Dahidah, S. Ali, S. Ethni, and V. Pickert, “Current Ripple

Minimisation Based on Phase-Shedding of DC-DC Interleaved Converters for EV Charging System," in *IECON 2019 - 45th Annual Conference of the IEEE Industrial Electronics Society*, 2019, vol. 1, pp. 3456–3462.

[77] F. Yang, X. Ruan, Q. Ji, and Z. Ye, "Input DM EMI filter design of interleaved CRM Boost PFC converter with coupled inductor," in *2011 IEEE Energy Conversion Congress and Exposition*, 2011, pp. 2614–2621.

[78] L. Bede, G. Gohil, T. Kerekes, and R. Teodorescu, "Optimal interleaving angle determination in multi paralleled converters considering the DC current ripple and grid Current THD," in *2015 9th International Conference on Power Electronics and ECCE Asia (ICPE-ECCE Asia)*, 2015, pp. 1195–1202.

[79] J. Mühlethaler, H. Uemura, and J. W. Kolar, "Optimal design of EMI filters for single-phase boost PFC circuits," in *IECON 2012 - 38th Annual Conference on IEEE Industrial Electronics Society*, 2012, pp. 632–638.

[80] K. Raggl, T. Nussbaumer, and J. W. Kolar, "Model based optimization of EMC input filters," in *2008 11th Workshop on Control and Modeling for Power Electronics*, 2008, pp. 1–6.

[81] T. Nussbaumer, M. L. Heldwein, and J. W. Kolar, "Differential Mode Input Filter Design for a Three-Phase Buck-Type PWM Rectifier Based on Modeling of the EMC Test Receiver," *IEEE Trans Ind Electron*, vol. 53, no. 5, pp. 1649–1661, 2006.

ISSN (online): 2446-1636
ISBN (online): 978-87-7210-943-5 AALBORG UNIVERSITY PRESS